

**AD-A251 731**  




2

## **RESEARCH ON COMPLEX III-V STRUCTURES**

Wright State University  
University Research Center  
Dayton, Ohio 45435

April 23, 1992

Final Report for Period Sep 86 - Dec 91

Approved for public release; distribution unlimited.

**DTIC**  
**ELECTE**  
**S D**  
**JUN 10 1992**

Solid State Electronics Directorate  
Wright Laboratory  
Air Force Systems Command  
Wright-Patterson AFB, Ohio 45433-6543

92 6 08 079

**92-15086**




## NOTICE

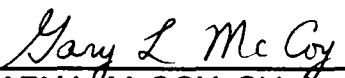
When Government drawings, specifications, or other data are used for any purpose other than in connection with a definitely Government-related procurement, the United State Government incurs no responsibility or any obligation whatsoever. The fact that the government may have formulated or in any way supplied the said drawings, specifications, or other data, is not to be regarded by implication, or otherwise in any manner construed, as licensing the holder, or any other person or corporation; or as conveying any rights or permission to manufacture, use, or sell any patented invention that may in any way be related thereto.

This report is releasable to the National Technical Information Service (NTIS). At NTIS, it will be available to the general public, including foreign nations.

This technical report has been reviewed and is approved for publication.

  
DAVID L. KINGSTON  
Project Engineer  
Characterization & Analysis Branch

  
KENICHI NAKANO, Chief  
Device Research Branch  
Research Division

  
GARY L. McCOY, Chief  
Research Division  
S.S. Electronics Directorate

If your address has changed, if you wish to be removed from our mailing list, or if the addressee is no longer employed by your organization please notify WL/ELRA, WPAFB, OH 45433-6543 to help us maintain a current mailing list.

Copies of this report should not be returned unless return is required by security considerations, contractual obligations, or notice on specific document.

REPORT DOCUMENTATION PAGE			Form Approved OMB No. 0704-0188	
Public reporting burden for this collection of information is estimated to average 1 hour per response, including the time for reviewing instructions, searching existing data sources, gathering and maintaining the data needed, and completing and reviewing the collection of information. Send comments regarding this burden estimate or any other aspect of this collection of information, including suggestions for reducing this burden, to Washington Headquarters Services, Directorate for Information Operations and Reports, 1215 Jefferson Davis Highway, Suite 1204, Arlington, VA 22202-4302, and to the Office of Management and Budget, Paperwork Reduction Project (0704-0188), Washington, DC 20503.				
1. AGENCY USE ONLY (Leave blank)	2. REPORT DATE 23 Apr 92	3. REPORT TYPE AND DATES COVERED Final: 23 Sep 86 - 23 Dec 91		
4. TITLE AND SUBTITLE  Research on Complex III-V Structures		5. FUNDING NUMBERS  C: F33615-86-C-1062  PR: 2306 TA: R1 WU: 00		
6. AUTHOR(S)		7. PERFORMING ORGANIZATION NAME(S) AND ADDRESS(ES)  Wright State University University Research Center Dayton, OH 45435		
8. PERFORMING ORGANIZATION REPORT NUMBER		9. SPONSORING / MONITORING AGENCY NAME(S) AND ADDRESS(ES) David Kingston (513) 255-1188 Research Division, WL/ELR Solid State Electronics Directorate Wright Laboratory Wright-Patterson Air Force Base, OH 45433-6543		
10. SPONSORING / MONITORING AGENCY REPORT NUMBER  WL-TR-92-5008		11. SUPPLEMENTARY NOTES		
12a. DISTRIBUTION / AVAILABILITY STATEMENT  Approved for public release; distribution is unlimited.		12b. DISTRIBUTION CODE		
13. ABSTRACT (Maximum 200 words)  Impurities and defects in bulk, ion-implanted, and epitaxial III-V compound homostructures and heterostructures have been studied by various electrical and optical techniques. Results have been applied to device design and implementation, with emphasis on MIMIC circuits.				
14. SUBJECT TERMS GaAs, AlGaAs, Antisite, Heterostructure, MIMIC, Hall effect, Photoluminescence, Photoreflectance			15. NUMBER OF PAGES 119	
16. PRICE CODE			17. SECURITY CLASSIFICATION OF REPORT Unclassified	
18. SECURITY CLASSIFICATION OF THIS PAGE Unclassified		19. SECURITY CLASSIFICATION OF ABSTRACT Unclassified		20. LIMITATION OF ABSTRACT Unlimited

# TABLE OF CONTENTS

	<u>Page</u>
1.0 Semiconducting/Semi-insulating Reversibility in Bulk GaAs	1
2.0 Defect Production in Electron-Irradiated, n-type GaAs	5
3.0 A New Technique for Contact Evaluation of MODFET Structures	10
4.0 Electrical Properties of MBE GaAs Grown at 200°C	15
5.0 Alloy Scattering in p-type $\text{Al}_x\text{Ga}_{1-x}\text{As}$	19
6.0 Optical Properties of Bulk Materials	23
7.0 Optical Properties of Epitaxial Materials	42
8.0 Optical Properties of Quantum Wells and Superlattices	51
9.0 Photocurrent Spectroscopy in AlGaAs/GaAs and InGaAs/GaAs Quantum Wells	59
10.0 Time Resolved and Magnetic-Field Dependent Photoluminescence in Quantum Wells	69
11.0 MIMIC Materials/Device Correlation Program	78
References	94
List of Publications	99
Patents	110



<b>Accession For</b>	
NTIS GRA&I	<input checked="" type="checkbox"/>
DTIC TAB	<input type="checkbox"/>
Unannounced	<input type="checkbox"/>
Justification	
By _____	
Distribution/	
<b>Availability Codes</b>	
Dist	Avail and/or Special
A-1	

## List of Figures

<u>Figure</u>	<u>Page</u>
1-1 Hall carrier concentration ( $n_H = 1/eR$ ) vs. inverse temperature for as-grown and heat-treated samples.	3
2-1 Carrier concentration as a function of temperature for various fluences.	7
3-1 A two-layer distributed-resistance circuit applicable to MODFET material.	12
3-2 Resistance versus contact spacing for MODFET material at 77 K.	14
4-1 The resistivity $\rho$ and apparent carrier concentration $n$ as a function of measurement temperature, for various annealing temperatures.	16
4-2 The deep-donor concentration $N_D$ , calculated separately from Hall-effect and infrared-absorption data, as a function of annealing temperature.	17
4-3 Surface potential energy $-e\phi_s$ , as a function of annealing temperature for the control and capped samples.	18
5-1 A comparison of the theoretical Hall mobilities for relatively pure p-type samples of GaAs, AlAs, and $Al_{0.5}Ga_{0.5}As$ ( $N_A = 6.5 \times 10^{13} \text{ cm}^{-3}$ , $N_D = 2.5 \times 10^{12} \text{ cm}^{-3}$ , and $E_A = 0.025 \text{ eV}$ , for each); and (b) the Hall $r$ factors for these same samples.	20
5.2 The experimental (circles, squares, and triangles) and theoretical (solid line) Hall mobility as a function of $x$ for p-type $Al_xGa_{1-x}As$ .	21
6.1 Pressure vs. transition energy relation for compensated p-type GaAs.	24
6.2 PL spectra under various pressure from 0 to 30 Kbar at 10 K. All the $\Gamma$ -transitions are due to the defects at the As site.	25
6.3 PL spectra from $Ga_{As}$ center in p-type GaAs.	27
6.4 PL of quenched GaAs at various temperatures.	28
6.5 Energy levels in indium-alloyed GaAs.	29
6.6 The variation of half-width of ELO emission with temperature.	31
6.7 Two different photo quenching spectra.	32
6.8 PL of Sb-doped GaAs.	35
6.9 Room-temperature photoreflexion spectrum of indium-alloyed GaAs.	36

6.10	$\text{Ga}_{\text{As}}^0$ and $\text{Ga}_{\text{As}}^-$ absorption spectra.	37
6.11	Photoconductivity of $(\text{Ga}_{\text{As}})^0/(\text{Ga}_{\text{As}})^-$ transition.	39
6.12	Variation of PL emission in In-alloyed GaAs across a 3-inch diameter wafer.	40
7.1	AlGaAs excitonic linewidth vs. Al concentration.	43
7.2	Variation of the lines at 1.5040– to 1.5110 eV range.	44
7.3	PL of AlGaAs with different growth conditions.	46
7.4	Excitation intensity vs. energy in GaInAs/GaAs.	47
7.5	Excitation intensity vs. transition energy in GaInAs/GaAs.	48
7.6	Reflection patterns of GaSbAs grown by MBE.	50
8.1	Well-resolved exciton lines of three GaAs–AlGaAs wells.	52
8–2	High-resolution PL and PR spectra of an AlGaAs–GaAs QW.	54
8–3	Theoretical calculation of the band-offset of the InGaAs/GaAs system.	58
9–1	Comparison of PC and PL spectra for a GaAs/AlGaAs MQW.	60
9–2	Monolayer fluctuation revealed by the PC method.	61
9–3	Variation of the oscillator strength of several exciton transitions	63
9–4	Electric field dependence of various exciton transition energies of a GaAs/AlGaAs MQW.	64
9–5	Electric field dependence of the oscillator strength of various excitons in a GaAs/AlGaAs MQW.	66
9–6	Electric field dependence of exciton transitions in an InGaAs/GaAs MQW.	67
9–7	Electric field dependence of exciton transitions in a triangular GaAs/AlGaAs well.	68
10–1	PL spectra obtained at 2 K showing the optical transitions from a 350–Å $\text{Al}_x\text{Ga}_{1-x}\text{As}/\text{GaAs}$ MQW structure in a zero magnetic field (solid line) and an magnetic field of 36 KG (dashed line).	71
10–2	Photoluminescence spectra from a 200–Å GaAs/AlGaAs/ $\text{Al}_{0.3}\text{Ga}_{0.7}\text{As}$ QW.	72
10–3	Time response for the HHFE of the sample shown in Fig. 10–2 (solid curve) and for the peak at 1.5239 eV (dashed curve).	73

10-4	PL spectrum for an undoped, two monolayer-wide $\text{In}_{0.1}\text{Ga}_{0.9}\text{As}/\text{GaAs}$ QW structure showing the HHFE and BB transitions.	75
10-5	Time resolved PL decay curves for the HHFE (solid) and BB (dashed) transitions for the undoped, two monolayer-wide $\text{In}_{0.1}\text{Ga}_{0.9}\text{As}/\text{GaAs}$ QW structure.	77
11-1	(a) Map of $I_{ds}-C$ after standard implant, gradient lower-left to upper-right, (b) rotated wafer.	84
11-2	Map of $I_{ds}-R$ for dip-etched wafer (a), spray-etched wafer (b) on same grey scale.	86
11-3	(a) Percentile plot illustrating local etch effects, (b) wafermap illustrating local testing effects.	87
11-4	Vector map of breakdown voltage variation.	88
11-5	Change in $I_{ds}$ (V vs. H) occurring between post-gate and final DC testing for seven process lines.	90
11-6	Correlation plot of $G_m\text{-RF}$ vs. $G_m\text{-DC}$ .	90
11-7	$I_{ds}\text{-F}$ (mA/mm) boxplots of six lots for one process line.	92

## LIST OF TABLES

<u>Table</u>		<u>Page</u>
1-1	Electrical properties of ingot No. 3, seed end, after anneal and quench cycles	2
2-1	Energies and production rates of primary defects produced by 1-MeV electrons in GaAs	6
11-1	Measurements and Test Times	82
11-2	Wafer Process Related Problems	82



## FOREWORD

This contract, which was largely of a basic-research nature, involved approximately 42.5 man-years of professional, technical, and clerical effort, and covered the period 29 September 1986 – 23 December 1991, or 5.23 years. The participants, including both full-time and part-time workers, were Christopher Blouch, Stewart Cummins, Timothy Cooper, Robin Heil, John Hoelscher, Jeffery Layne, David Look, James Prichard, Donald Reynolds, Harold Ritter, Patter Schwenke, Gregory Smith, Ivan Soper, John Stephenson, William Theis, Dennis Walters, and Phil Yu. There are perhaps many ways to measure success or failure of a contract such as ours, but we believe that the 135 professional-journal articles and 4 patents, listed at the end of this report, are a good indication of a productive effort. Whatever success we have had would not have been possible without the strong support of Air Force personnel in the Research Division of the Solid State Electronics Directorate, Wright Laboratory, especially Mr. David Kingston, Contract Monitor, Mr. Gary McCoy, Division Chief, Lt Col. Kenneth Soda, former Branch Chief, and Dr. Robert Walline, present Branch Chief. We also owe a debt of gratitude to several Wright State University colleagues involved in contract administration and negotiation, especially Mr. Leon Testas, Mr. Philip Spina, Dr. Joseph Thomas, and Dr. Donald Thomas. Many other colleagues, both at Wright Laboratory and Wright State University, have directly contributed to our research endeavors, and some of their names can be found as co-authors in the various publications listed at the end of this report.

This work was performed by the University Research Center, School of Graduate Studies, Wright State University, 106 Oelman Hall, 3640 Col. Glenn Highway, Dayton, Oh, 45435, under Contract F33615-86-C-1062. The project, task, and work unit number was 2306R100, and the project engineer was David L. Kingston, WL/ELR, Wright-Patterson AFB, OH, 45433-6543. The report was submitted on 23 April 1992.

## 1.0 Semiconducting/Semi-insulating Reversibility in Bulk GaAs

### 1.1 Introduction

Bulk, undoped, semi-insulating (SI) GaAs is generally considered to be of high resistivity because of a balance between a shallow donor, Si (or S), a shallow acceptor, C, and a deep donor, EL2, with relative magnitudes as follows:  $[C] > [Si]$  and  $[EL2] > [C] - [Si]$ . However, it is possible with present low-pressure liquid-encapsulated Czochralski (LPLEC) and high-pressure liquid-encapsulated Czochralski (HPLEC) technology to grow crystals with  $[C]$  and  $[Si] < 5 \times 10^{14} \text{ cm}^{-3}$ . With such materials, the compensation is almost entirely due to native defects. We show that it is possible to make LPLEC crystals uniformly conducting or semi-insulating by variations of a simple heat treatment which changes the relative concentrations of donor and acceptor defects. As reported earlier,<sup>1</sup> the process leads to improved uniformity of direct-implant metal-semiconductor field-effect transistors.

### 1.2 Experimental Results

The crystals were grown under near-stoichiometric conditions, in PbN crucibles, with 2 atm of  $N_2$  gas. The ingots were 2 1/2 - 3 inches in diameter, and 2 - 5 inches long. As grown, the boules were, in general, not semiinsulating and not uniform from seed to tail. However, after a 5-hour,  $950^\circ\text{C}$  soak in an evacuated quartz ampoule, and subsequent quench by rapidly removing the ampoule from the furnace, the ingots were both uniform and semi-insulating. Table 1-1 illustrates the reversibility of the conducting and semi-insulating states for ingot No. 3. Here " $950^\circ\text{C-Q}$ " means the sample was quenched, as described above, and " $950^\circ\text{C-A}$ " means the sample was "annealed" after the  $950^\circ\text{C}$  soak, i.e., the furnace was simply turned off. It is clear from Table 1-1 that the electrical properties can be cycled back and forth between the two states. A similar phenomenon was observed by Woodall and Woods,<sup>2</sup> although over a much reduced resistance range.

Table 1-1 Electrical properties of ingot No. 3, seed end, after anneal and quench cycles.

Treatment	$\rho(\Omega \text{ cm})$	$\mu(10^3 \text{ cm}^2/\text{Vs})$	$n(\text{cm}^{-3})$
1. as-grown	2.5	5.2	$4.7 \times 10^{14}$
2. 950°C-Q	$9.4 \times 10^6$	5.2	$1.3 \times 10^8$
3. 950°C-A	7.8	4.6	$1.7 \times 10^{14}$
4. 950°C-Q	$9.6 \times 10^6$	5.1	$1.3 \times 10^8$
5. 950°C-A	3.3	7.1	$2.7 \times 10^{14}$
6. 950°C-Q	$2.7 \times 10^7$	6.7	$3.4 \times 10^7$

The impurity concentrations were checked by local vibrational mode (LVM) absorption spectroscopy, secondary-ion mass spectroscopy (SIMS), and spark source mass spectroscopy (SSMS). For sample 950°C-A, the results were  $[B] \approx 8 \times 10^{16} \text{ cm}^{-3}$ ,  $[C] \approx 3 \times 10^{14} \text{ cm}^{-3}$ ,  $[\text{Si}] \lesssim 2 \times 10^{14} \text{ cm}^{-3}$  with all other individual impurity concentrations  $\lesssim 1 \times 10^{15} \text{ cm}^{-3}$  and with total impurity donor and acceptor concentrations each  $\lesssim 2 \times 10^{15} \text{ cm}^{-3}$ . (Note that no  $B_{\text{As}}$  was detected by LVM absorption and  $B_{\text{Ga}}$  is not electrically active.) The EL2 concentration was measured by deep level transient spectroscopy (DLTS) and absorption, and was nearly identical at  $1.0 \times 10^{16} \text{ cm}^{-3}$  in both the quenched and annealed crystals. In the as-grown sample,  $[\text{EL2}]$  was found to be about  $6 \times 10^{15} \text{ cm}^{-3}$ , by a DLTS measurement.

The Hall electron concentrations ( $n_{\text{H}} \equiv 1/eR$ ) of as-grown, annealed, and quenched samples are shown in Fig. 1-1. The as-grown sample is controlled mainly by a shallow donor ( $E_{\text{DS}} \approx 3.0 \text{ meV}$ ) at room temperature and below, with a small amount of a deeper donor ( $E_{\text{C}}$

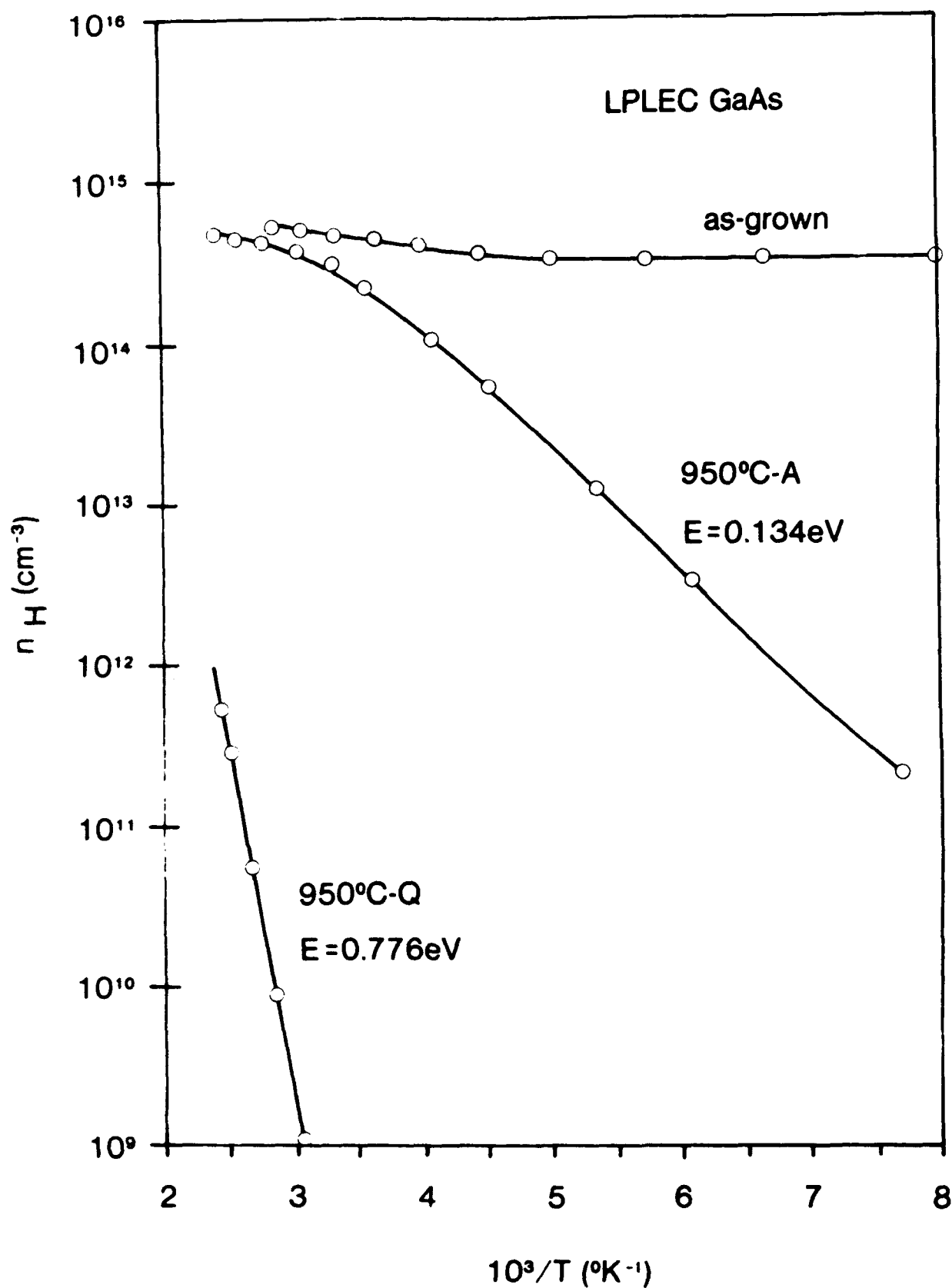


Fig. 1-1. Hall carrier concentration ( $n_H = 1/eR$ ) vs. inverse temperature for as-grown and heat-treated samples. The symbol "A" designates slow cooling, and "Q" fast cooling, following a 5-h, 950°C anneal. The solid lines are theoretical fits.

– 0.13 eV) becoming noticeable at higher temperatures. (It will be assumed here that the 0.13 eV center is a donor, although we as yet have no proof of that fact.) The annealed sample (950°C–A), on the other hand, has a greatly increased concentration of the 0.13 eV center, but also an increased acceptor concentration. Finally, the quenched sample (950°C–Q) shows the EL2 activation energy, but accurate quantitative information cannot be obtained from the Hall-effect data since the room-temperature EL2 energy is not precisely known.<sup>3</sup> A significant observation from all of these data is that both the as-grown and annealed states show very close compensation. Another observation is that the donor and acceptor concentrations are significantly higher than the electrically active impurity concentrations, at least for sample 950°C–A. Thus, the electrical properties of this sample are primarily controlled by defects.

### 1.3 Model

In our model, a rapid cooldown (quench) freezes in significant amounts ( $10^{15} - 10^{16} \text{ cm}^{-3}$ ) of  $V_{As} - As_{Ga}$  and  $V_{Ga} - Ga_{As}$ . The latter complexes (plus other acceptors below midgap) dominate the former complexes (plus other donors above midgap) so that the deep donor EL2 can render the sample semi-insulating ( $[A] > [D]$  and  $[EL2] > [A] - [D]$ ). A slow cooldown (anneal), on the other hand, permits the rather unstable  $V_{Ga} - Ga_{As}$  to break up as  $E_F$  rises, so that  $[D] > [A]$  and the sample is conductive. Other electron traps, as observed by DLTS, may influence this picture, but are of lower concentrations than the  $E_C - 0.13 \text{ eV}$  center. Hole traps have not yet been investigated. Further information may be found in Publ. No's. 1, 2, 15, and 34 in the List of Publications.

## 2.0 Defect Production in Electron-Irradiated, n-type GaAs

### 2.1 Introduction

Electron-irradiation experiments in GaAs have been carried out extensively since the early 1960's. The results prior to 1977 have been reviewed by Lang,<sup>4</sup> and those up to 1985 by Pons and Bourgoin.<sup>5</sup> In spite of the results available from a wide variety of experimental techniques, no defect produced in quantity by 1-MeV irradiation has been conclusively identified, although the involvement of the As vacancy ( $V_{As}$ ) is fairly certain.<sup>5,6</sup> The primary characterization tool used for electron-irradiation investigations in the last decade is deep-level transient spectroscopy (DLTS),<sup>7</sup> which allows many deep-level centers to be seen in the same sample. One disadvantage of DLTS, however, is that it requires either a Schottky barrier or a p-n junction diode in order to have a region in which the majority carrier concentration is adjustable by applying a voltage pulse. Thus, the main usefulness of DLTS lies in the study of majority-carrier traps, i.e., electron traps in n-type material and hole traps in p-type material. Although minority carriers can sometimes be injected, by voltage or light, still only qualitative information may be obtained on minority-carrier traps in most cases.<sup>8</sup> In GaAs, it is easy to make a good Schottky diode on n-type material, and therefore, most of the DLTS work has been carried out on electron traps in n-type GaAs. At present, there are two major dilemmas concerning the DLTS data. The first is that a reconciliation of Hall-effect and DLTS results seems to demand that at least one of the two major electron traps, E1 and E2 ( $C_1$  and  $C_2$  in our notation) must be an acceptor.<sup>5,9</sup> But  $C_1$  and  $C_2$  have also been identified with the As vacancy,<sup>2</sup> which intuitively should have donor nature. The second dilemma is that all of the electron and hole traps observed by DLTS have been attributed, with good evidence, to As sublattice damage.<sup>5</sup> If so, then the Ga sublattice damage, which certainly is created in roughly the same amount, is missing. The results of our study can resolve both dilemmas.

## 2.2 Results

Carrier concentration  $n$  vs.  $T^{-1}$  data as a function of irradiation fluence are presented in Fig. 2-1. The production rates of the various defects can be determined by fitting these data. The principal defects are  $C_2$ ,  $C_3$ , and  $C_{AS}$ , where the first two are undoubtedly the same as the well-known electron traps E2 and E3, deduced by DLTS, and the third,  $C_{AS}$ , is a new acceptor trap. The situation is summarized in Table 2-1. As can be seen, the agreement with DLTS is very good for  $C_2$  and  $C_3$ .

Table 2.1. Energies and production rates of primary defects produced by 1-MeV electrons in GaAs.

Defect		Energy (eV)		Production rate ( $\text{cm}^{-1}$ )	
Hall <sup>a</sup>	DLTS <sup>b</sup>	Hall <sup>a</sup>	DLTS <sup>b</sup>	Hall <sup>a</sup>	DLTS <sup>b</sup>
	E1 <sup>c</sup>		$E_C - 0.045$		1.5
$C_2^c$	E2 <sup>c</sup>	$E_C - 0.148$	$E_C - 0.14$	$2.0 \pm 0.2$	1.5
$C_3^c$	E3 <sup>c</sup>	$E_C - 0.295$	$E_C - 0.30$	$0.5 \pm 0.2$	0.4
	E4 <sup>c</sup>		$E_C - 0.76$		0.1
	E5 <sup>c</sup>		$E_C - 0.96$		0.1
	H0 <sup>d</sup>		$E_V + 0.06$		0.8
	H1 <sup>d</sup>		$E_V + 0.29$		0.1
$C_{AS}^c$		below $E_C - 0.3$		$4 \pm 1$	

<sup>a</sup>This work.

<sup>b</sup>From Ref. 5

<sup>c</sup>Measured in n-type GaAs.

<sup>d</sup>Measured in p-type GaAs.

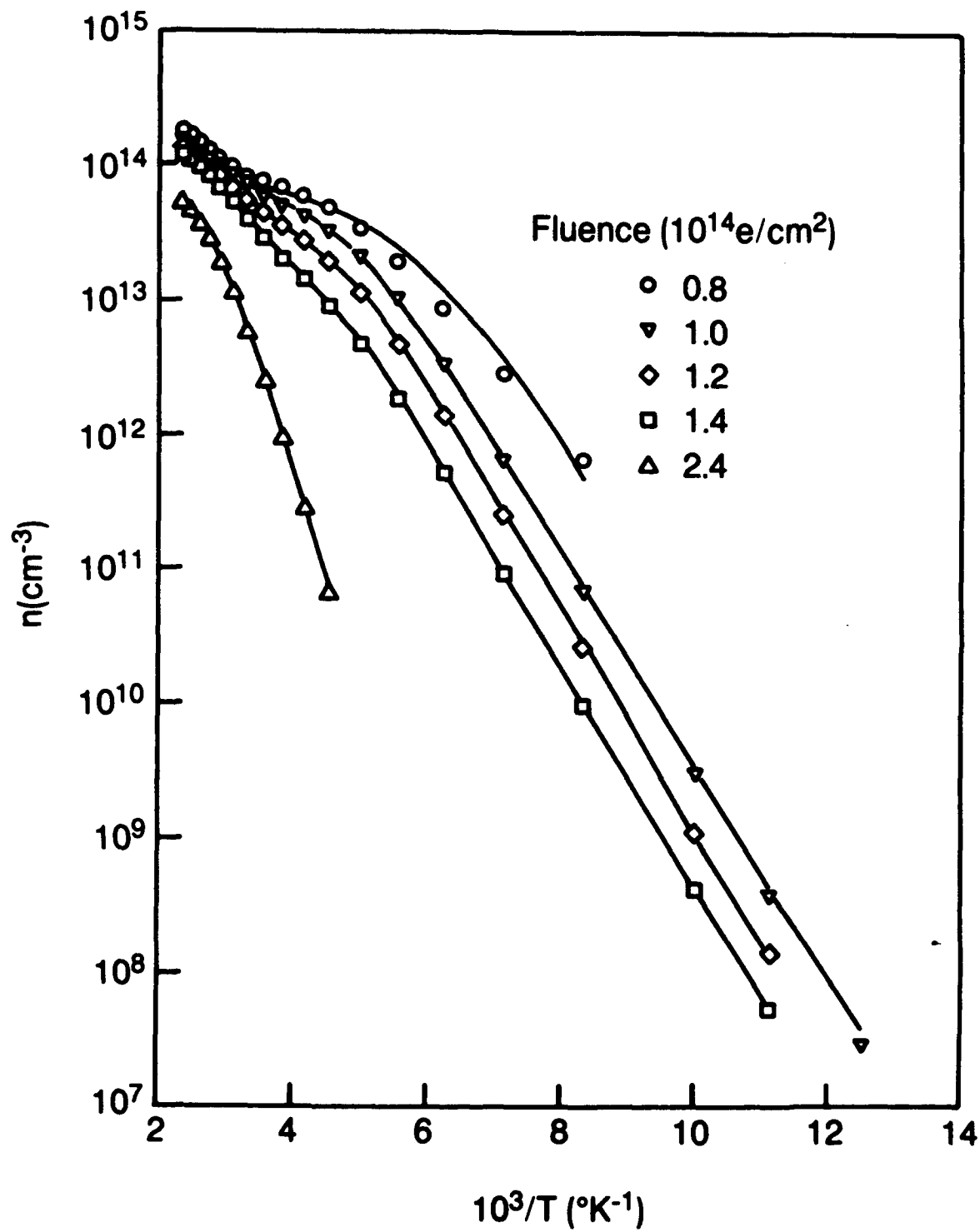


Fig. 2-1. Carrier concentration as a function of temperature for various fluences. The solid lines are theoretical fits.



### 2.3 Model

An intriguing model, which satisfies most, if not all, of the experimental and theoretical observations, is that  $C_{AS}$  is mainly Ga-sublattice damage (GSLD), which has not been identified up to now.<sup>5</sup> The GSLD would probably consist primarily of  $V_{Ga}$ , or the Frenkel pairs  $V_{Ga}-Ga_i$ , just as the As-sublattice damage (ASLD) is expected to be mostly  $V_{As}$  and/or  $V_{As}-As_i$  pairs. First, the ASLD is known, from DLTS data,<sup>5</sup> to have a total production rate of about  $5\text{ cm}^{-1}$ . The GSLD would be expected to have nearly the same rate, and indeed, the rate for  $C_{AS}$  is  $4 \pm 1\text{ cm}^{-1}$ . Second, the GSLD defects, i.e.,  $V_{Ga} - Ga_i$ , should have primarily acceptor nature,<sup>10</sup> and we have shown that the  $C_{AS}$  are acceptors. Third, the GSLD might be expected to be unstable in p-type GaAs, since  $V_{Ga}$  can then transform to the more stable configuration  $As_{Ga} - V_{As}$  by a simple nearest-neighbor hop,<sup>11</sup> and  $V_{Ga}-Ga_i$  should have a high probability of recombination if the  $Ga_i$  is positively charged. In agreement, the  $C_{AS}$  must be unstable in p-type material, or else the Fermi level would not move up, toward midgap, in electron-irradiated p-type GaAs.<sup>4,12</sup> Also, the nonobservation by DLTS of any high-production-rate ( $\tau \sim 4\text{ cm}^{-1}$ ) centers in p-type GaAs is consistent with this model. It would be interesting to make a more concerted DLTS effort to find and quantify the  $C_{AS}$  centers in n-type GaAs by applying injection techniques. Furthermore, detailed isothermal annealing experiments should be performed to determine the thermal stability.

Finally, the  $\tau_{AS}$  results have important implications for any theoretical attempts to identify  $C_1$  and  $C_2$ . A starting point for many of the current models is that either  $C_1$  or  $C_2$  must be an acceptor;<sup>5,9</sup> otherwise, as seen in Table 2-1, there are no other electron or hole traps with a high enough production rate to explain the well-known fact that electron irradiation depletes n-type GaAs of electrons. Since there is now good evidence to associate  $C_1$  and  $C_2$  with the As vacancy, it has even been claimed<sup>9</sup> that these levels represent the two double-acceptor states of  $V_{As}$ , a model which seems to violate intuition, as well as the

observed capture cross sections. We do not wish to debate the relative merits of this model or any other, but simply to point out that the high measured value of  $\tau_{AS}$  makes it entirely unnecessary to assume that either  $C_1$  or  $C_2$  has an acceptor nature; i.e., the electron depletion in n-type GaAs can be basically explained by the  $C_{AS}$  acceptors alone. Further information can be found in Publ. No's. 21, 22, 23, 39, and 80 in the List of Publications.

### 3.0 A New Technique for Contact Evaluation of MODFET Structures

#### 3.1 Introduction

The problems of contact resistance have become more acute in recent years with the advent of submicron devices, which can have very small intrinsic resistances.<sup>13</sup> Thus, much effort has been expended in an attempt to improve ohmic contacts, and also to improve the techniques by which they are measured. For planar devices, such as metal–semiconductor field–effect transistors (MESFETs), the transmission–line model (TLM) has been widely used to extract the intrinsic metal–semiconductor (M/S) barrier resistance, in a form called the specific contact resistivity  $\rho_c$ , which is a figure of merit for the ohmic contacts.<sup>14</sup> This model gives two parameters:  $r_s$ , the sheet resistance of the bulk material between the contacts, and  $\rho_c R_s$ , where  $R_s$  is the sheet resistance of the material under the contacts. To determine  $\rho_c$  it is usually assumed that  $R_s = r_s$ , which may be true if the contacting materials do not diffuse or alloy appreciably, but is not true in general. It is sometimes possible, by means of an additional measurement, to determine the "end resistance," which gives the correct  $R_s$  and thus  $\rho_c$ .<sup>15</sup>

Earlier, we introduced a new technique based on the magneto–transmission line model (MTLM), which, besides  $r_s$  and  $\rho_c R_s$ , also gives the bulk mobility  $\mu$ , the bulk sheet carrier concentration  $n_s$ , and the mobility of the material under the contact  $\mu_c$ .<sup>16</sup> The determinations of  $\mu$  and  $n_s$  make an additional Hall–effect measurement unnecessary. Also, if  $\mu_c = \mu$ , then it can be safely assumed that  $R_s = r_s$  and  $\rho_c$  can be accurately calculated. If  $\mu_c \neq \mu$  it still may be possible to estimate  $R_s$  from the value of  $\mu_c$ .

Unfortunately, all the techniques discussed above work only for single–layer devices such as MESFETs, and are not applicable to the heterostructure devices, in particular the modulation–doped FETs (MODFETs). Recently, Feuer<sup>17</sup> has developed a two–layer model in which the space between the contacts (bulk) is treated as a distributed resistance, but the contacts themselves are evidently treated as equipotential vertical surfaces, through both

layers. Thus, no information concerning the material beneath the contact metallization can be obtained. In this report, we treat both the bulk and contact regions as two-layer distributed resistances, and also include magnetic-field effects. The model fits MODFET data very well, with reasonable parameters, over a wide range of magnetic-field strengths (0–18kG) and temperatures (5–300°K).

### 3.2 Model

Both the one-layer TLM and one-layer MTLM have been discussed in detail elsewhere.<sup>14,16</sup> The basic two-layer circuit considered here, shown in Fig. 3–1, consists of two contacts of length  $\ell_c$  separated by bulk semiconductor material of length  $\ell$ . In practice, the contacting materials may diffuse through one or both layers<sup>13,18</sup> so that  $R_{s1} \neq r_{s1}$ , and  $R_{s2} \neq r_{s2}$ . For example, in the MODFET structure shown in Fig. 3–1, if the contacts are the commonly used Au/Ge/Ni, then it is well known that all three materials can diffuse more than 1000Å under typical anneal conditions.<sup>18</sup> The specific contact resistivity  $\rho_{c1}$  denotes the M/S barrier resistance between layer 1 and the metal, while  $\rho_{c2}$  denotes the barrier resistance between layers 1 and 2, both in the contact region and in the bulk. If a GaAs cap layer has been added in order to decrease the overall parasitic resistance, then the two-layer model does not strictly apply, although  $\rho_{c2}$  could then be considered to represent the barrier between layer 2 and the GaAs cap, i.e., the barrier through all of the AlGaAs material. The cap would normally not add a third layer in the material between the contacts since in this region it would be depleted by the surface potential.

### 3.3 Results

The MODFET material discussed here had the following structure, from bottom to top: semi-insulating substrate, 1μm p<sup>−</sup>–GaAs buffer layer, 200Å p<sup>−</sup>–In<sub>0.15</sub>Ga<sub>0.85</sub>As, 30Å p<sup>−</sup>–Al<sub>0.15</sub>Ga<sub>0.85</sub>As, 350Å n<sup>+</sup>–Al<sub>0.15</sub>Ga<sub>0.85</sub>As, and finally, a cap layer, 200Å n<sup>+</sup>–GaAs. We may consider it as a generic MODFET structure for testing our two-layer model.

The TLM pattern used for this study had contact separations, as measured by an

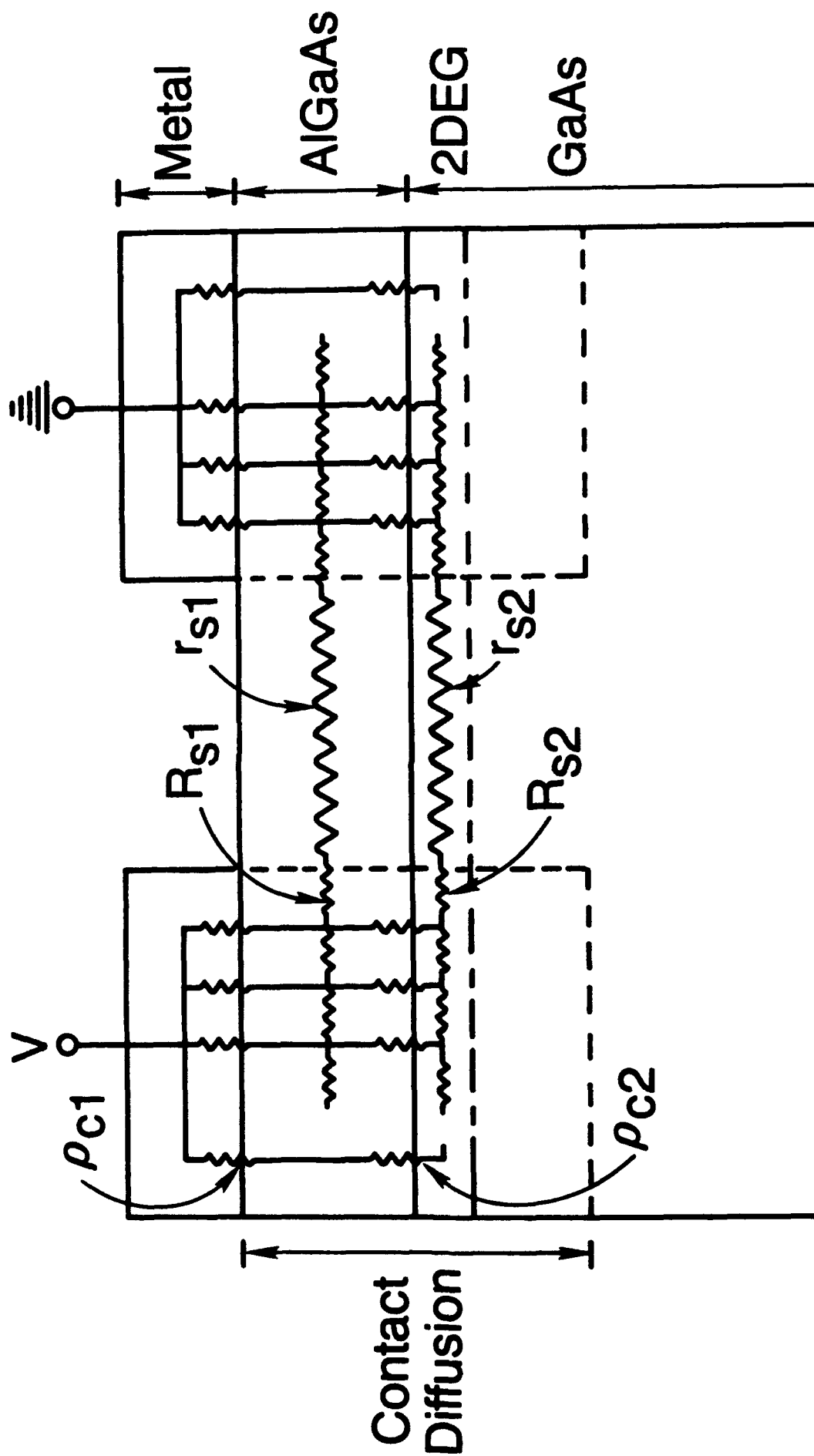


Fig. 3-1. A two-layer distributed-resistance circuit applicable to MODFET material. Layer 2 is assumed to be mainly due to the 2D electron gas, while layer 1 is due to parallel conduction in the doping layer.

optical microscope, of 1.5, 3.6, 5.9, and 9.8  $\mu\text{m}$ . The voltage used was 20 mV, and magnetic field strengths  $B$  ranged from 0 to 18 kG. The  $R$  vs.  $\ell$  data are shown in Fig. 3-2 along with fits using one-layer and two-layer MTLM theories. The two-layer model fits very well while the one-layer model does not. (In this case, the one-layer model was fitted at  $B=0$  for all  $\ell$ , and at  $B = 18$  kG for  $\ell = 1.5$   $\mu\text{m}$ , somewhat arbitrarily. However, other combinations looked just as bad.) Also, the one-layer TLM theory (no magnetic field) was fitted and was very close to the  $B = 0$  curve. Thus, each model fits the  $B = 0$  data fairly well.

In this brief report, we will not list the fitting parameters found from the one-layer and two-layer fits, because they can be found, along with other information on this technique, in Publ. No's. 16, 18, 19, 40, 41, and 50 in the List of Publications. However, it appears that the two-layer MTLM method will be useful for both bulk and contact studies in MODFET materials.

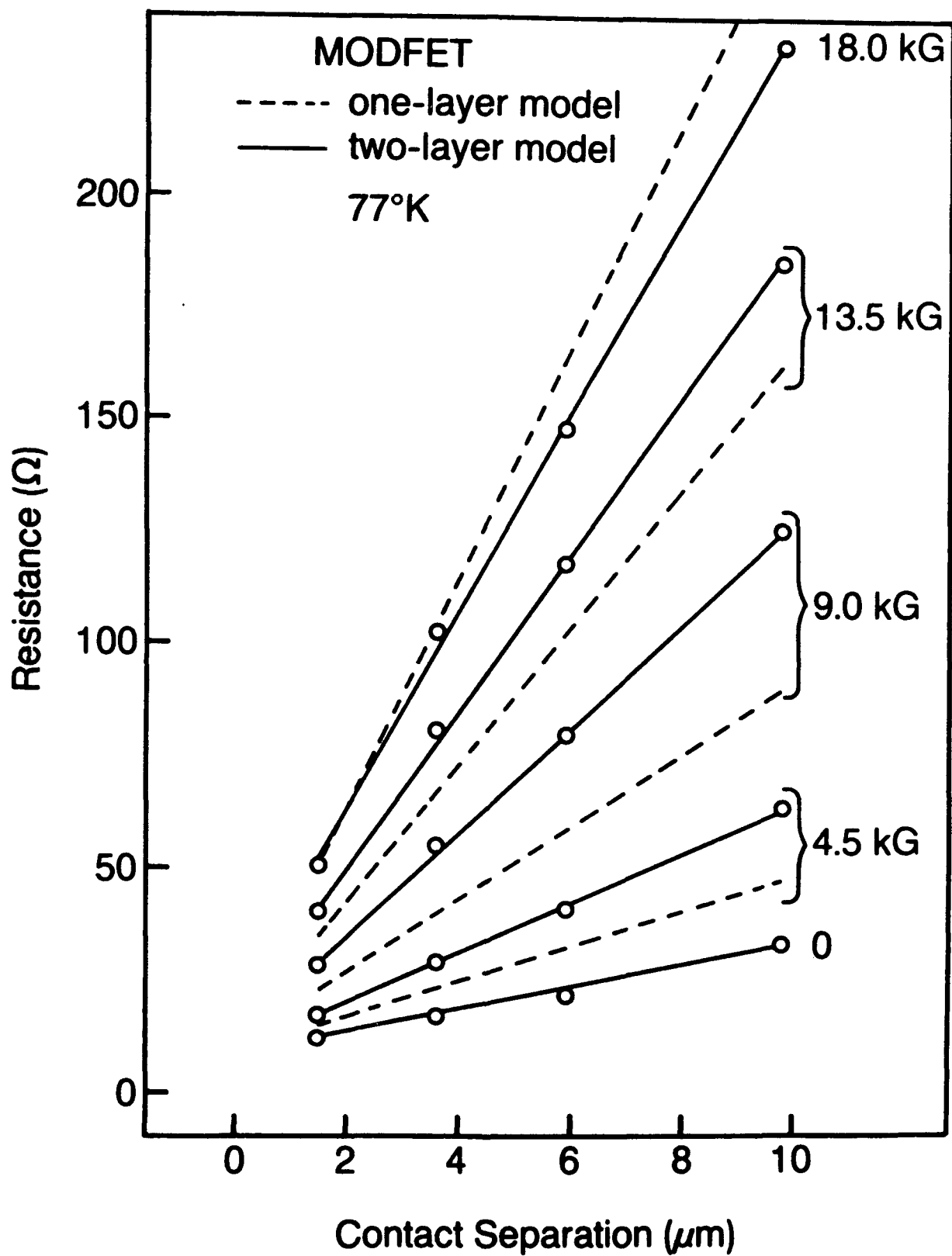


Fig. 3-2. Resistance versus contact spacing for MODFET material at 77 K. The solid line is a two-layer fit and the dashed line is a one-layer fit.

## 4.0 Electrical Properties of MBE GaAs Grown at 200°C

### 4.1 Introduction

Molecular beam epitaxial (MBE) GaAs is normally grown at temperatures of 580–600°C and, at these temperatures, it is relatively routine to attain shallow donor ( $N_D$ ) and acceptor ( $N_A$ ) concentrations in the  $10^{14} \text{ cm}^{-3}$  range, and even smaller deep donor ( $N_{DD}$ ) and acceptor ( $N_{AA}$ ) concentrations. Recently, however, Smith et al.<sup>19</sup> showed that MBE GaAs grown at 200°C had much different properties, and that when used as a buffer layer could remarkably improve some critical characteristics of GaAs MESFET devices; since then many groups have studied the application of this material to a variety of other devices.<sup>20–24</sup> The outstanding characteristic of low-temperature grown MBE (LTMBE) GaAs is a large excess of As (1–2%), which leads to a deep donor ( $\text{As}_{\text{Ga}}$ -related) concentration  $N_{DD} > 10^{19} \text{ cm}^{-3}$ , and, after a 600°C anneal, large ( $\sim 60 \text{ \AA}$ ), dense ( $\sim 10^{17} \text{ cm}^{-3}$ ) precipitates of As.<sup>25–31</sup>

We began working on LTMBE GaAs in April 1989, about 1 year after the initial report on the material.<sup>19</sup> Our major contributions, so far, have included: (1) the first Hall-effect measurements (Fig. 4-1), and the model to explain Hall effect and conductivity;<sup>28</sup> (2) the first absorption measurements,<sup>27</sup> which gave an independent confirmation to the Hall results on deep donor concentration vs. annealing temperature (Fig. 4-2); (3) the first report<sup>32</sup> on the reduction in effective surface potential energy ( $-e\phi_s$ ) caused by a 200°C MBE cap on an active layer (Fig. 4-3); and (4) a model for the immediate ohmic nature (without alloying) of a metal contact on 200°C MBE material.<sup>33</sup> Further information may be found in Publ. No's. 83, 84, 85, 86, 87, 89, 92, 93, 102, 126, 127, 128, and 131 in the List of Publications.



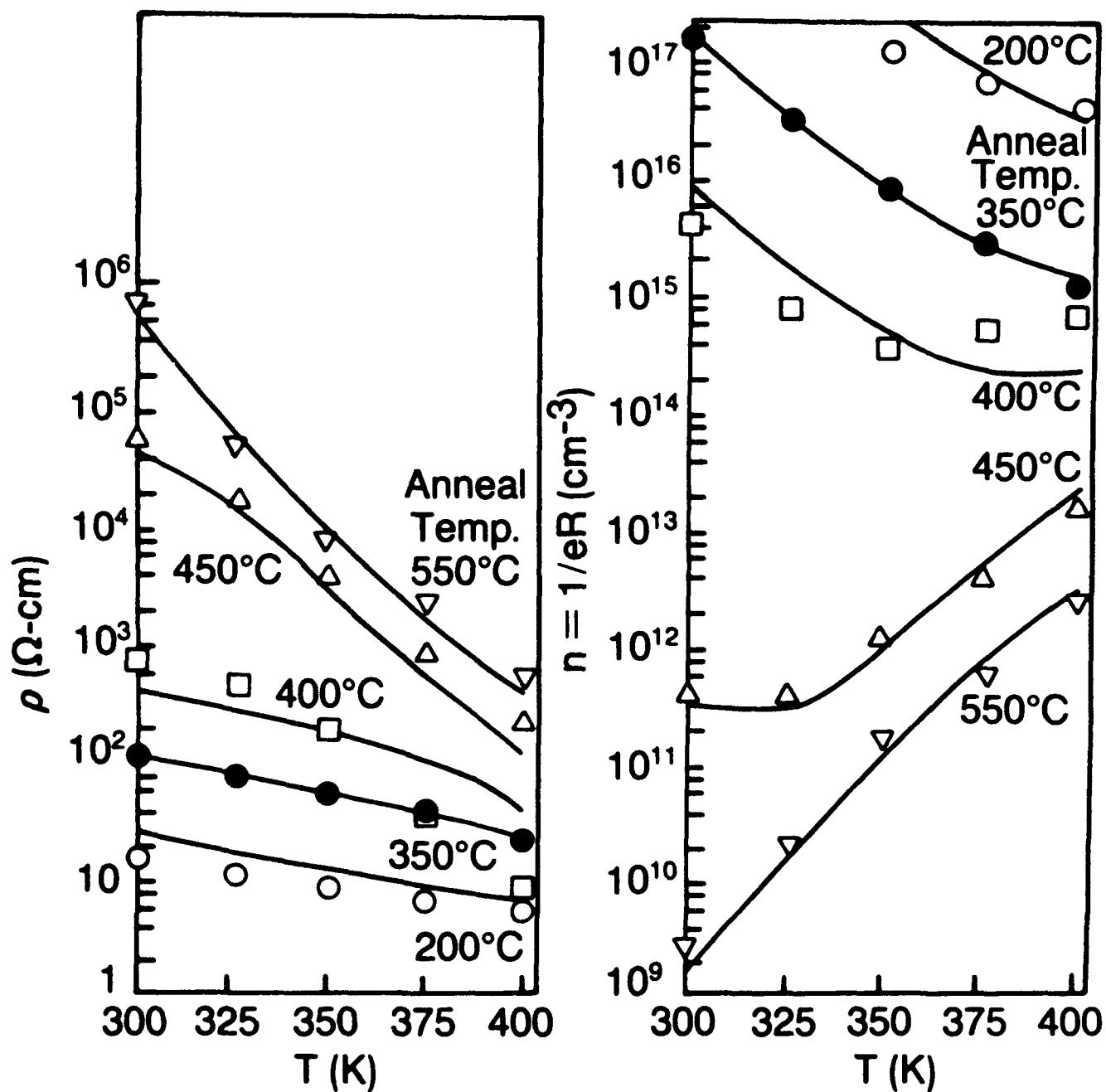


Fig. 4-1. The resistivity  $\rho$  and apparent carrier concentration  $n$  as a function of measurement temperature, for various annealing temperatures. The solid lines are theoretical fits with  $N_D$  as the only fitting parameter.

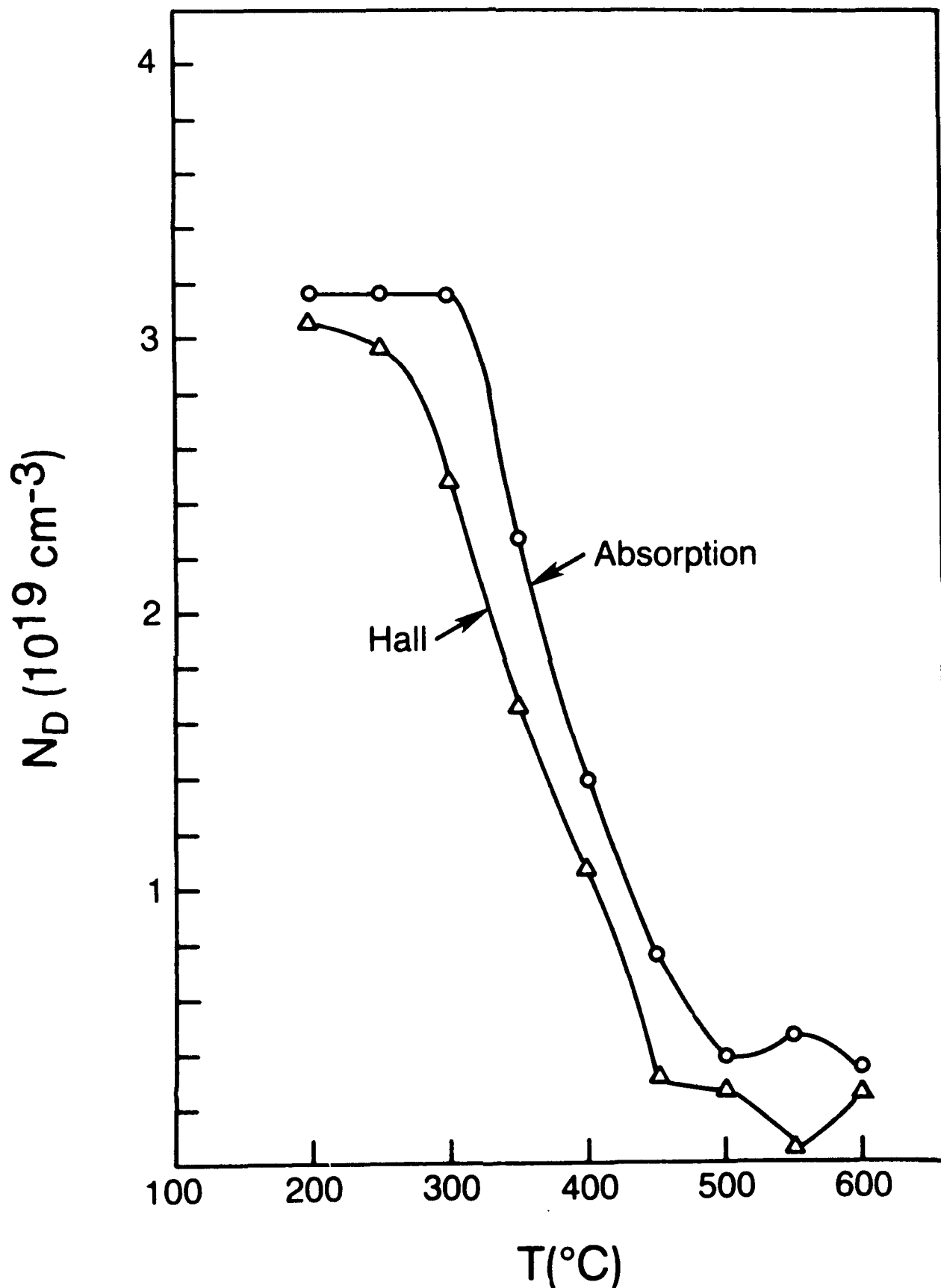


Fig. 4-2. The deep-donor concentration  $N_D$ , calculated separately from Hall-effect and infrared-absorption data, as a function of annealing temperature.

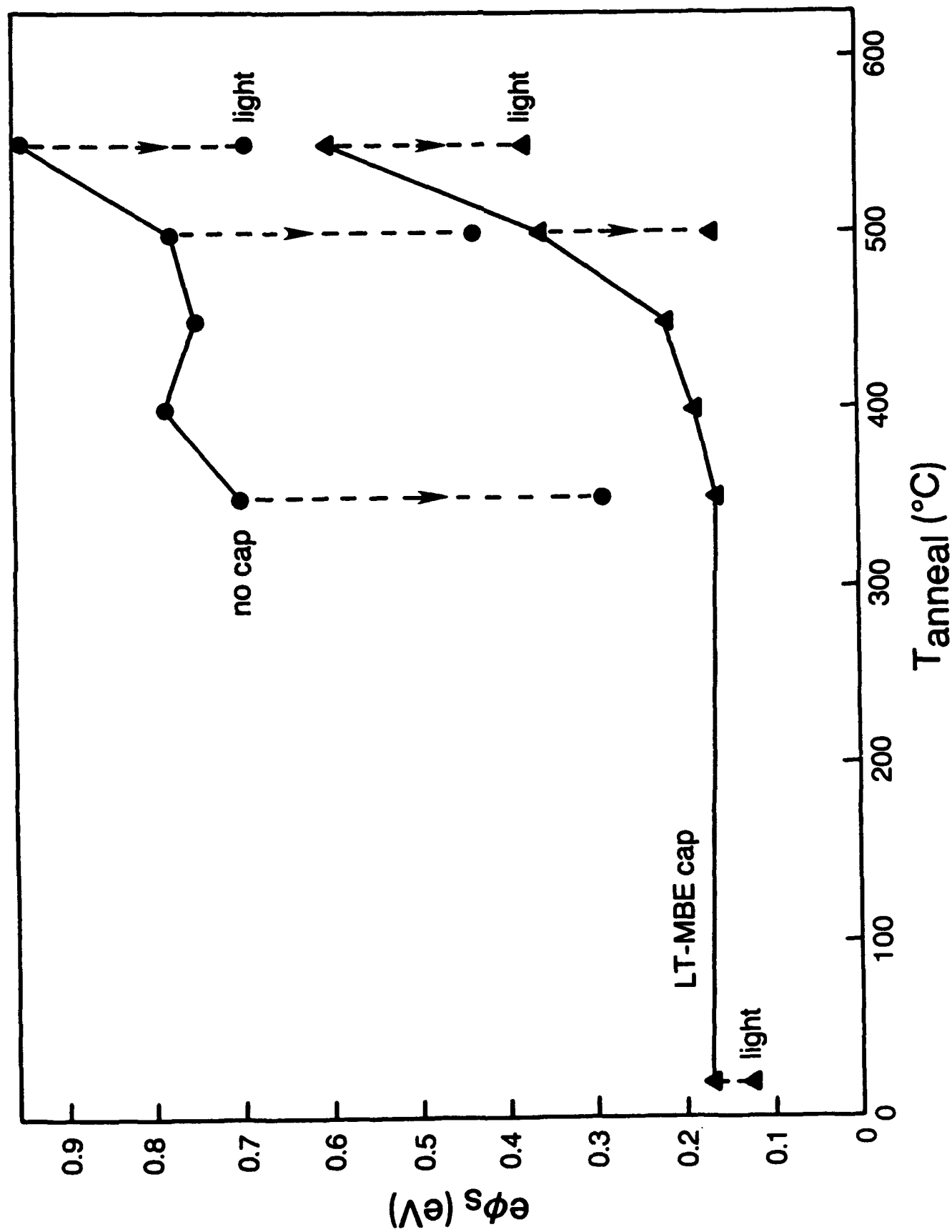


Fig. 4-3. Surface potential energy  $-e\phi_s$ , as a function of annealing temperature for the control and capped samples. Also, the effects of a strong white light are shown.

## 5.0 Alloy Scattering in p-type $\text{Al}_x\text{Ga}_{1-x}\text{As}$

### 5.1 Introduction

Hall-effect measurements constitute one of the most useful and effective ways to assess the quality of semiconductor materials, with the Hall mobility being a widely used figure of merit. Mobility data are especially useful when they can be compared with theory, allowing parameters such as impurity concentrations to be extracted. Such theory is well developed for simple systems which involve carriers in only a single, spherical band, such as for electrons in GaAs.<sup>34</sup> For holes in such semiconductors, on the other hand, the situation is usually much more complex because of degenerate valence bands.<sup>35</sup> A further complexity is added when alloys, such as  $\text{Al}_x\text{Ga}_{1-x}\text{As}$ , are considered because of electron or hole scattering from the alloy potential.<sup>36-38</sup> Alloy scattering is relatively weak for carriers with small effective masses, but can be strong for heavy carriers. Thus, it is very important to include alloy scattering when calculating hole mobilities in  $\text{Al}_x\text{Ga}_{1-x}\text{As}$ .<sup>39-41</sup> Such a calculation was carried out by Masu et al.<sup>41</sup> several years ago, and was compared with hole-mobility data in Be-doped  $\text{Al}_x\text{Ga}_{1-x}\text{As}$ . However, we have carried out a more accurate calculation, and also have obtained a more complete set of data, with  $x$  ranging from 0 to 1. Our fit of data and theory is excellent and an improved value of the alloy scattering potential is obtained.<sup>42</sup>

### 5.2 Theory and Results

The theory includes separate scattering calculations for the heavy- and light-hole bands, by direct solutions of the Boltzmann equation, and then proper mixing of the two bands to get the conductivity and Hall coefficient. Alloy parameters, such as effective masses and dielectric constants, were obtained from several sources,<sup>43</sup> including some of our results. The theoretical results for GaAs, AlAs, and  $\text{Al}_{0.5}\text{Ga}_{0.5}\text{As}$  are shown in Fig. 5-1. An alloy scattering potential of 0.53 eV, as found from the fit in Fig. 5-2, was used for the  $\text{Al}_{0.5}\text{Ga}_{0.5}\text{As}$  curve. Several conclusions may be drawn from Figs. 5-1 and 5-2: (1) alloy

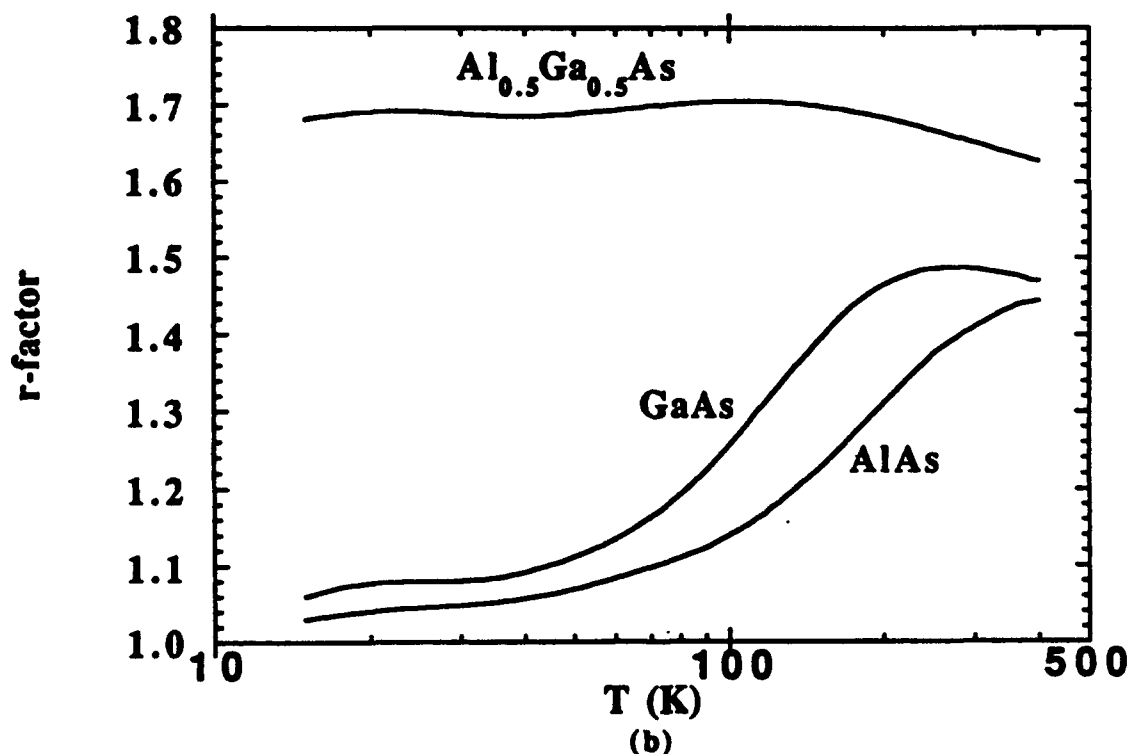
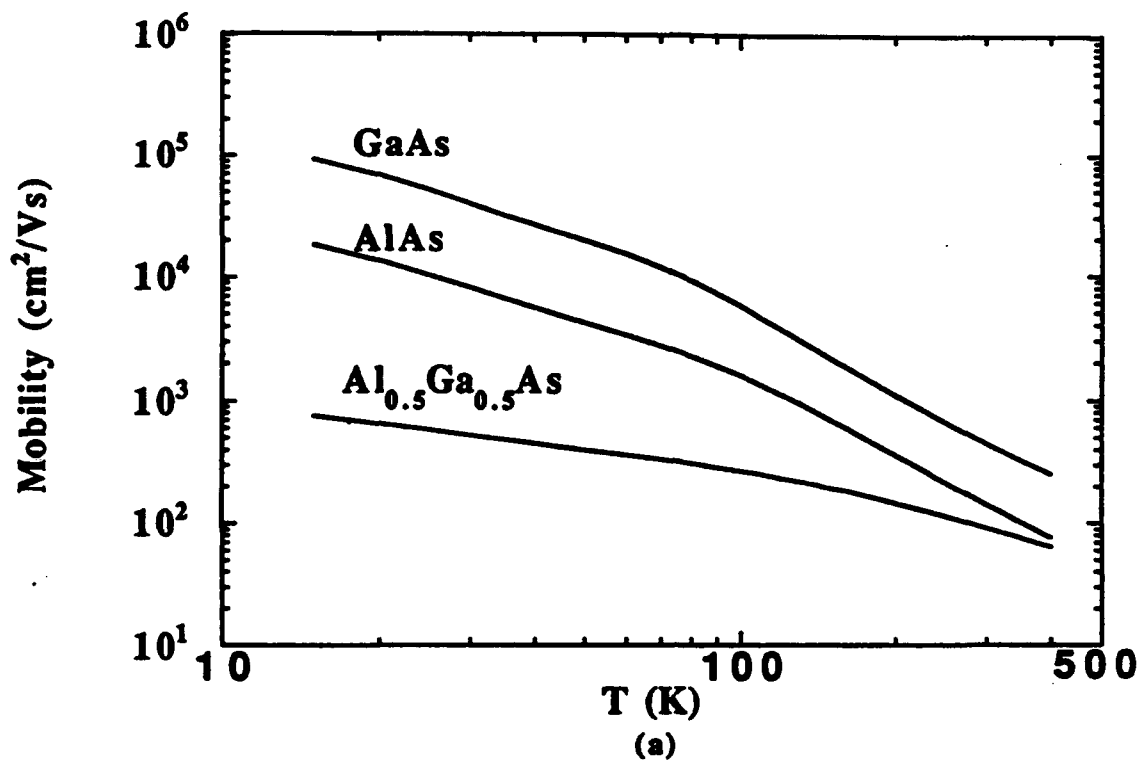


Fig. 5-1. A comparison of the theoretical Hall mobilities for relatively pure p-type samples of GaAs, AlAs, and  $\text{Al}_{0.5}\text{Ga}_{0.5}\text{As}$  ( $N_A = 6.5 \times 10^{13} \text{ cm}^{-3}$ ,  $N_D = 2.5 \times 10^{12} \text{ cm}^{-3}$ , and  $E_A = 0.025 \text{ eV}$ , for each); (b) the Hall  $r$  factors for these same samples.

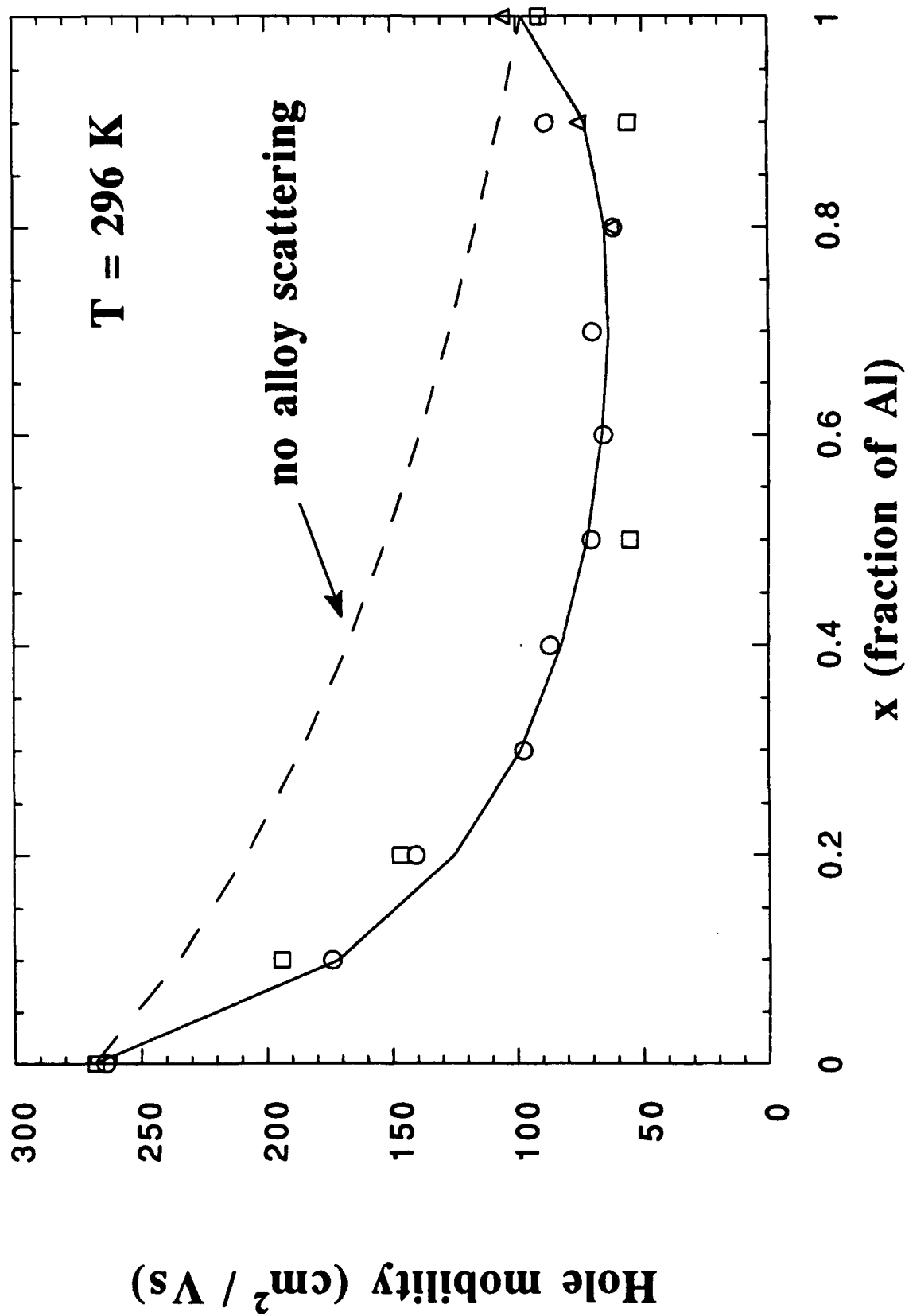


Fig. 5-2. The experimental (circles, squares, and triangles) and theoretical (solid line) Hall mobility as a function of  $x$  for p-type  $\text{Al}_x\text{Ga}_{1-x}\text{As}$ . Also shown is the case of no alloy scattering (dashed line).

scattering is very important in p-type  $\text{Al}_x\text{Ga}_{1-x}\text{As}$ , even near the end points ( $x < 0.2$  or  $x > 0.8$ ); (2) the effect on mobility is amplified at low temperatures (Fig. 5-1a); and (3) the Hall  $r$ -factor is quite high ( $\sim 1.7$ ), but nearly temperature-independent for  $\text{Al}_{0.5}\text{Ga}_{0.5}\text{As}$ . The last conclusion suggests that the usual assumption of  $r = 1$  is dangerous in p-type  $\text{Al}_{0.5}\text{Ga}_{0.5}\text{As}$ , but that at least the determination of acceptor activation energies from  $T$ -dependent Hall measurements would be accurate, since  $r$  is only a weak function of  $T$ .

## 6.0 Optical Properties of Bulk Materials

### 6.1 Pressure Effects on the Intrinsic Acceptor $\text{Ga}_{\text{As}}$ in Uncompensated GaAs<sup>44</sup>

The photoluminescence of  $\text{Si}_{\text{As}}$  and gallium antisite  $\text{Ga}_{\text{As}}$  related emissions of Si-doped p-type GaAs have been measured as a function of hydrostatic pressure using a diamond anvil cell. The  $\text{Ga}_{\text{As}}$  related emissions have energies of  $\sim 1.32$  and  $1.44$  eV at 2 K and are due to the donor-acceptor pair transitions. The pressure coefficients of the binding energy of acceptors responsible for the two transitions are  $0.2\text{--}0.3$  meV/kbar in the direct gap  $\Gamma_{1c}\text{--}\Gamma_{15v}$  region. At pressures larger than the  $\Gamma_{1c}\text{--}X_{1c}$  crossover, the emission intensity of the  $1.44$  eV emission decreases drastically and the half-width of the emission increases considerably due to the transfer of electron from the  $\Gamma_{1c}$  minimum to the  $X_{1c}$  minimum. Fig. 6-1 shows the pressure vs. transition energy relation.

### 6.2 Pressure Effects on $\text{Ga}_{\text{As}}$ for Compensated p-type GaAs<sup>45</sup>

Photoluminescence is used to study the behavior of  $\text{C}_{\text{As}}$ -related and  $\text{Ga}_{\text{As}}$  cation antisite defect center in GaAs under hydrostatic pressure at 10 K. The pressure coefficients,  $\alpha$ , for these transitions were determined. We found  $\alpha(\text{C}_{\text{As}})$  to be about  $12$  meV/kbar which is very close to the band edge pressure dependence. The  $\text{Ga}_{\text{As}}$  center demonstrated only slightly smaller coefficient. This makes the binding energy of  $\text{C}_{\text{As}}$  and  $\text{Ga}_{\text{As}}$ , at  $26$  and  $77$  meV, respectively, almost independent of pressure. At pressures above  $30$  kbar relatively strong transitions were observed that displayed very small pressure dependence. The deepening of the  $\Gamma\text{X}$ -mixed donor levels interacting with these acceptor levels is primarily responsible for small pressure coefficients of the transitions above  $30$  kbar. A deepening of  $\sim 160$  meV is observed for the donors. Fig. 6-2 shows the variation of PL spectrum under pressure.

### 6.3 Photoluminescence of the $\text{Ga}_{\text{As}}$ -Related $1.32$ eV Emission in Bulk GaAs<sup>46</sup>

A detailed study of the  $1.32$  eV photoluminescence emission present in p-type GaAs was made at various temperatures and excitation intensities in conjunction with the



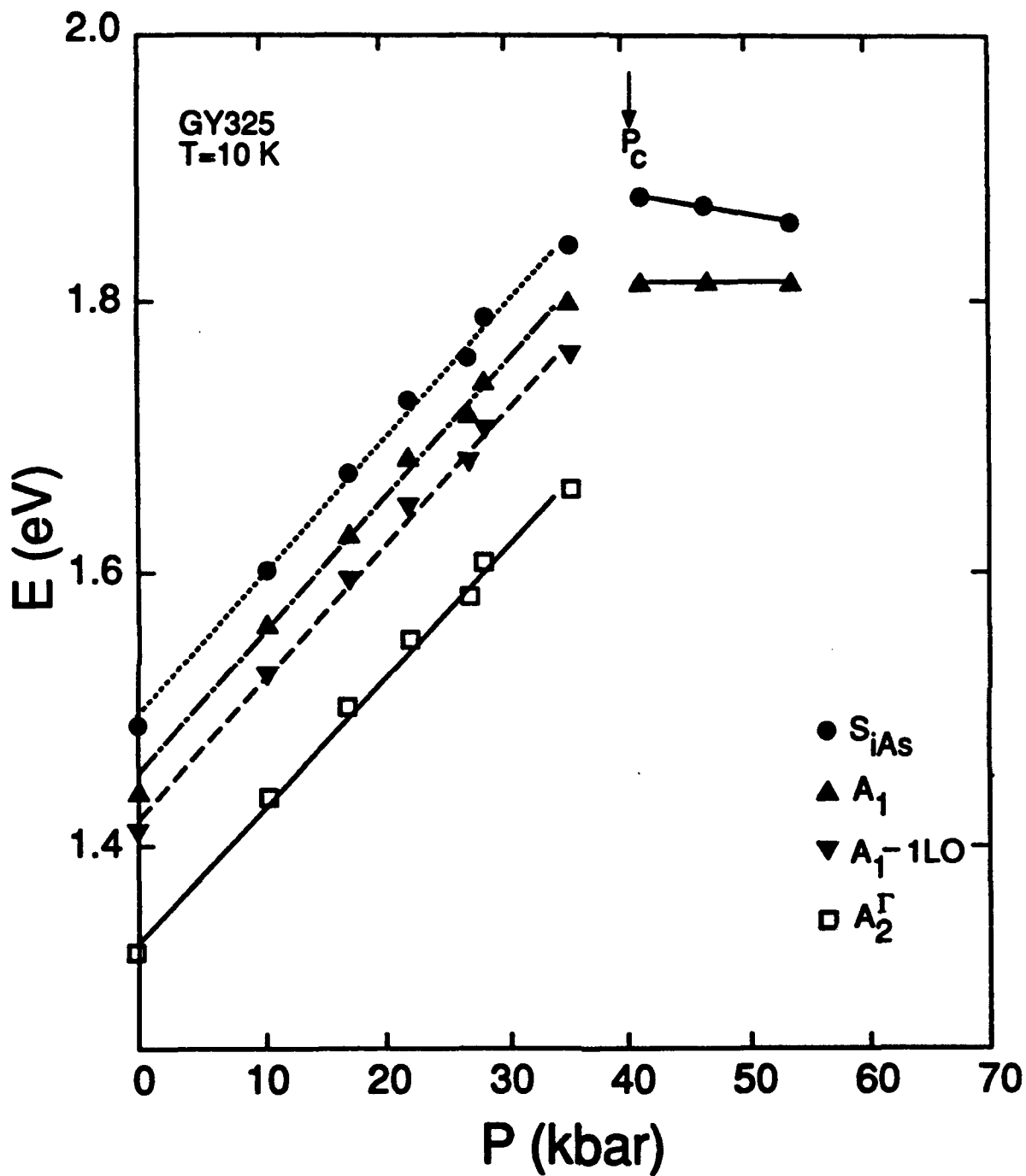


Fig. 6-1. Pressure vs. transition energy relation for compensated p-type GaAs.  $A_1$  and  $A_2$  are, respectively, due to the first level of  $Ga_{As}$  and  $Ga_{As}-Si_{Ga}$ .

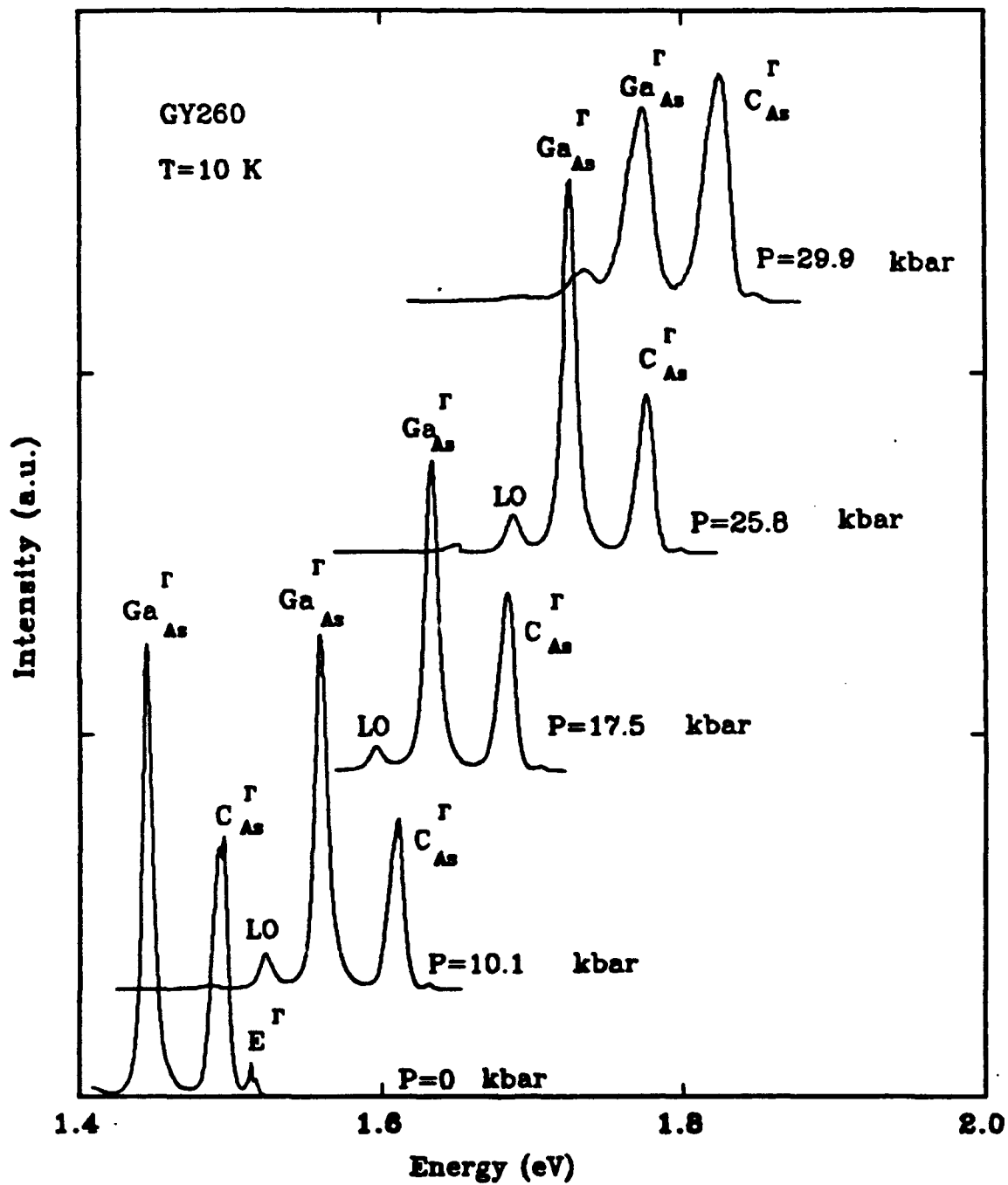


Fig. 6-2. PL spectra under various pressure from 0 to 30 Kbar at 10 K. All the  $\Gamma$ - transitions are due to the defects at the As site.

effects of electron irradiation and infrared absorption measurements. We find that the acceptor responsible for the 1.32 eV emission is not the same as that of the  $\text{Ga}_{\text{As}}^-/\text{Ga}_{\text{As}}^{--}$  transition as commonly believed. It is proposed instead that the acceptor responsible for this luminescence is a gallium antisite double acceptor—effective mass donor pair complex,  $\text{Ga}_{\text{As}}$ —donor. The activation energy of this complex acceptor is determined to be  $\sim 197$  meV. Fig. 6-3 shows a 4.2 K PL spectrum related to  $\text{Ga}_{\text{As}}$ .

#### 6.4 Photoluminescence in Electrically Reversible Bulk GaAs<sup>1,47,48</sup>

A photoluminescence study has been made of electrically reversible, bulk, liquid-encapsulated Czochralski GaAs at temperatures 2–300 K. The reversibility from the semiconducting to the semi-insulating state is made by slow or fast cooling, respectively, following a 5-hour, 950°C heat treatment in an evacuated quartz ampoule. A donor level at  $E_C - 0.13$  eV and two acceptor levels at  $E_V + 0.069$  eV and  $E_V + 0.174$  eV are produced after the heat treatment. Only the acceptor levels were detected by photoluminescence. A tentative model assigning the acceptor to the intrinsic defect pair  $V_{\text{Ga}} - \text{Ga}_{\text{As}}$  is discussed. Fig. 6-4 shows the PL spectrum of a quenched sample.

#### 6.5 Photoluminescence of Indium-Alloyed Semi-insulating GaAs Subjected to Bulk Heat Treatments<sup>49</sup>

A photoluminescence study has been made, at temperatures 2–300 K, on indium-alloyed semi-insulating GaAs subjected to bulk heat treatments. Heat treatments were made by slow and fast cooling following a 15-hour, 950°C soak. Two intrinsic acceptors at  $E_V + 0.069$  eV and  $E_V + 0.17$  eV are produced after heat treatments. The acceptor at  $E_V + 0.069$  eV is attributed to the intrinsic pair defect  $\text{Ga}_{\text{As}} - V_{\text{Ga}}$  and is produced more in the fast-cooled materials than in the slow-cooled materials. The deficiency of intermediate deep donors causes no drastic variation of the electron concentration after the heat treatments. Energy levels in In-alloyed GaAs are shown in Fig. 6-5.

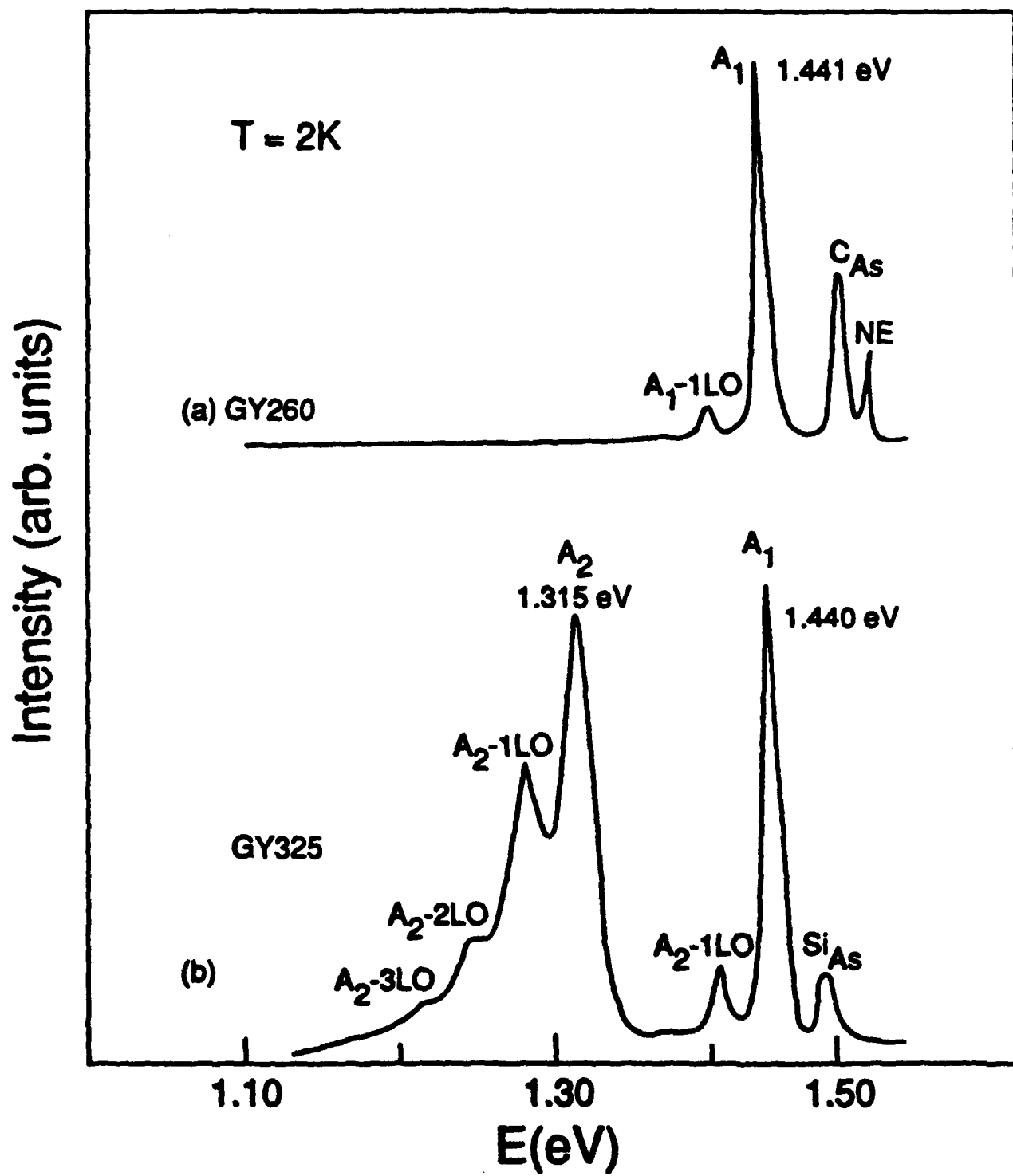


Fig. 6-3. PL spectra from  $Ga_{As}$  center in p-type GaAs.

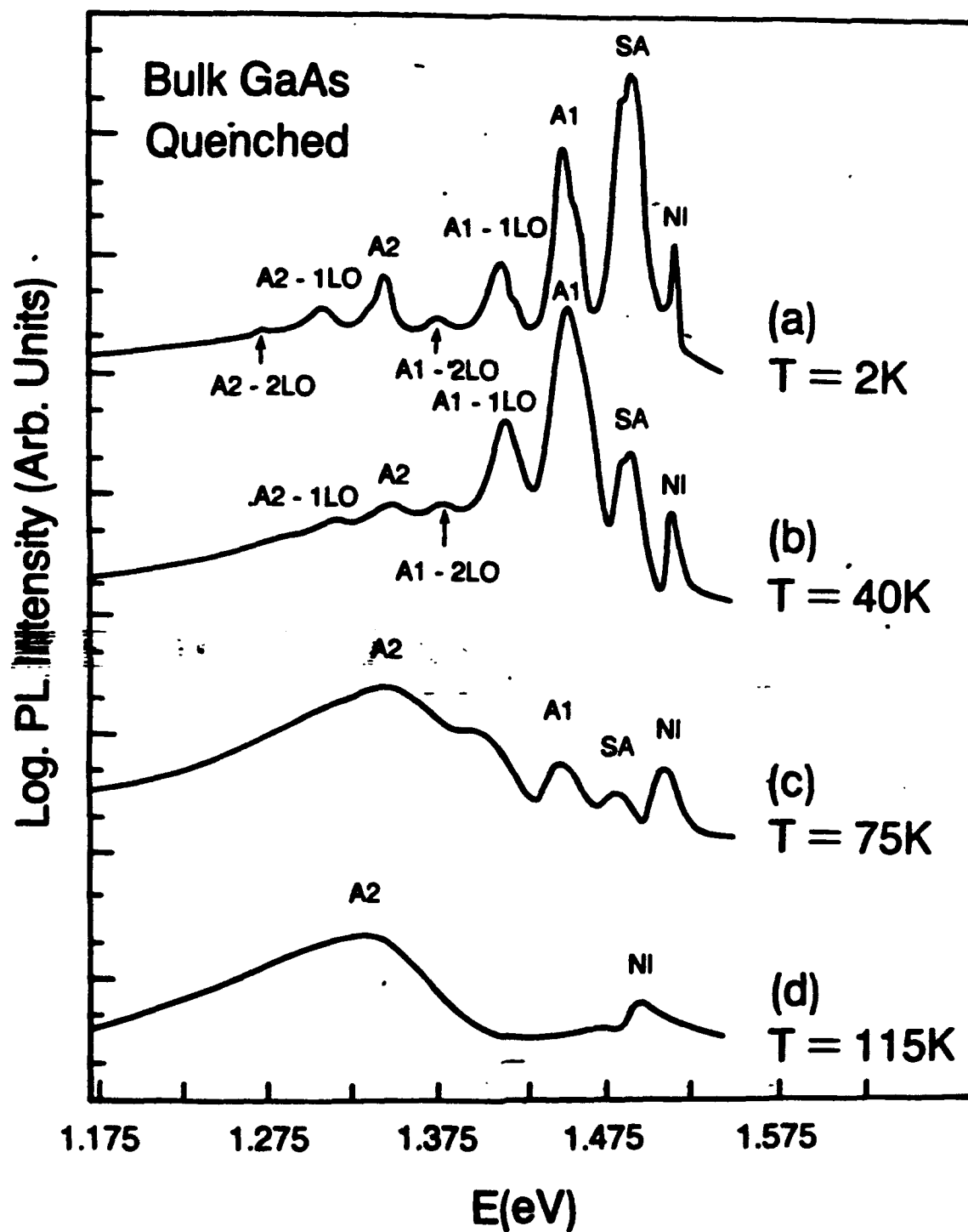


Fig. 6-4. PL of quenched GaAs at various temperatures.

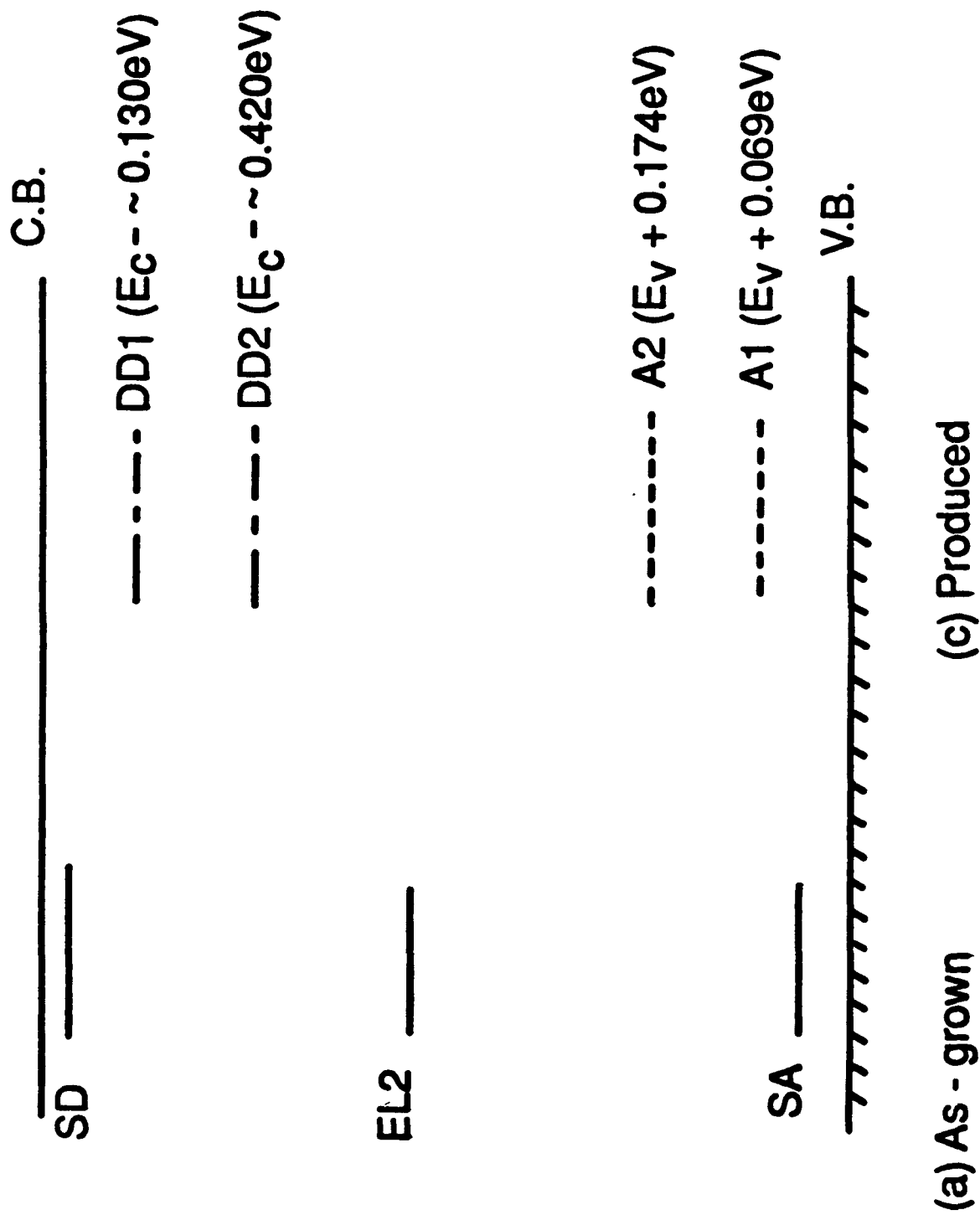


Fig. 6-5. Energy levels in indium-alloyed GaAs.

#### 6.6 Photoluminescence and Photoluminescence Excitation of the 0.635 eV ELO Emission in Oxygen-Doped Semi-insulating GaAs<sup>50</sup>

The 0.635-eV photoluminescence emission present in oxygen-doped semi-insulating GaAs was studied with respect to temperature variation and photoluminescence excitation. The photoluminescence characteristics of the 0.635-eV emission are distinctly different compared to those of 0.68-eV EL2 emission. The radiative mechanism is explained well by the configuration coordinate model, which involves a complex center involving the deep oxygen donor on an arsenic site and a gallium vacancy as a nearest neighbor. The Frank-Condon shift and vibration energy of the excited state of the center were determined to be 0.16 and 0.025 eV, respectively. Fig. 6-6 shows the variation of the half-width of the ELO band with temperature.

#### 6.7 Observation of a Difference in the Quenching of the Photocurrent in GaAs Containing EL2 and ELO<sup>51,52</sup>

An anomalous reduction in the photoquenching efficiency at 80 K has been observed in some semi-insulating GaAs samples during illumination with 1.1 eV light. The effect has been observed in photocurrent and infrared-absorption quenching experiments. Photoluminescence experiments on normal and anomalous samples indicate that the effects are produced by the presence of oxygen as indicated by the photoluminescence emission from the oxygen-related deep donor ELO. Oxygen was found to produce a photoassisted thermal-recovery effect with 1.1 eV light that competes with the EL2 photoquenching effect. No infrared absorption was found that could be attributed directly to ELO. In contrast, the photocurrent was found to be dominated by photoionization of ELO rather than EL2, and the anomalous effect is attributed to the reduced photoquenching temperature of ELO. Fig. 6-7 shows two different photoquenching spectra.

The quenching of the photocurrent and photo-Hall effect of several undoped semi-insulating gallium arsenide samples has been measured and compared with the

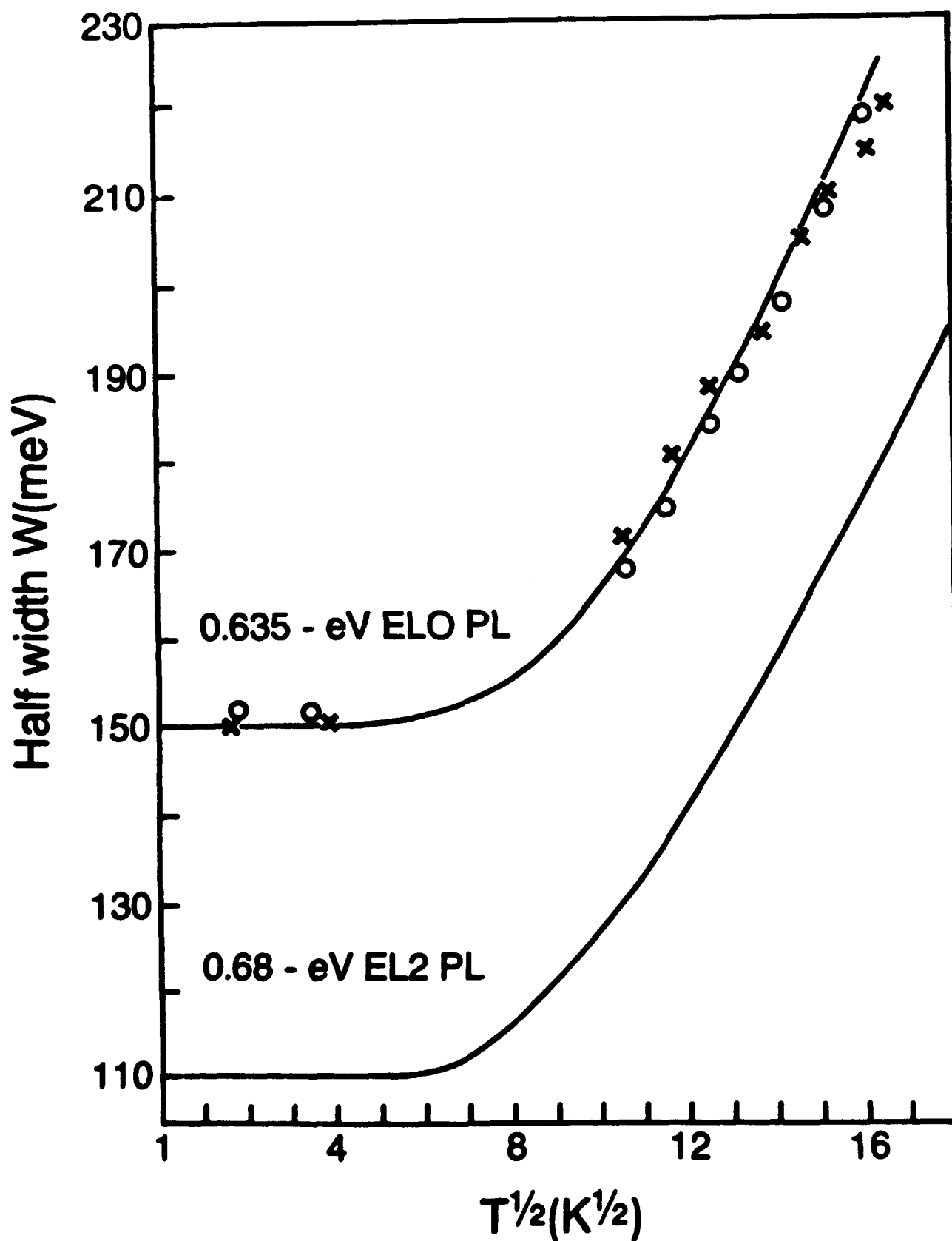


Fig. 6-6. The variation of half-width of ELO emission with temperature.



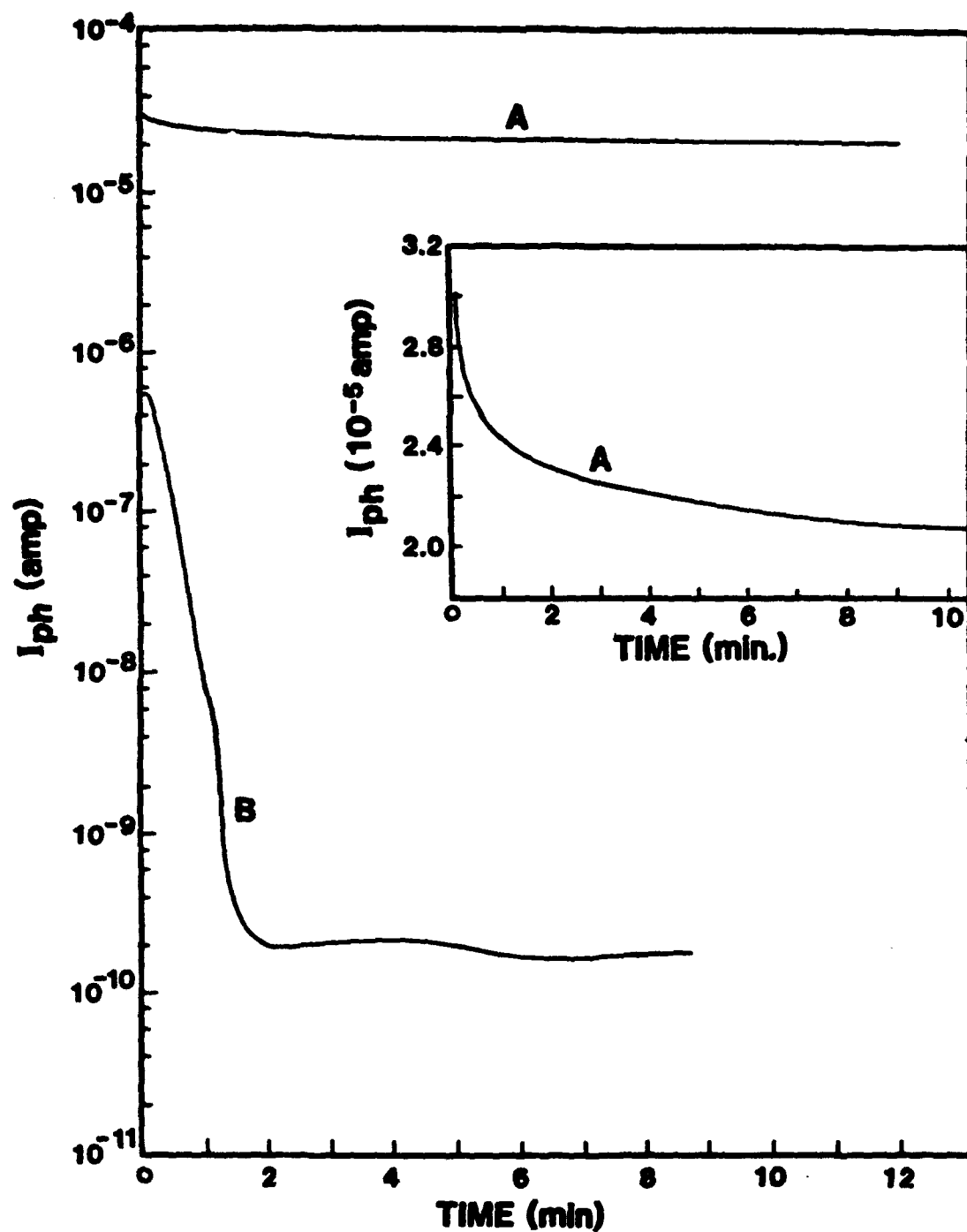


Fig. 6-7. Two different photo quenching spectra.

deep-level photoluminescence spectra from neighboring samples. Samples that show either EL2 (0.68 eV) or ELO (0.63 eV) photoluminescence have distinctly different photocurrent quenching behaviors. EL2 samples show a photocurrent decrease of several orders of magnitude, and a change from n-type to p-type conduction during quenching at 80 K with 1.1 eV light. ELO samples show a reduction in photocurrent of less than an order of magnitude with no change in the carrier type at this temperature. Photo-Hall effect experiments at 80 K indicate that the conduction is n-type for the ELO samples, but changes from n- to p-type during the quench for the EL2 samples. The temperature dependence of the quenching has also been studied. EL2 samples show little variation in the range 10–80 K, while ELO samples show significant quenching similar to EL2 after the temperature is reduced below 70 K. These results indicate that defects other than EL2 can significantly affect photocurrent quenching experiments.

#### 6.8 An Antimony Related Electronic Level in Isovalently Doped Bulk GaAs<sup>53,54</sup>

Temperature-dependent Hall-effect and photoluminescence measurements have been performed on a series of antimony-doped bulk GaAs samples that were otherwise undoped. A new donor level located 0.48 eV below the conduction-band edge has been detected by both experiments in all antimony-doped samples studied. This level reduces the resistivity of antimony-doped material below the semi-insulating limit. Comparisons with known intrinsic levels in undoped material have been made and it is shown that the 0.48-eV donor is distinct from any of these. It is concluded that the defect responsible for the 0.48-eV donor involves an impurity antisite  $\text{Sb}_{\text{Ga}}$  either isolated or in a complex with intrinsic defects.

GaAs doped with antimony (Sb) to a level of  $10^{19} \text{ cm}^{-3}$  has been studied by electron paramagnetic resonance (EPR). A new EPR spectrum has been discovered which is identified as the  $\text{Sb}_{\text{Ga}}$  heteroantisite defect. The electronic structure of this defect is practically identical with that of the intrinsic-anion antisite defects in GaP, GaAs, and InP. The EPR

results show that Sb can be incorporated as an electrically active defect and, therefore, is not a suitable isovalent dopant in the growth of low-dislocation-density semi-insulating GaAs. Fig. 6-8 shows deep-center PL of Sb doped GaAs.

#### 6.9 Photoreflectance Measurements of the Indium Content in Indium-Alloyed Semi-insulating GaAs Substrates<sup>55,56</sup>

Room-temperature photoreflectance measurements were used to determine the radial and axial distribution of low levels of indium in 3-inch-diameter semi-insulating bulk GaAs materials grown by the liquid-encapsulated Czochralski method. These results were compared with 4.2-K photoluminescence data and found to be accurate and more convenient for this application. Room-temperature photoreflectance allows accurate determination of the indium content in the range of 0.1 – 2.0% with standard deviation of 0.03%. Two types of radial inhomogeneity were found in commercially available GaAs wafers. This is discussed in terms of indium segregation and shape of solid and liquid interface during the crystal growth. Fig. 6-9 shows a typical room-temperature PR spectrum.

#### 6.10 Infrared Absorption and Photoluminescence of Defect Levels in the 204 to 205 meV Range in p-type GaAs<sup>57</sup>

Infrared absorption and photoluminescence measurements have been performed on a series of p-type GaAs materials, all of which exhibited the so-called 78-meV double acceptor. Additional details concerning the negative charge state of the acceptor (204-meV level) were obtained. A new infrared absorption spectrum which appears to be due to a level at about 225 meV was found and might be related to the 1.284-eV photoluminescence line. Direct evidence for the existence of the boron antisite defect in as-grown material is shown for the first time but is not the source of the double-acceptor spectra. Fig. 6-10 shows the absorption spectra due to  $\text{Ga}_{\text{As}}^0$  and  $\text{Ga}_{\text{As}}^-$ .

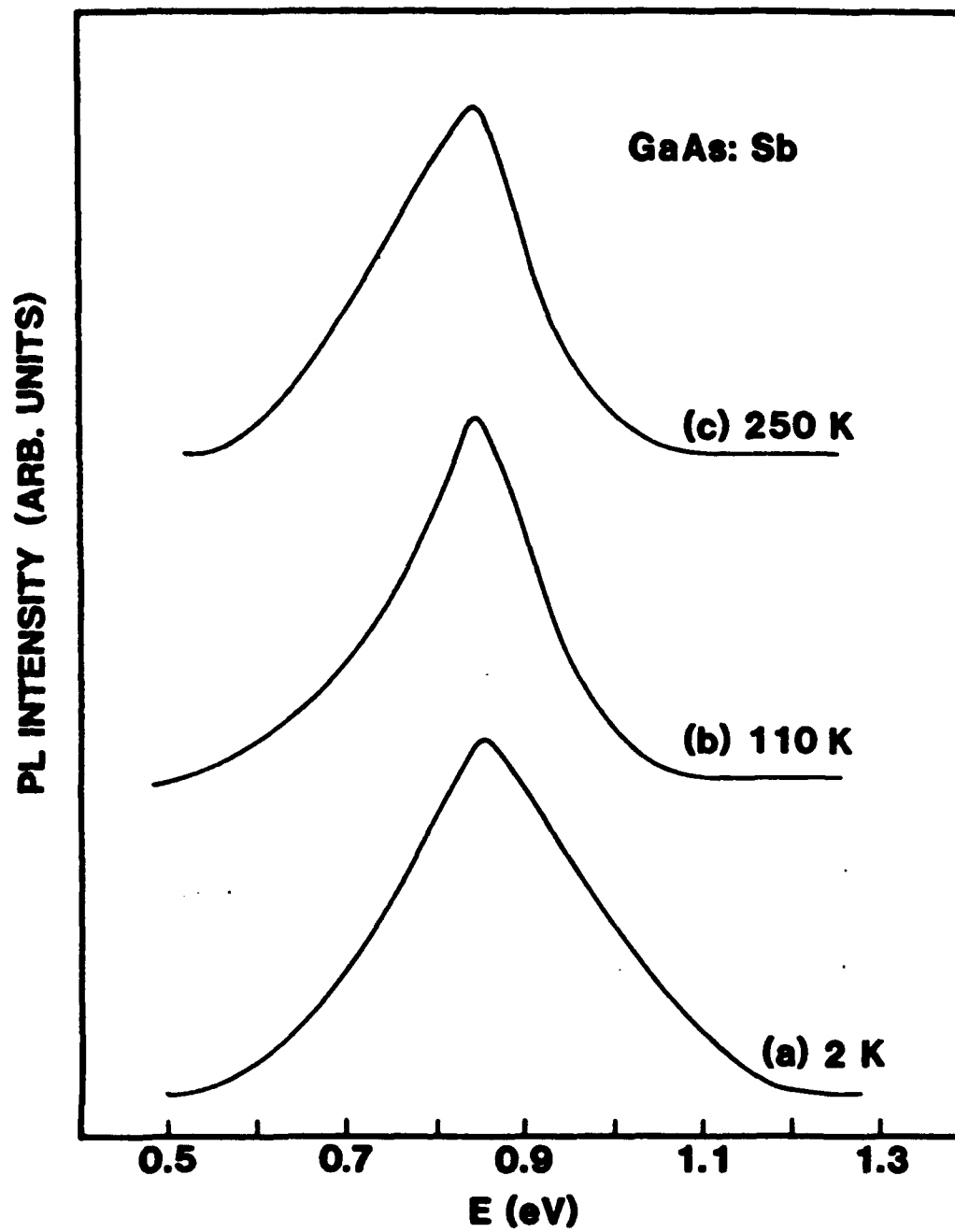


Fig. 6-8. PL of Sb-doped GaAs.

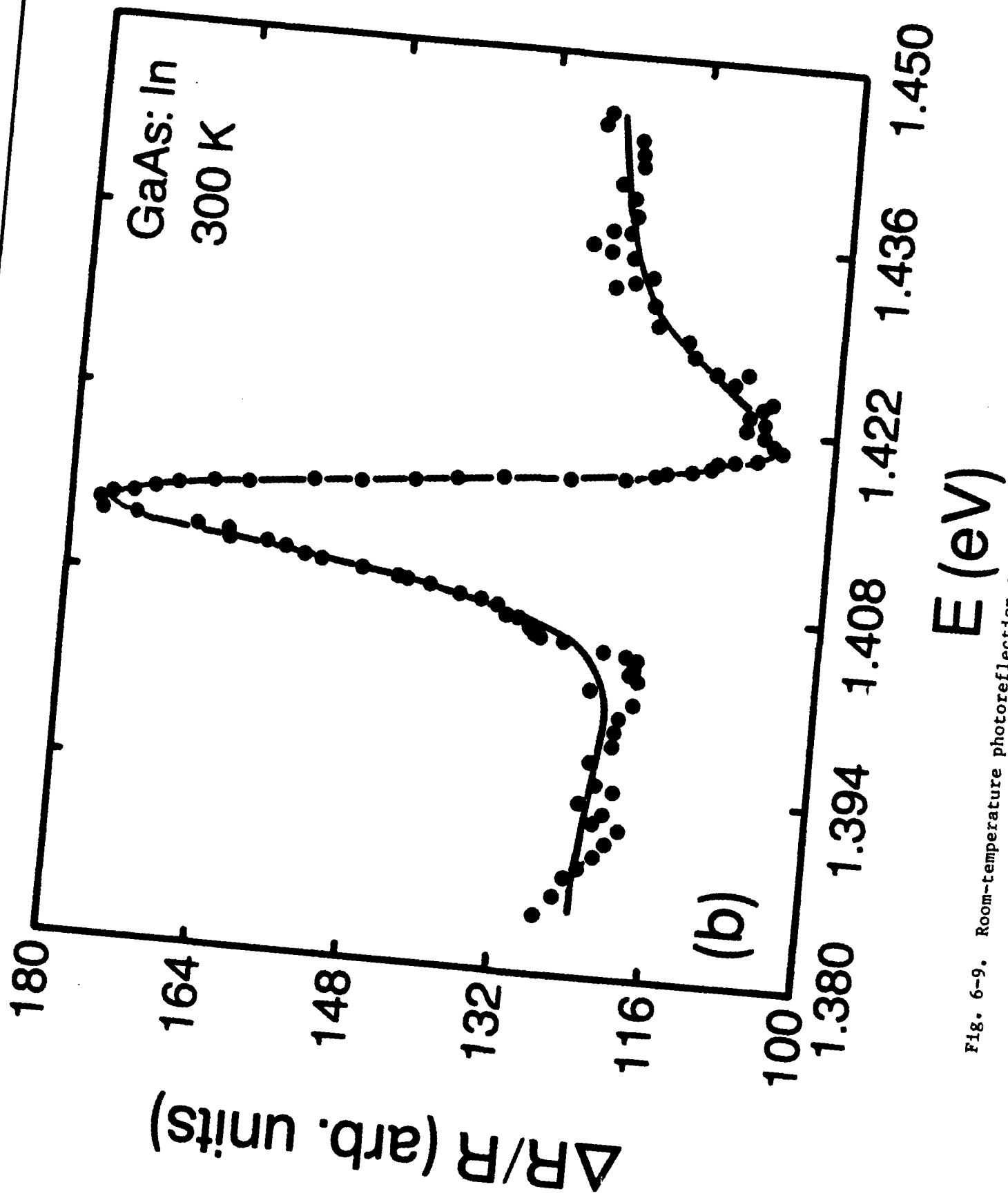


Fig. 6-9. Room-temperature photoreflection spectrum of indium-alloyed GaAs.

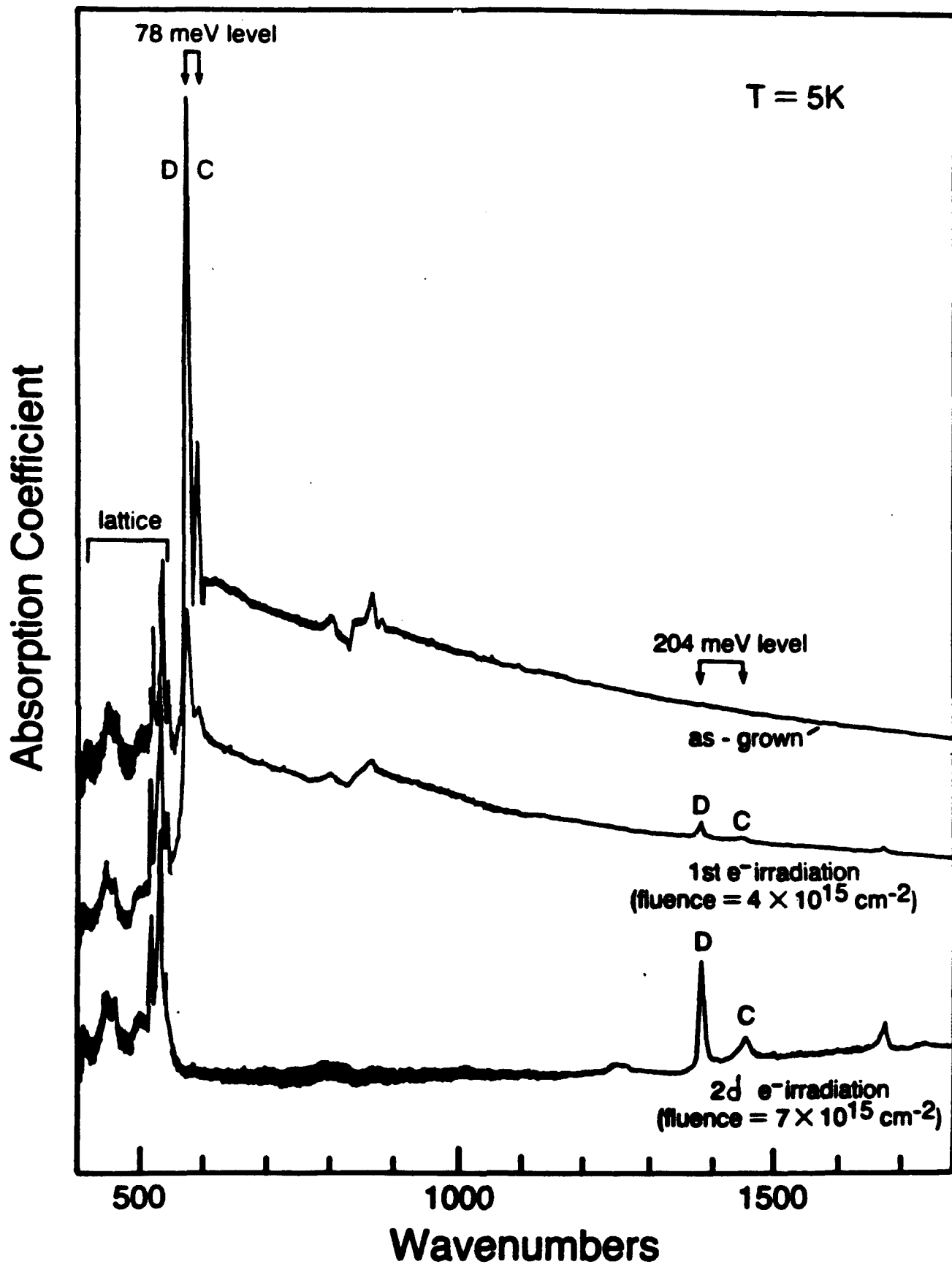


Fig. 6-10.  $\text{GaAs}^0$  and  $\text{GaAs}^-$  absorption spectra.

### 6.11 Characterization of the $\text{Ga}_{\text{As}}$ Spectrum in Undoped p-type GaAs<sup>58</sup>

A detailed study of the dominant double acceptor found in p-type, undoped GaAs grown by the liquid-encapsulated Czochralski technique has been performed using temperature-dependent Hall effect, infrared absorption, spectral photoconductivity, and photoluminescence. Improved fitting techniques are presented for analyzing the temperature-dependent Hall-effect data. A dependence of the activation energy of the neutral state of the double acceptor as determined by Hall effect on the concentration of the defect has been observed and is discussed in terms of prevalent theories. The ionization energy of this level as determined by all three optical techniques is constant and independent of any concentration. Additional data on the correlation between the concentration of the double acceptor and the boron concentration in the material are presented. A model for this correlation is presented that is consistent with the isolated gallium antisite model for the double acceptor. Aluminum and indium alloyed samples were studied and no additional acceptors that could be attributed to these isovalent dopants were discovered. The PC signal due to  $(\text{Ga}^0/\text{Ga}_{\text{As}}^-)$  is seen in Fig. 6-11.

### 6.12 Photoluminescence Determination of Effects Due to In in In-alloyed Semi-insulating GaAs<sup>59</sup>

Photoluminescence measurements at 2 and 2-40 K were made to study effects due to In alloying for  $\text{In}_x\text{Ga}_{1-x}\text{As}$  semi-insulating substrate materials grown by the liquid-encapsulated Czochralski method. The neutral  $\text{C}_{\text{As}}$  bound exciton is a good photoluminescence transition to determine a small variation of In composition in the range of  $0 < x < 0.014$ . The band-gap reduction  $\Delta E_g$  (eV) can be expressed by  $-1.59x$ . The radial nonuniformity of In concentration and photoluminescence intensity were determined. The axial segregation of In was also analyzed with the help of the neutron activation analysis and spark-source mass spectrometry. Fig. 6-12 shows the variation of the energy level due to In in a 3-inch-diameter wafer.

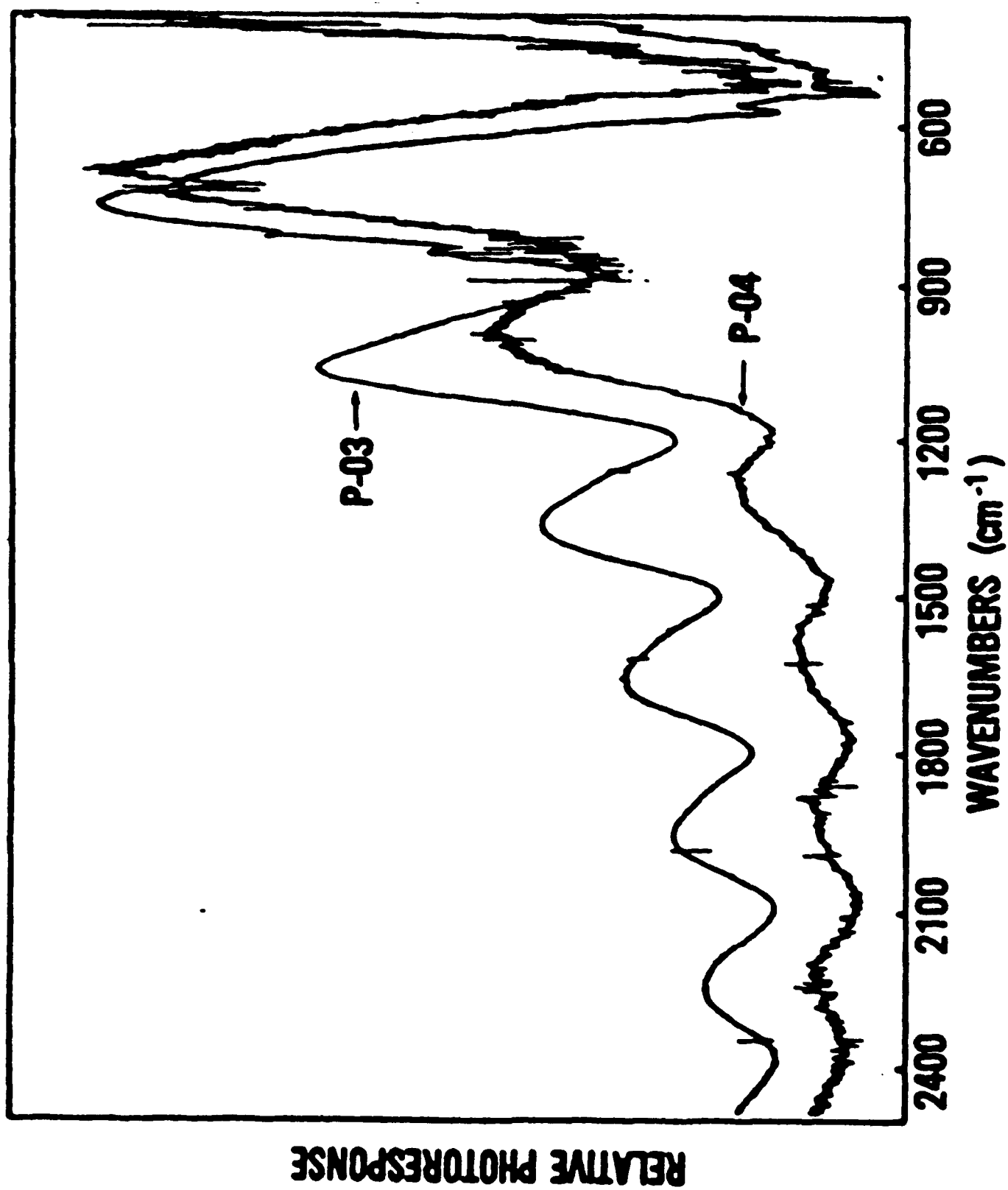


Fig. 6-11. Photoconductivity of  $(\text{GaAs})^0/(\text{GaAs})^-$  transition.



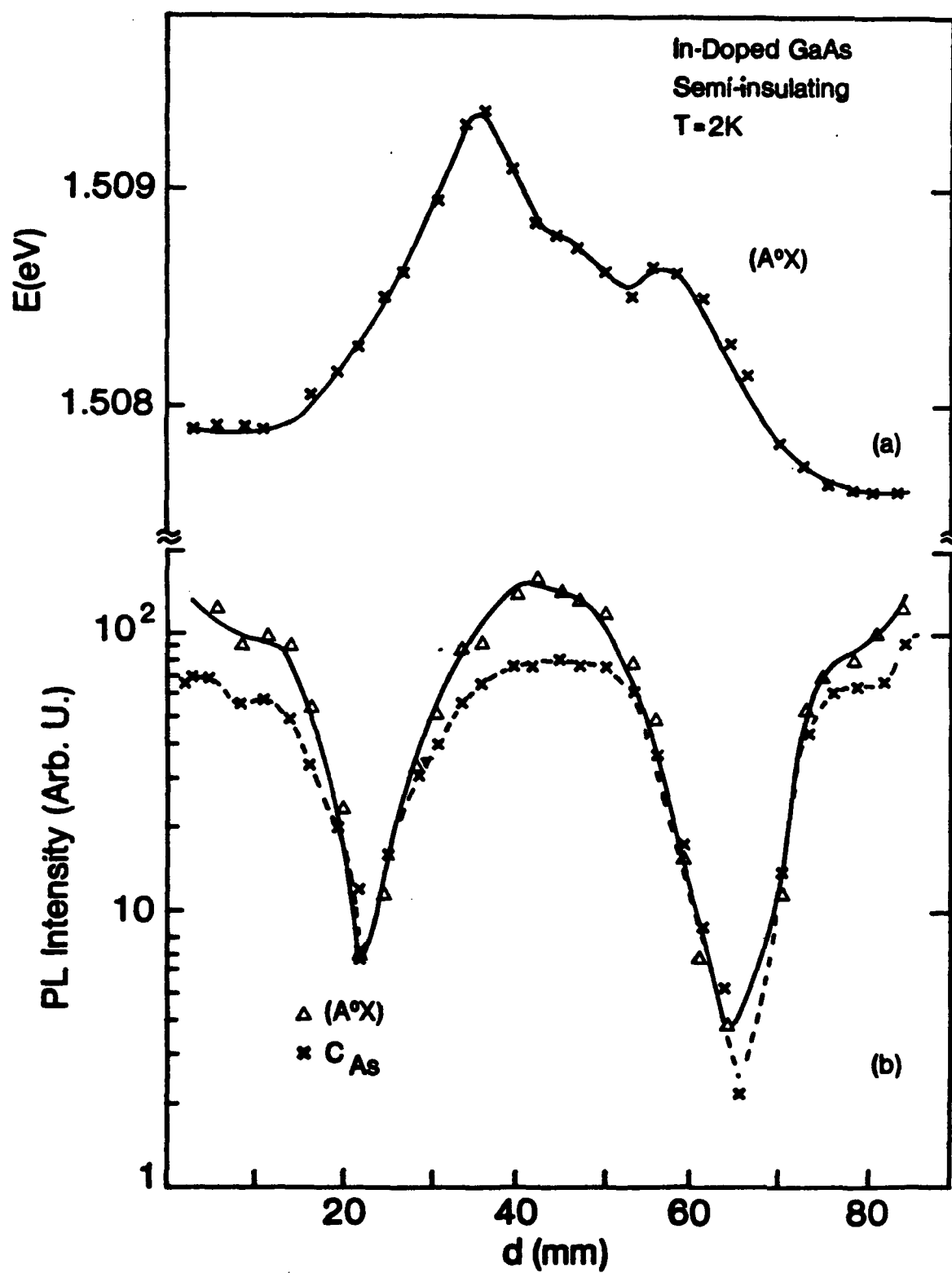


Fig. 6-12. Variation of PL emission in In-alloyed GaAs across a 3-inch diameter wafer.

### 6.13 Thermal Properties of Semi-insulating GaAs Dilutely Alloyed with InAs<sup>60</sup>

The thermal diffusivity, specific heat, and thermal conductivity of  $\text{In}_x\text{Ga}_{1-x}\text{As}$  dilute alloys for  $0 < x < 0.013$  were determined at 25°C. For  $x = 0.005$ , the diffusivity and conductivity are reduced to 60% and 50% of the values for GaAs, respectively. The implications of a reduction in thermal transport due to In alloying are discussed in terms of both crystal growth of dislocation-free GaAs and potential circuit reliability problems associated with lower heat dissipation.

## 7.0 Optical Properties of Epitaxial Materials

### 7.1 Excitonic Photoluminescence Linewidths in AlGaAs Grown by Molecular Beam Epitaxy<sup>61</sup>

The linewidths of excitonic transitions were measured in  $\text{Al}_x\text{Ga}_{1-x}\text{As}$ , grown by molecular beam epitaxy as a function of alloy composition  $x$  for values of  $x \lesssim 0.43$  using high resolution photoluminescence spectroscopy at liquid helium temperature. The values of the linewidths thus measured are compared with the results of several theoretical calculations in which the dominant broadening mechanism is assumed to be the statistical potential fluctuations caused by the components of the alloy. An increase in the linewidth as a function of  $x$  is observed which is in essential agreement with the prediction of the various theoretical calculations. The linewidths of the excitonic transitions in  $\text{Al}_x\text{Ga}_{1-x}\text{As}$  observed in the present work are the narrowest ever reported in the literature, for example  $\sigma = 2.1$  meV for  $x = 0.36$ , thus indicating very high quality material. Fig. 7-1 shows the line variation dependence on  $x$ .

### 7.2 Magnetic Field Splitting of the Emission Lines in the 1.5040- to 1.5110-eV Range.<sup>62</sup>

The magnetic field splitting and strain splitting of the emission lines in the 1.5040- to 1.5110-eV range in GaAs are reported. In the Voigt configuration the lines show doublet splittings in applied magnetic fields. In combined magnetic and strain fields four lines are observed in this configuration. All of the lines show a similar splitting. The splittings agree with what would be expected for shallow donor-acceptor pair centers in a zinc-blende structure. The temperature variation of the emissions is shown in Fig. 7-2.

### 7.3 Low-Pressure $\text{AsH}_3$ Cracking Cells in Gas Source MBE Growth of GaAs and AlGaAs<sup>63</sup>

MBE growth of GaAs and AlGaAs layers with good surface morphology and reasonably good PL spectral response has been achieved using two versions of a low-pressure,

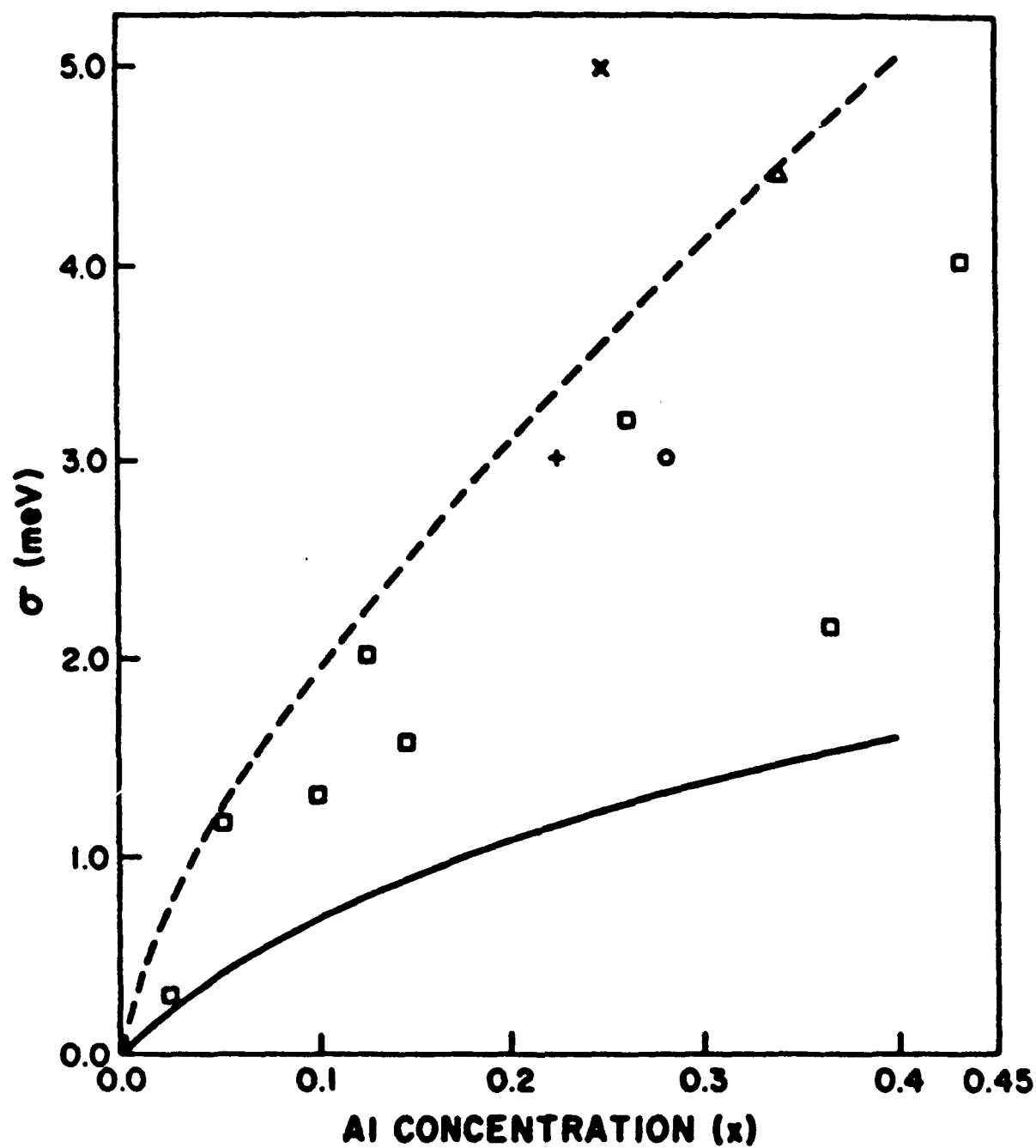


Fig. 7-1. AlGaAs excitonic linewidth vs. Al concentration.

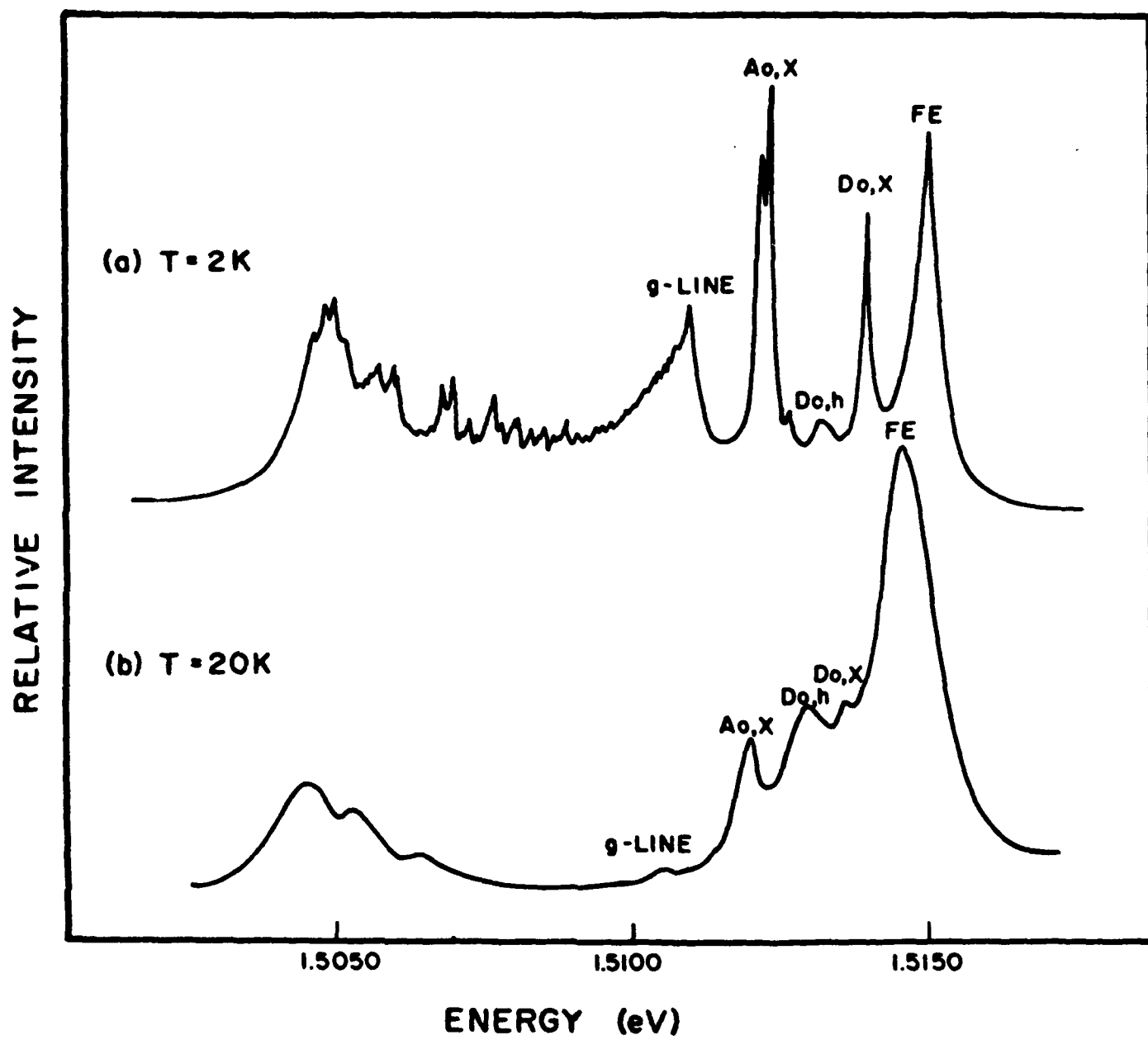


Fig. 7-2. Variation of the lines at 1.5040- to 1.5110-eV range.

Calawa-type  $\text{AsH}_3$  cracker (long-quartz-tube containing a filamentary Ta catalyst) which produced predominantly  $\text{As}_4$  and  $\text{As}_2$  and smaller concentrations of  $\text{As}_1$  for the MBE growth. Quadruple mass analyzer measurements of the cracking patterns and the  $\text{As}_4$ ,  $\text{As}_2$ , and  $\text{As}_1$  molecular species produced by the gas cracking furnaces are also reported. Fig. 7-3 shows the dependence of the AlGaAs PL on growth parameters.

#### 7.4 Quasi-Donor-Acceptor Pair in GaInAs/InP<sup>64</sup>

The low-temperature properties of the excitation-dependent photoluminescence emission, in nominally undoped n-type  $\text{Ga}_x\text{In}_{1-x}\text{As}$  ( $0.44 < x < 0.48$ ) layers grown on InP by molecular beam epitaxy, are investigated with changes of temperature and excitation intensity. The excitation-dependent emission is attributed to the quasi-donor-acceptor pair transition in impure compensated crystals. The random impurity potential arising from residual impurities causes a larger energy shift than expected for the usual donor-acceptor pair transitions. Fig. 7-4 shows the excitation dependence of the transition energy.

#### 7.5 Photoluminescence from Carriers Confined at a GaInAs/InP Interface<sup>65</sup>

The low-temperature properties of the interface photoluminescence emission in  $\text{Ga}_x\text{In}_{1-x}\text{As}$ -InP single heterojunctions grown by molecular beam epitaxy are investigated with changes of temperature and excitation intensity at different depths across the interface. The emission energy shifts to higher energy with increasing excitation intensity and lies between the three-dimensional  $\text{Ga}_x\text{In}_{1-x}\text{As}$ -InP near-band-edge exciton and the quasi-donor-acceptor pair transition. The new emission is attributed to the interface exciton which is indirect in real space. Fig. 7-5 shows the different energy variations depending on the type of PL emission.

#### 7.6 Mass-Spectroscopic Determination of Sb Incorporation During III-V Molecular Beam Epitaxy<sup>66</sup>

The antimony incorporation rate  $\alpha$  (Sb) during molecular-beam epitaxy (MBE) of  $\text{GaAs}_{1-y}\text{Sb}_y$ ,  $\text{AlAs}_{1-y}\text{Sb}_y$ , and  $\text{Al}_{0.5}\text{Ga}_{0.5}\text{As}_{1-x}\text{Sb}_y$  is determined as a function of growth

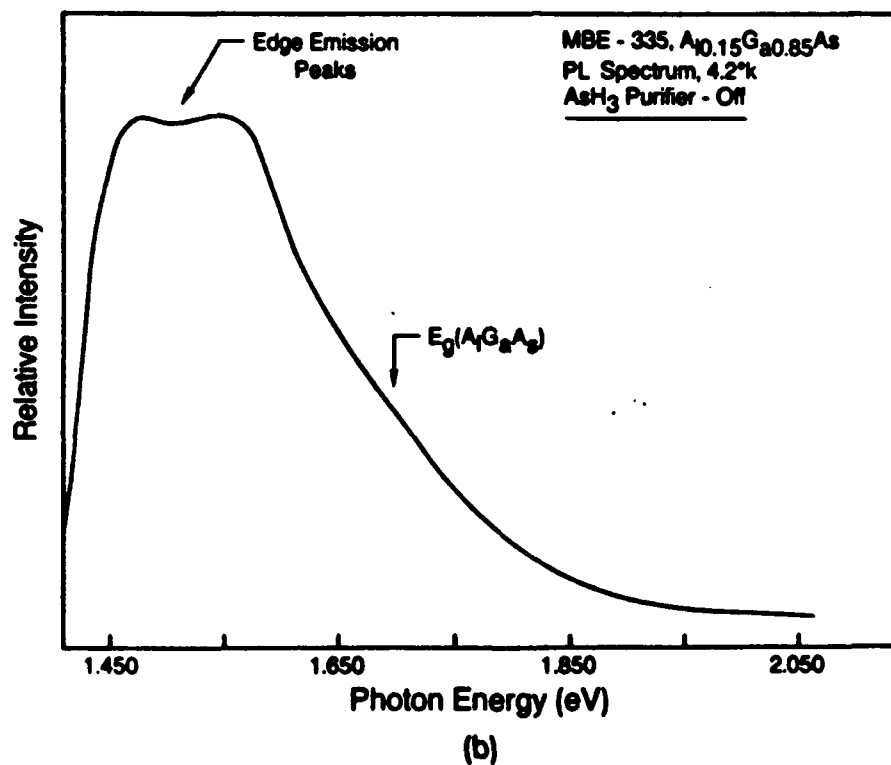
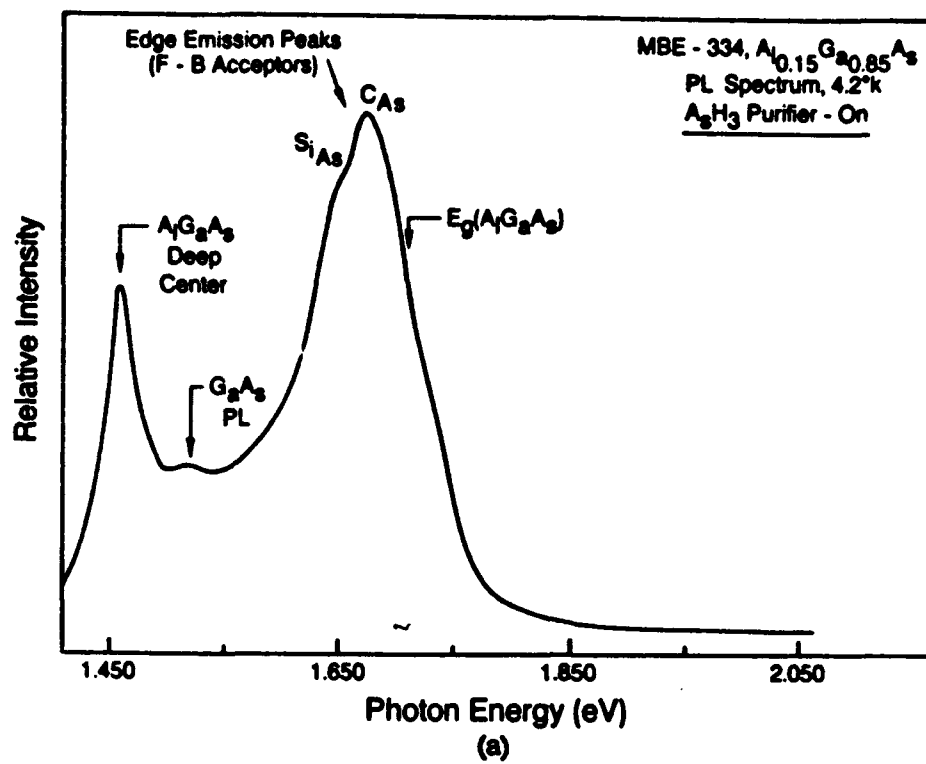


Fig. 7-3. PL of AlGaAs with different growth conditions.

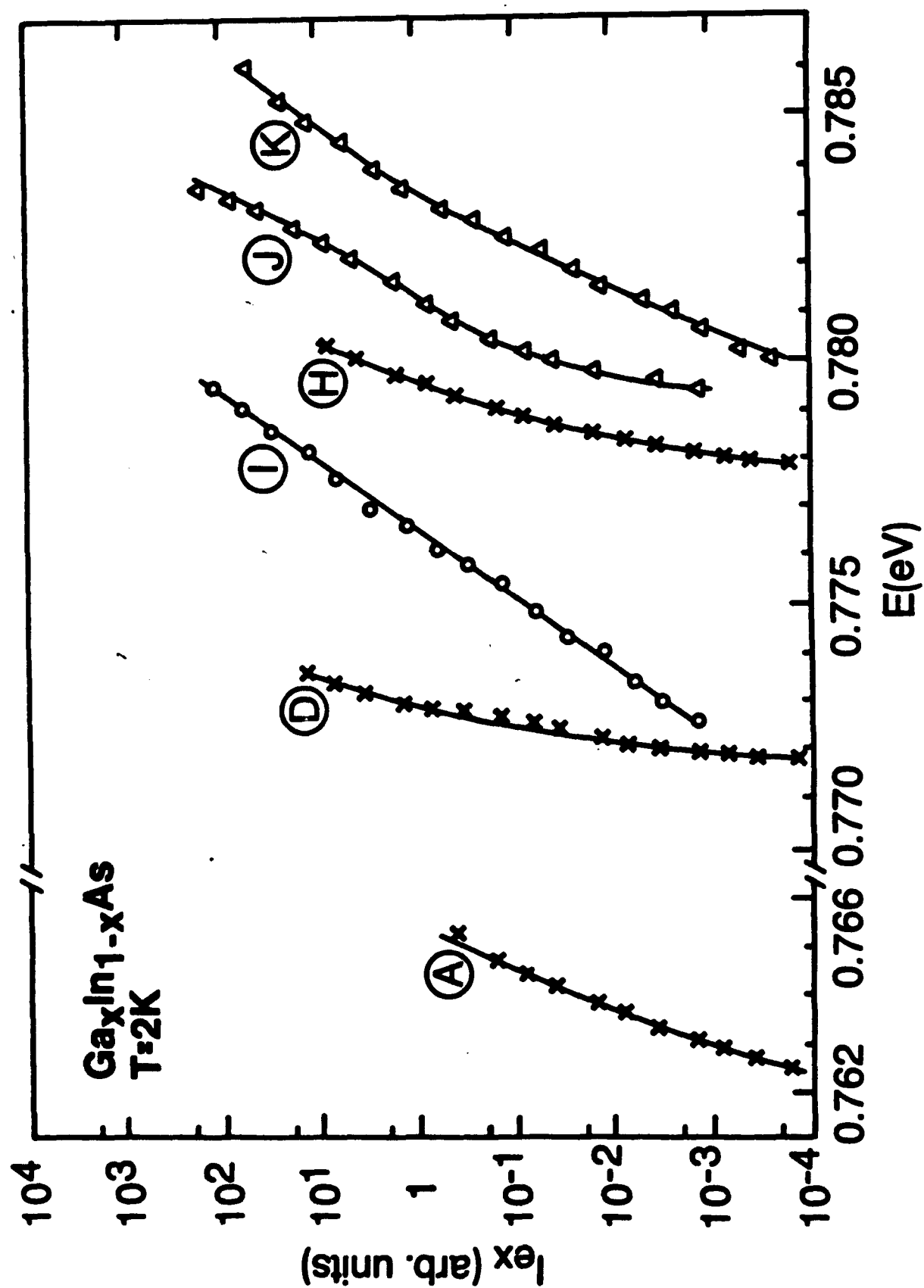


Fig. 7-4. Excitation intensity vs. energy in GaInAs/GaAs.



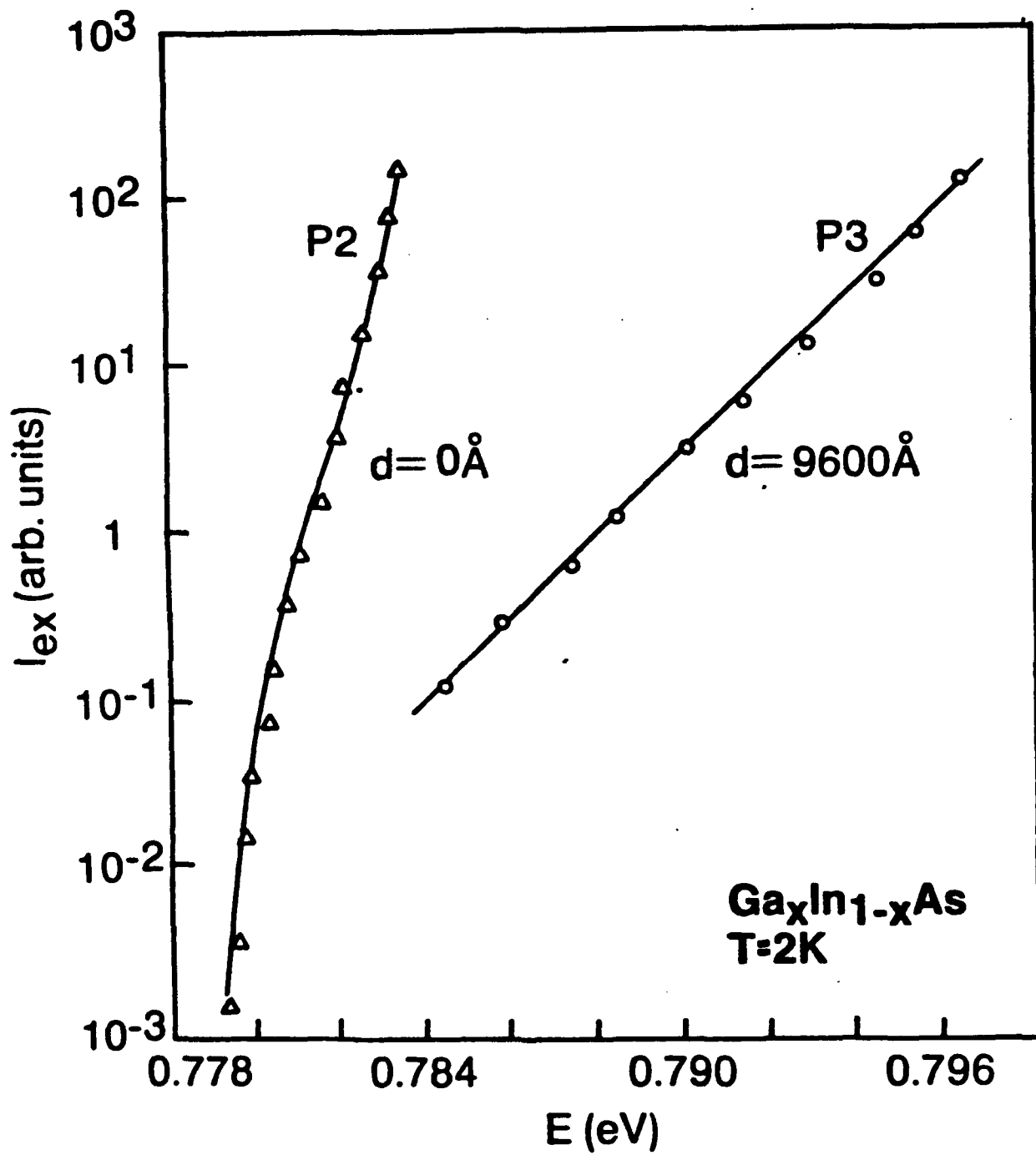


Fig. 7-5. Excitation intensity vs. transition energy in  $GaInAs/GaAs$ .

conditions via mass-spectrometric measurements of the nonincorporated fraction of the incident antimony flux. The observed trends of an increase in Sb incorporation rate with decreasing substrate temperature and increasing group III flux, and an increase in resulting Sb content with Sb flux, are found to be in agreement with previous studies using ex situ techniques only. Additionally, the process of GaAsSb on GaAs interface formation is shown to result in a time dependent  $\alpha(\text{Sb})$  and is understood on the basis of a surface Sb-content dependent Sb desorption rate. Similarly, the Sb desorption rate is found to be time dependent when an incoming Sb flux reacts with a growth interrupted GaAs surface to form a GaAsSb surface layer which is likely to be graded in composition. Fig. 7-6 shows the reflection spectra of the GaSbAs layer.

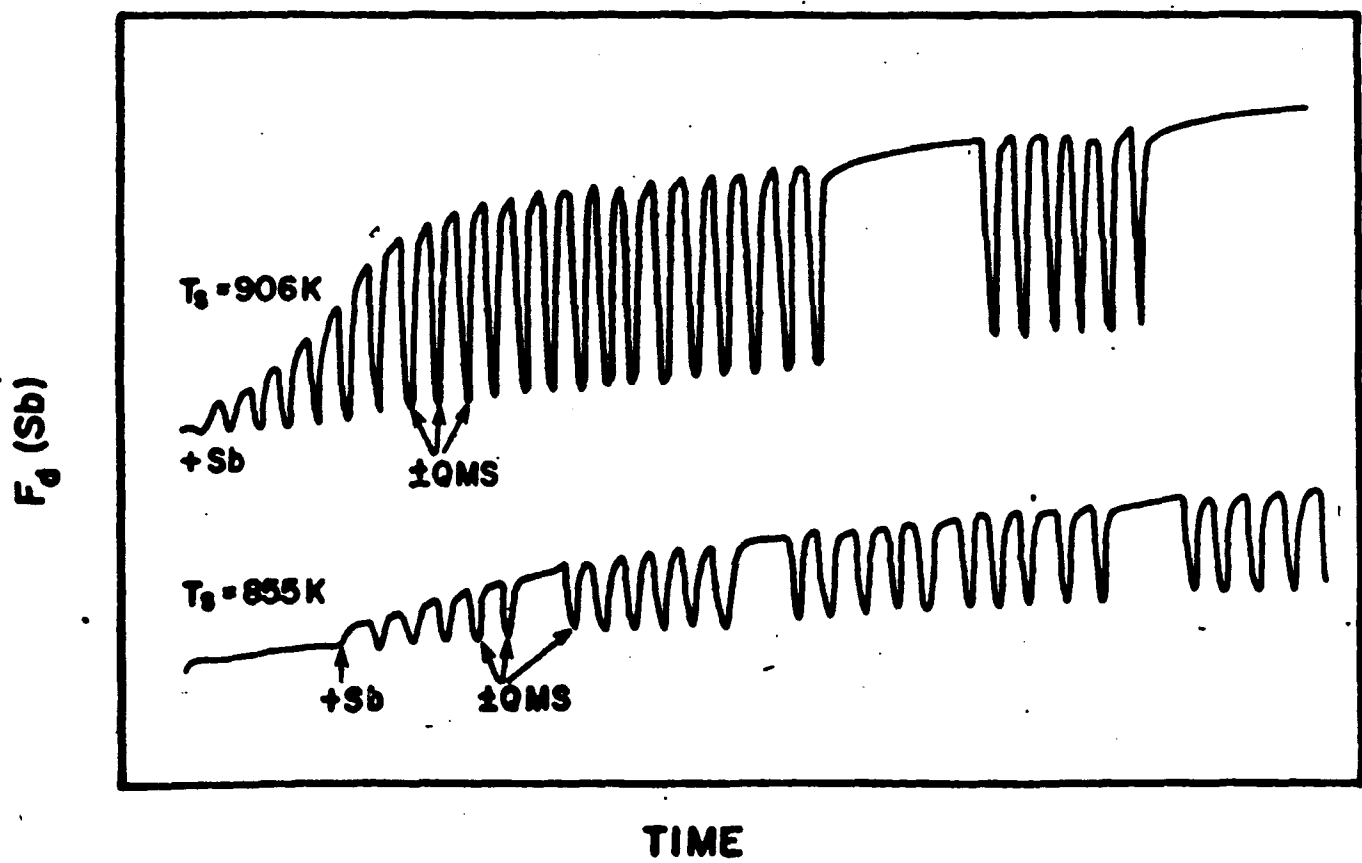


Fig. 7-6. Reflection patterns of GaSbAs grown by MBE.

## 8.0 Optical Properties of Quantum Wells and Superlattices

### 8.1 Shallow Impurity Levels and High Resolution Photoluminescence in AlGaAs/GaAs Quantum Wells<sup>67,68</sup>

Recent developments in the studies of GaAs/GaAlAs multiquantum-well (MQW) structures using high-resolution photoluminescence spectroscopy are reviewed. Results discussed in this report are all obtained in quantum wells grown using molecular-beam epitaxy (MBE). The observed linewidths of the excitonic transitions are very small (in many cases  $< 0.2$  meV), thus indicating a high quality of the quantum wells. Theories of crystal growth by MBE using Monte Carlo techniques and of excitonic lineshape in quantum wells are reviewed. Based on the observed linewidths of the excitonic transitions, a microscopic model for the GaAs/GaAlAs interface is proposed. Variations of the energies of the various transitions in MQW structures as a function of the well size are presented and are compared with the available calculations. The behavior of the excitonic transitions as a function of temperature and applied electric field is also reviewed. Fig. 8-1 shows the well-resolved exciton lines.

This report reviews current knowledge of shallow impurity states (donors and acceptors) in AlGaAs/GaAs multiple-quantum-well structures. Calculations of these levels have been performed by a number of groups, most of which solved an effective-mass Schrodinger equation using the variational method. These results are generally consistent with each other, any differences being related to different approximations made in each calculation. The ground states of some of these shallow impurity levels have also been measured in several laboratories using low-temperature photoluminescence, Raman and far-infrared absorption techniques. These methods yield similar results which are consistent with the calculations. Both theoretical and experimental methods and results are discussed.

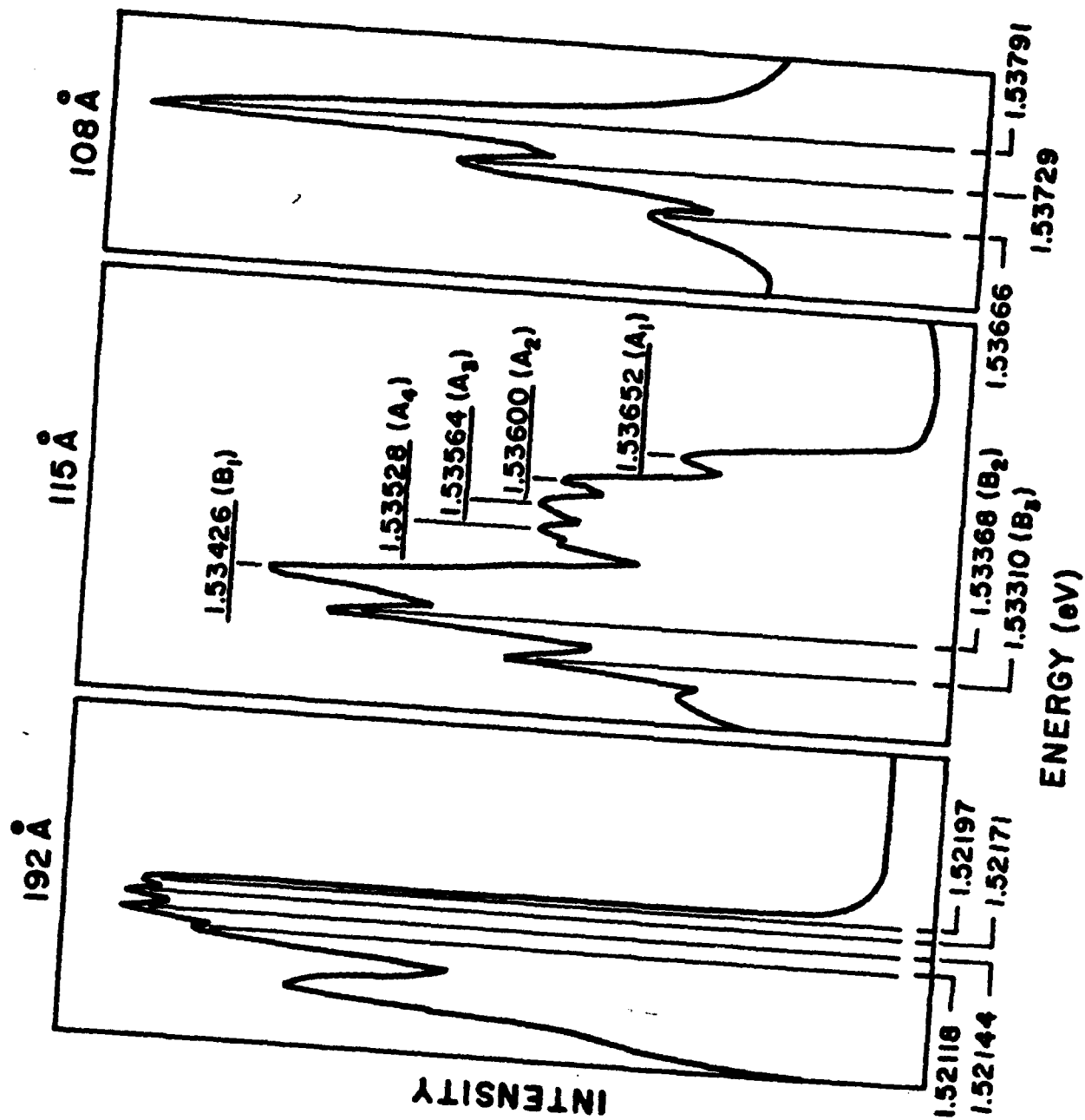


Fig. 8-1. Well-resolved exciton lines of three GaAs-AlGaAs wells.

## 8.2 High Resolution Photoluminescence and Reflection Studies of GaAs-AlGaAs Quantum Wells<sup>69-73</sup>

High-resolution photoluminescence and reflection measurements on two sets of GaAs-Al<sub>x</sub>Ga<sub>1-x</sub>As multiquantum-well (MQW) structures grown by molecular-beam epitaxy (MBE) are reported. Both the heavy-hole and the light-hole excitonic spectra reveal considerable structure with very sharp lines, some as narrow as 0.05 meV. We believe that these are the sharpest lines ever reported for such systems. Samples from different parts of the same wafer for each MQW system exhibit very different excitonic structures. To explain these observations a theoretical model is proposed which is based on our studies of the formation of heterointerfaces by MBE and the theory of the effects of interface roughness on the excitonic linewidths. Typical examples of high-resolution spectra are given in Fig. 8-2.

We have measured the diamagnetic shifts of both the heavy-hole and the light-hole excitons as a function of the well size and the magnetic field (up to 36 kG) in GaAs-Al<sub>x</sub>Ga<sub>1-x</sub>As multiquantum well (MQW) structures using high-resolution optical spectroscopy at liquid-helium temperatures. The applied magnetic field is parallel to the plane of the MQW structures which were grown by molecular-beam epitaxy. We find that in this range of the magnetic field, the diamagnetic shift varies quadratically with the applied field. At a given value of the magnetic field, the diamagnetic shifts of both exciton systems vary almost linearly with the well size. We have also determined, for the first time, the variation of the effective *g* values of the heavy and light holes as a function of the well size assuming that the electron *g* value is independent of the well width. A comparison of our measured values of the diamagnetic shifts with those of another group and with the results of a recent calculation is discussed.

Sharp line structure associated with both the light-hole free exciton (LHFE) and heavy-hole free exciton (HHFE) in multiple-quantum-well structures of GaAs-Al<sub>x</sub>Ga<sub>1-x</sub>As in photoluminescence and reflection spectra has been deconvoluted by using

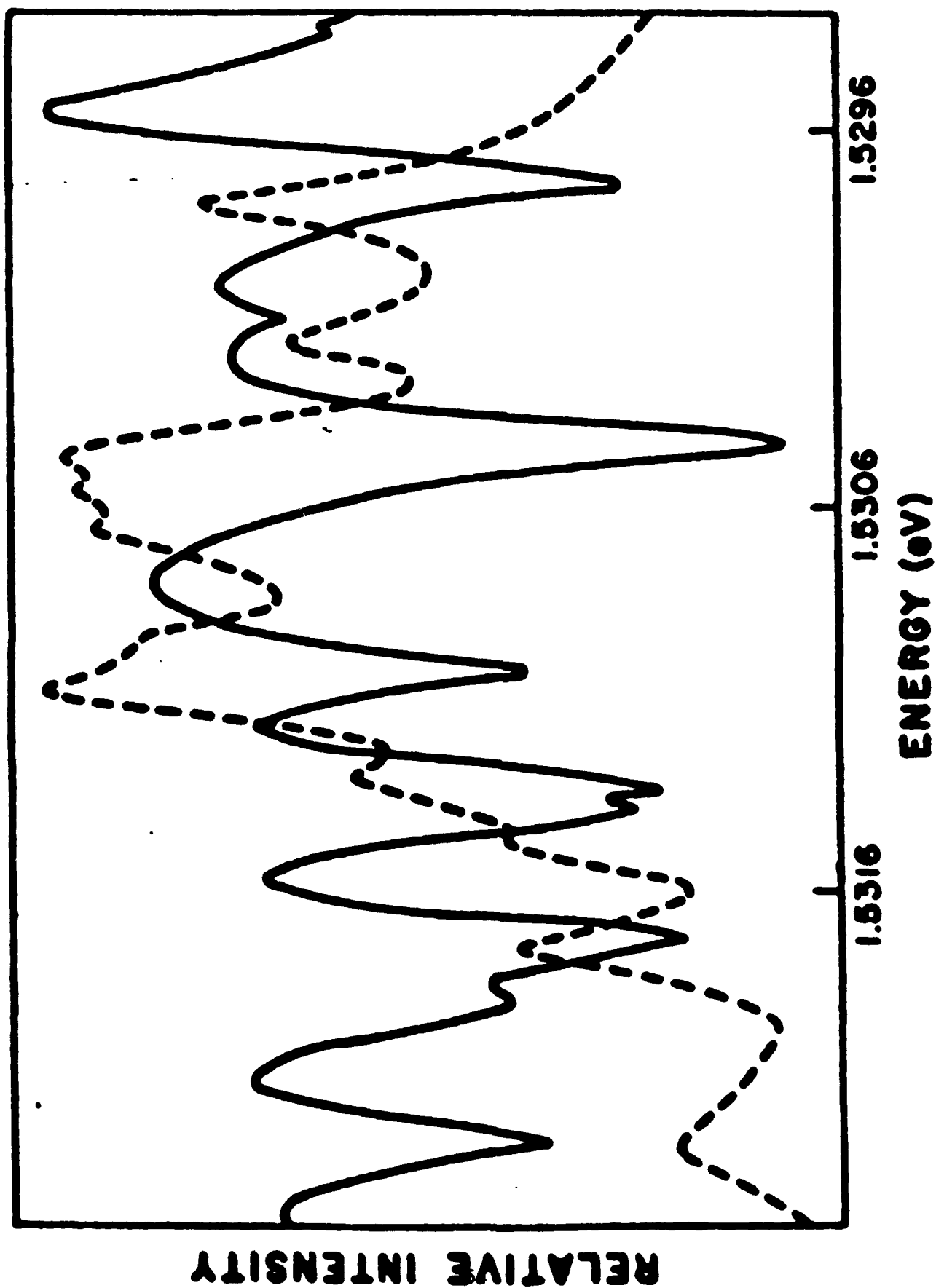


Fig. 8-2. High-resolution PL and PR spectra of an AlGaAs-GaAs QW.

photoluminescence excitation spectroscopy. A correlation is established between particular LHFE fine-structure components and specific HHFE fine-structure components. A model is developed to account for the LHFE and HHFE fine structure in these samples which exploits the nonrandom character of the observed spectra. The physical location of the excitons is demonstrated to be in regions of the wells(s) with essentially identical interfacial microstructure. Evidence of diffusion from effectively-narrow-well regions to wide-well regions is presented.

Observation of several optical transitions associated with the recombination of a free-heavy hole with a neutral donor ( $D^0, HH$ ) and with heavy- and light-hole excitons bound to shallow donors and acceptors in a  $GaAs-Al_xGa_{1-x}As$  multiple-quantum-well (MQW) structure with a nominal well width of 350Å is reported. These transitions are identified using high-resolution photoluminescence and photoluminescence excitation spectroscopies at 2 K. Temperature-dependent (2–20 K) data are also analyzed. To further aid in identifying these transitions, their behavior in the presence of a magnetic field applied parallel to the plane of the MQW structure is investigated. The measured diamagnetic shift agrees well with the calculated diamagnetic shift for the same size well.

The binding energy  $E_B$  of residual donors in nominally 300-Å-wide  $GaAs/Al_xGa_{1-x}As$  quantum wells has been determined from the results of low-temperature photoluminescence (PL), PL-excitation (PLE), and resonant-excitation (RE) measurements. The center of each quantum well was  $\delta$  doped with  $3 \times 10^9 \text{ cm}^{-2}$  Be acceptors, resulting in ionization of residual donors and allowing the observation of free-heavy-hole-to-donor ( $D^0, h$ ) transitions. The  $n = 1(D^0, h)$ , transition for center-well donors was observed in PL, and the  $n = 2(D^0, h)$  transition for center-well donors was observed in PLE. Two transitions associated with ( $D^0, h$ ) were observed in PLE; it is proposed that both the  $2s$  and  $2p_{\pm}$  excited states of the donor are being observed. The calculated binding energy of the  $2s$  and  $2p_{\pm}$  excited states can be added to the measured transition energy from the heavy-hole subband



to the respective excited states. This method gives a donor binding energy of  $8.0 \pm 0.5$  meV. The calculated binding energy of the donor for a 300-Å-wide well is 8.7 meV according to Greene and Bajaj. The observed energy separation between the 2s and  $2p_{\pm}$  excited states of the donor is 0.7 meV, in reasonably good agreement with the calculated value of 0.5 meV. We note that this work is an observation of the  $n = 2$  state of the donor from PLE spectra, as well as the detection of the 2s and  $2p_{\pm}$  levels.

### 8.3 Energy Levels in InGaAs/GaAs Quantum Wells<sup>74,75</sup>

The complete  $k \cdot p$  Hamiltonian with strain is solved numerically to obtain the energies and wave functions of  $\text{In}_x\text{Ga}_{1-x}\text{As}$ -GaAs superlattices. The electron, heavy-hole, light-hole, and split-off bands are treated in a unified description in which the only adjustable parameters are the respective zone-center effective masses in each material. It is shown that the theory accurately reproduces the spectra of a wide range of published samples for valence-band offsets ranging from 0.3 to 0.6. It is also found that the transition energies are relatively insensitive to the valence-band offset over a wide range of offsets. The electron-light-hole exciton energy is fitted more closely at the lower offset values, and suggests a valence-band offset close to 0.4. At this offset, the light holes exhibit borderline type-II behavior, and are only slightly localized in the GaAs layers.

The well-width dependence of the binding energy ( $E_{BE}$ ) of excitons to neutral donors in high-quality, narrow, pseudomorphic  $\text{In}_{0.1}\text{Ga}_{0.9}\text{As}$ /GaAs single-quantum-well structures was obtained via low-temperature photoluminescence measurements. It is observed that  $E_{BE}$  varies smoothly with well widths for wells that vary from 2 monolayers (5.7 Å) to 10 monolayers (28.5 Å) in width. The results are understood on the basis of simple physical arguments. Additionally, a previously unobserved transition was found for both undoped and donor-doped, two-monolayer-wide  $\text{In}_{0.1}\text{Ga}_{0.9}\text{As}$ /GaAs quantum wells. This transition is identified with a bound-to-bound transition and is shown to have significantly faster time-resolved photoluminescence response than those of both the heavy-hole-free-excitonic

and neutral-donor-bound-excitonic transitions. Fig. 8-3 shows the band offsets of the InGaAs/GaAs system.

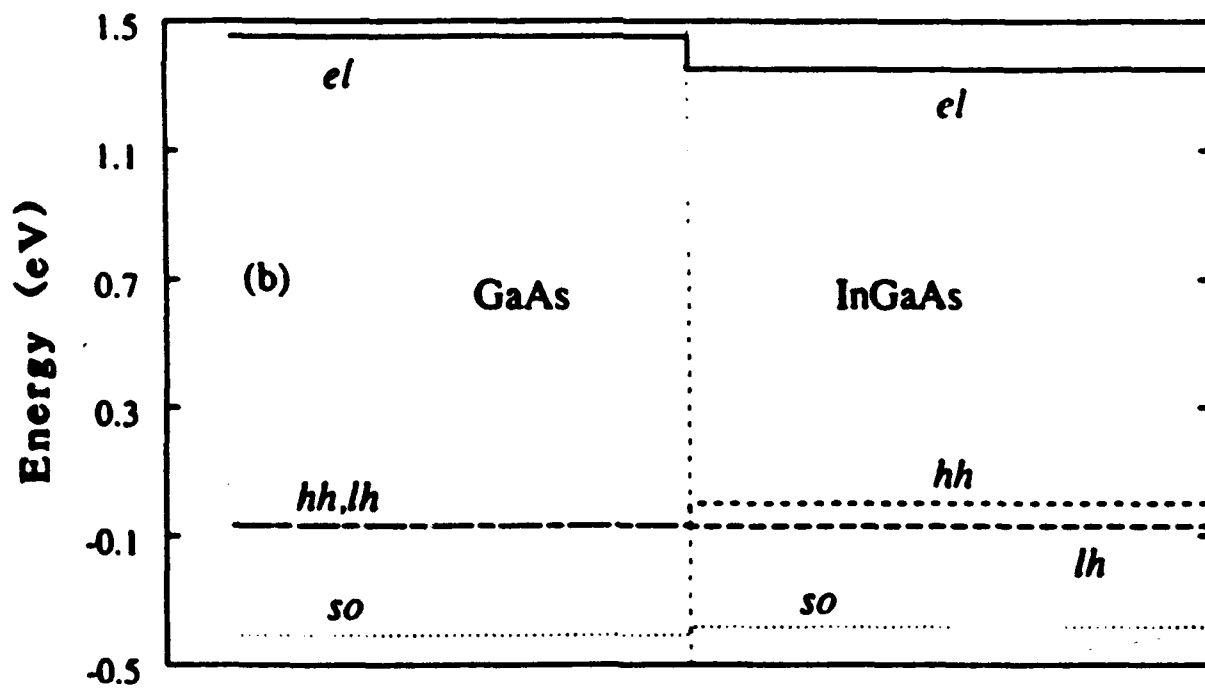
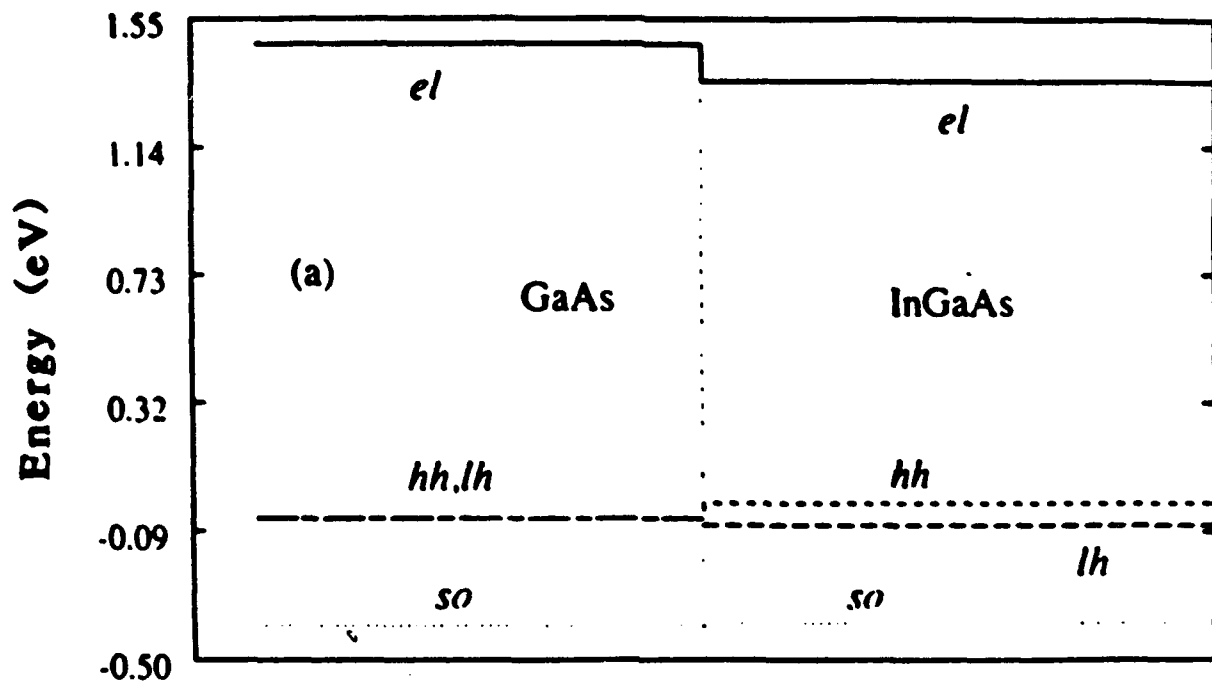


Fig. 8-3. Theoretical calculation of the band-offset of the InGaAs/GaAs system.

## 9.0 Photocurrent Spectroscopy in AlGaAs/GaAs and InGaAs/GaAs Quantum Wells

### 9.1 Photovoltaic Spectra of GaAs-AlGaAs Quantum Wells and Correlation with Photoluminescence<sup>76</sup>

The photovoltaic spectra of molecular beam epitaxy GaAs-Al<sub>0.25</sub>Ga<sub>0.75</sub>As multiple quantum wells in the vicinity of the  $n = 1$  subbandgap region and their correlation with the corresponding photoluminescence spectra have been studied in the temperature range 2–297 K. Photovoltaic and photoluminescence spectra are found to agree for the transition of the  $n = 1$  heavy- and light-hole excitons. The photovoltaic spectra in the Schottky-barrier configuration show as the relative maxima and minima at the corresponding exciton photoluminescence lines. A possible model of the observed coincidence of photoluminescence and photovoltage is discussed. Fig. 9–1 shows a comparison of the PL and PC spectra.

### 9.2 Monolayer Fluctuation in the Excited States of GaAs/AlGaAs Quantum Wells Using Photocurrent and Reflection Spectroscopy<sup>77</sup>

Low temperature photocurrent and reflection spectra are described for GaAs-Al<sub>x</sub>Ga<sub>1-x</sub>As multiple-quantum-well structures grown by molecular beam epitaxy. The spectra include well resolved multiple sharp components both in the ground-state exciton and higher-order allowed and forbidden exciton transitions. These multiple components are attributed to changes in well thickness of approximately 1 monolayer. The observed splittings both in the ground and excited states are in good agreement with calculated values. Fig. 9–2 shows monolayer fluctuations of the exciton transitions.

### 9.3 Determination of Transition Energies and Oscillator Strengths in GaAs-AlGaAs Quantum Wells Using Photocurrent Spectroscopy<sup>78</sup>

A careful study of excitonic lines in the photocurrent spectra of GaAs-Al<sub>0.25</sub>Ga<sub>0.75</sub>As multiple quantum well structures grown by molecular beam epitaxy is carried out for wells having widths in the range 35–245 Å. Transition energies and relative oscillator strengths are measured and compared with theoretical values obtained using a

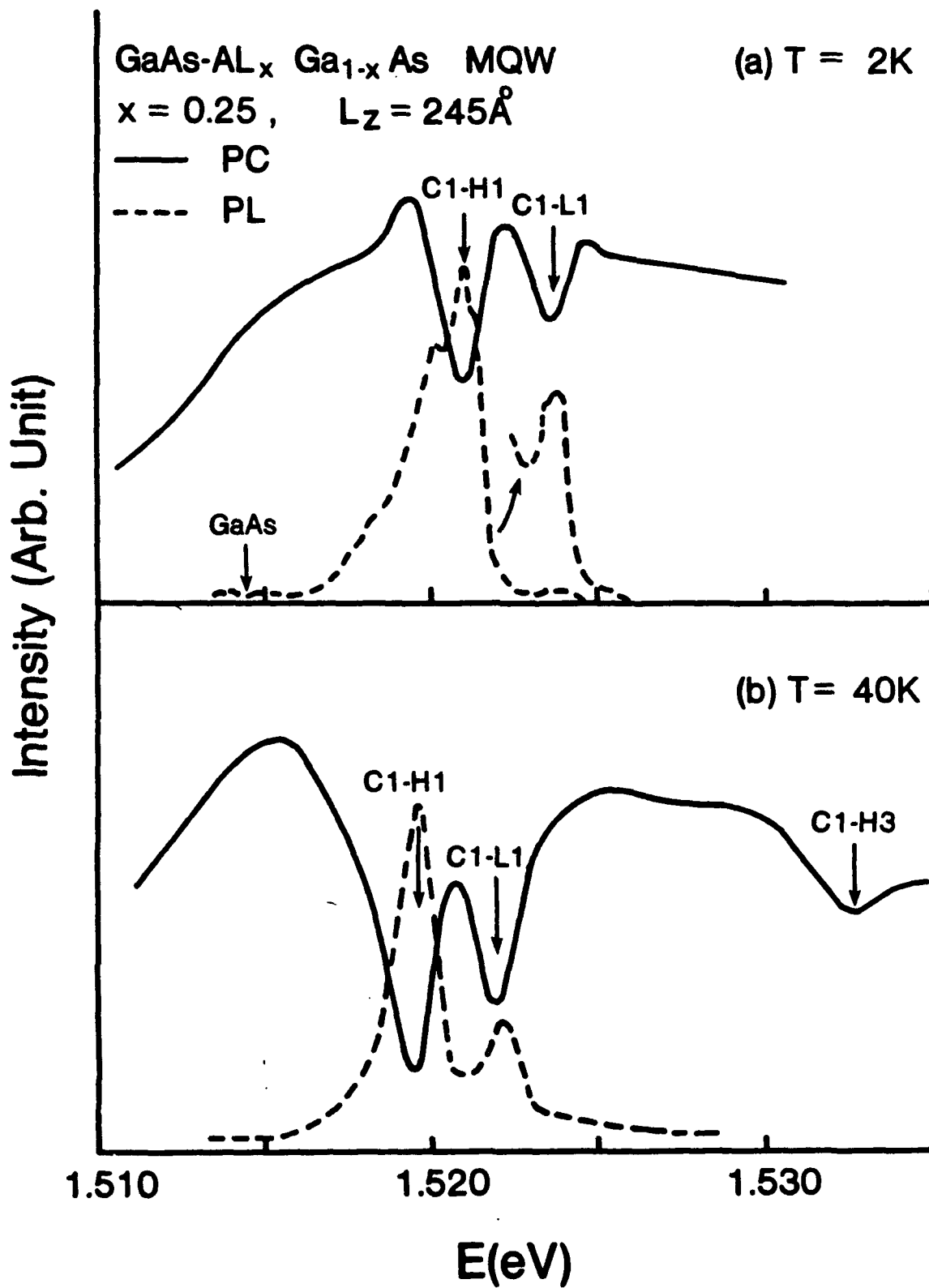


Fig. 9-1. Comparison of PC and PL spectra for a GaAs/AlGaAs MQW.

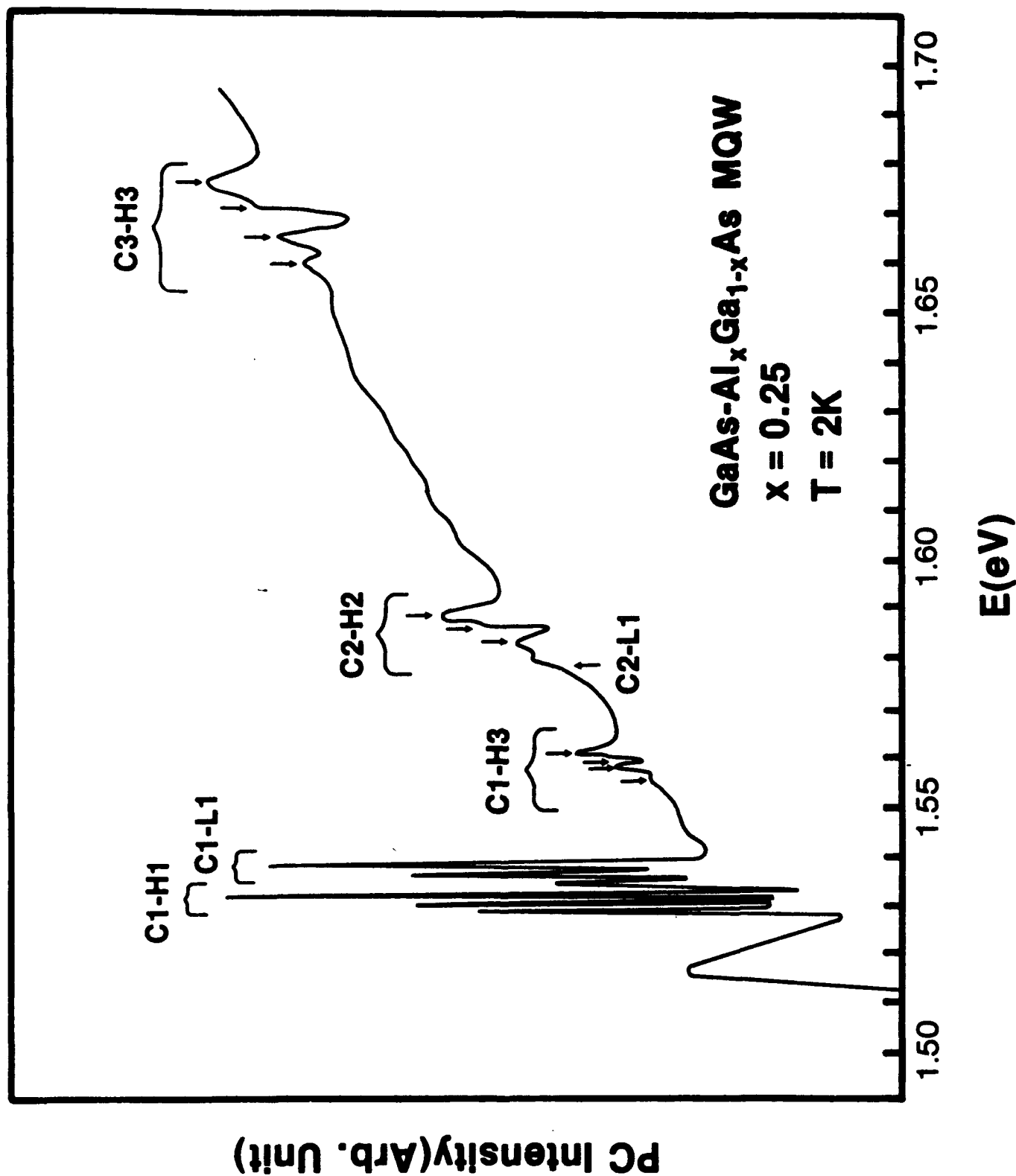


Fig. 9-2. Monolayer fluctuation revealed by the PC method.

multiband effective-mass approach and excellent agreement between experimental data and theory is found. A large number of transitions, as many as 13 excitons, of both allowed and forbidden types are identified and their anomalously large oscillator strengths are shown to be the result of strong mixing of valence subbands. Fig. 9-3 shows the variation of the oscillator strengths of the exciton transitions.

#### 9.4 Electric Field Dependence of Exciton Transition Energies in GaAs-AlGaAs<sup>79-81</sup>

Photocurrent spectroscopy of GaAs-Al<sub>x</sub>Ga<sub>1-x</sub>As multiple quantum well structures in an electric field perpendicular to the heterointerface is used to study exciton transition energies as a function of electric field up to  $\sim 10^5$  V/cm. A large number of excitonic transitions, as many as 16, are identified. The  $\Delta n \neq 0$  forbidden excitonic transitions grow in intensity with increasing electric field, while the  $\Delta n = 0$  allowed excitonic transitions show the opposite. Both negative and positive shifts of exciton transition energies are observed. The results of these observations are compared with those of a theoretical calculation based on a multiband effective-mass approach which incorporates valence-band mixing effects, and a good agreement is found. Fig. 9-4 shows the field dependence of the GaAs-AlGaAs exciton transitions.

#### 9.5 Electric Field Dependence of Exciton Oscillator Strengths in GaAs-AlGaAs<sup>82</sup>

Photocurrent spectroscopy of GaAs-Al<sub>x</sub>Ga<sub>1-x</sub>As multiple-quantum-well structures with an electric field applied perpendicular to the heterointerface is used to study exciton oscillator strengths as a function of electric field up to  $\sim 10^5$  V/cm. The electric field dependence of exciton oscillator strengths is attributed to a complicated interaction between local variation of zone-center electron- and hole-wave function overlap and strong valence-band mixing. The results of experiment are compared with a theoretical calculation based on a multiband effective-mass approach which incorporates valence-band mixing effects, and in which good agreement is found. Strong mixing between the 2s and 2p states of the  $n = 1$  light-hole exciton and the 1s state of the  $n = 2$  heavy-hole to  $n = 1$  electron

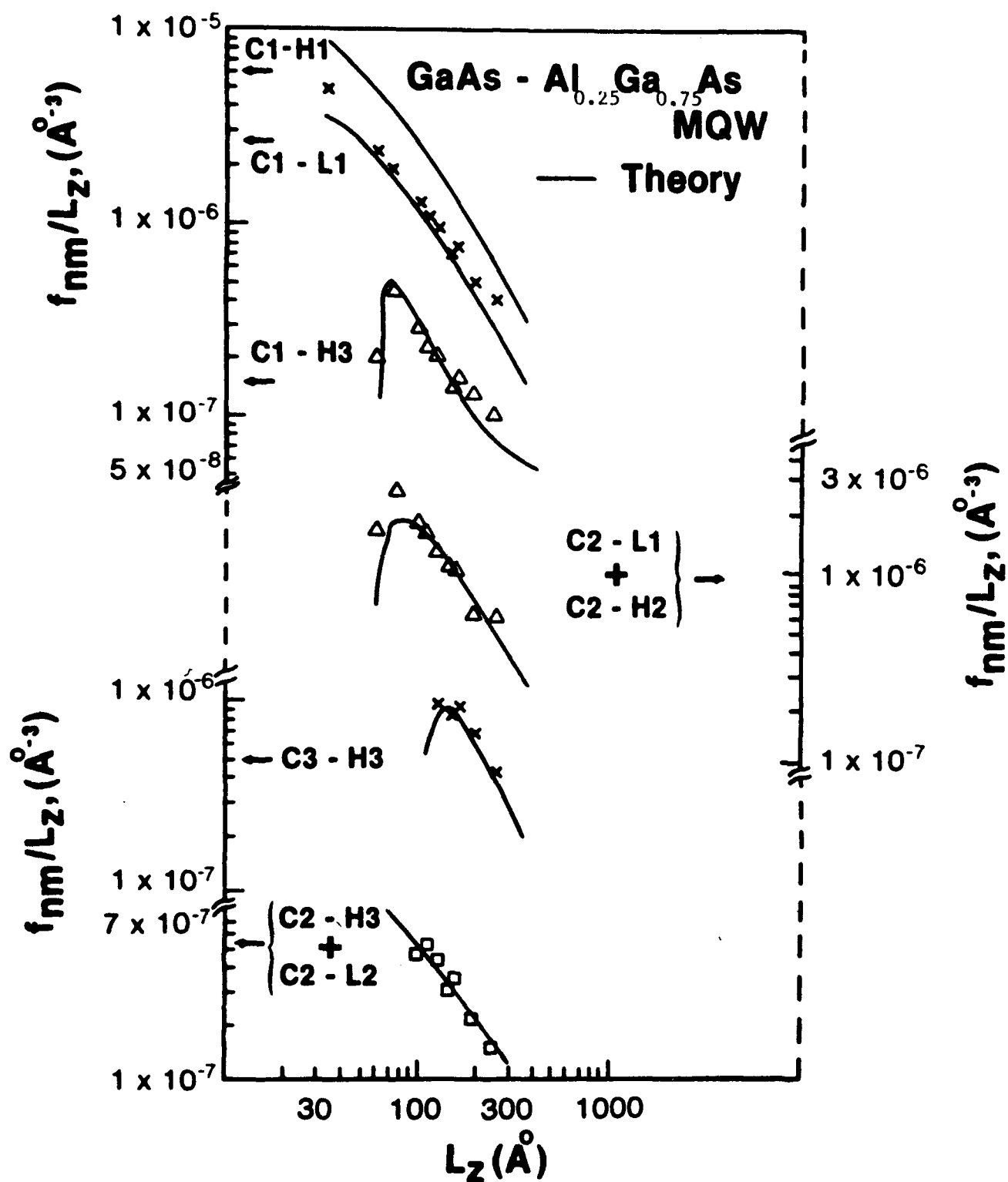


Fig. 9-3. Variation of the oscillator strength of several exciton transitions.



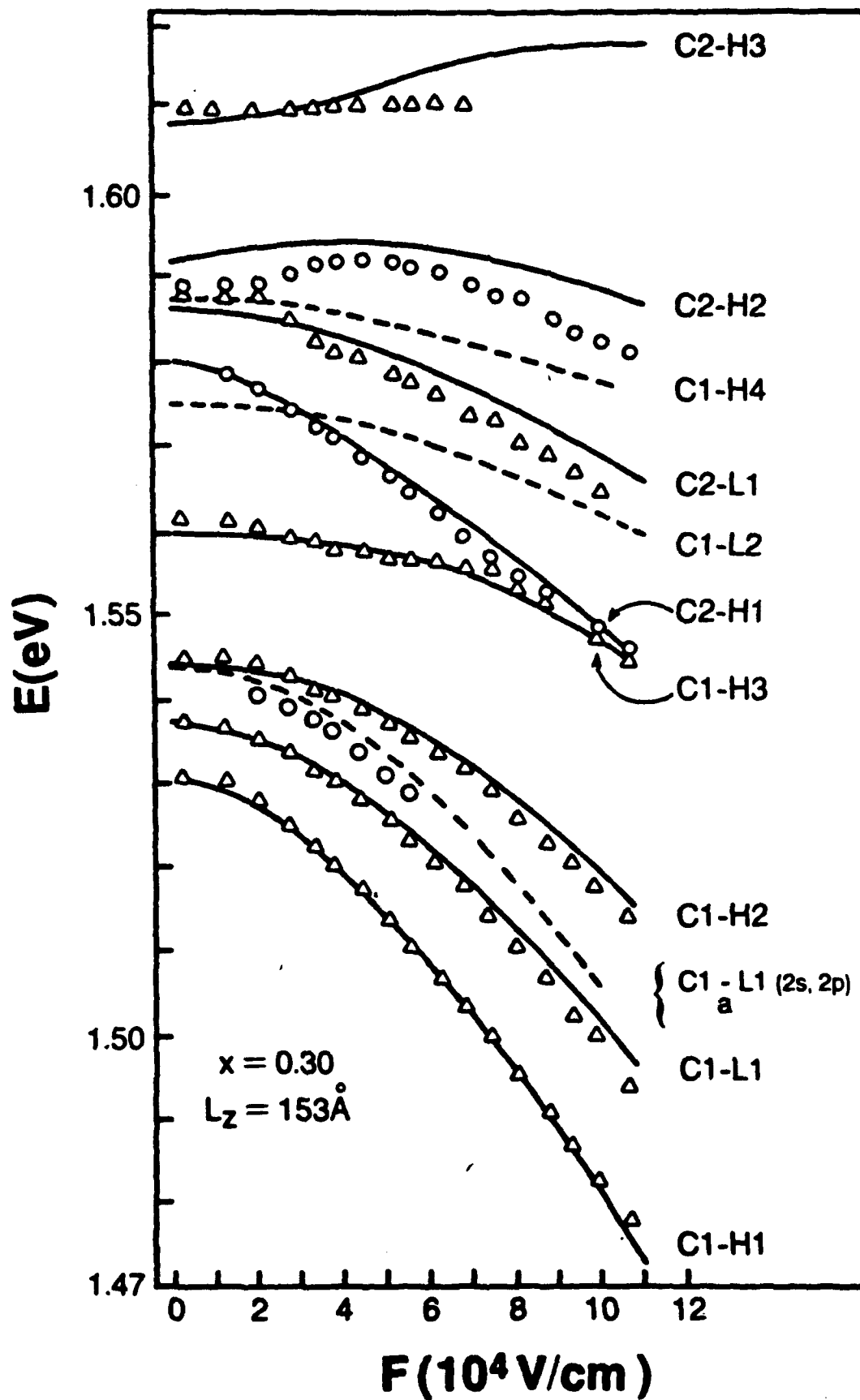


Fig. 9-4. Electric field dependence of various exciton transition energies of a GaAs/AlGaAs MQW.

exciton is identified. Fig 9-5 shows the variation of electric field dependence for several excitons.

#### 9.6 Photocurrent Spectroscopy of InGaAs/GaAs Quantum Wells<sup>83</sup>

Photocurrent spectra of  $\text{In}_x\text{Ga}_{1-x}\text{As}/\text{GaAs}$  multiple quantum wells structures grown by molecular-beam epitaxy are studied in the presence of electric fields perpendicular to the heterointerface. Several  $\Delta n = 0$  allowed and  $\Delta n \neq 0$  forbidden excitonic transitions are observed. Both negative and positive shifts of exciton transitions are found. Good agreement is found between the photocurrent observations and calculations using a multiband effective-mass approach, taking into account the strain-induced splitting. Fig. 9-6 is a typical example of the electric field dependence of exciton transition energies.

#### 9.7 Electric-Field Effects on the Exciton Spectrum in Asymmetric Triangular AlGaAs-GaAs Quantum Well<sup>84</sup>

Photocurrent spectroscopy of asymmetric triangular quantum wells in an electric field perpendicular to the heterointerface is used to study exciton transition energy and oscillator strength under electric fields ranging from  $-10^5\text{V/cm}$  to  $+10^5\text{V/cm}$ . The transition energy and oscillator strength strongly depend on the field direction and magnitude. The lowest-lying heavy- and light- hole excitons show linear Stark shifts that are small compared to that of the corresponding rectangular well. A large energy shift is seen for the transition of the  $n = 2$  electron subband to  $m = 1$  heavy-hole subband in the negative field region. The results of our experiment are in good agreement with a theoretical calculation based on a multiband effective mass approach which incorporates valence-band mixing. Fig. 9-7 shows the electric field dependence of the exciton transitions in a triangular well.

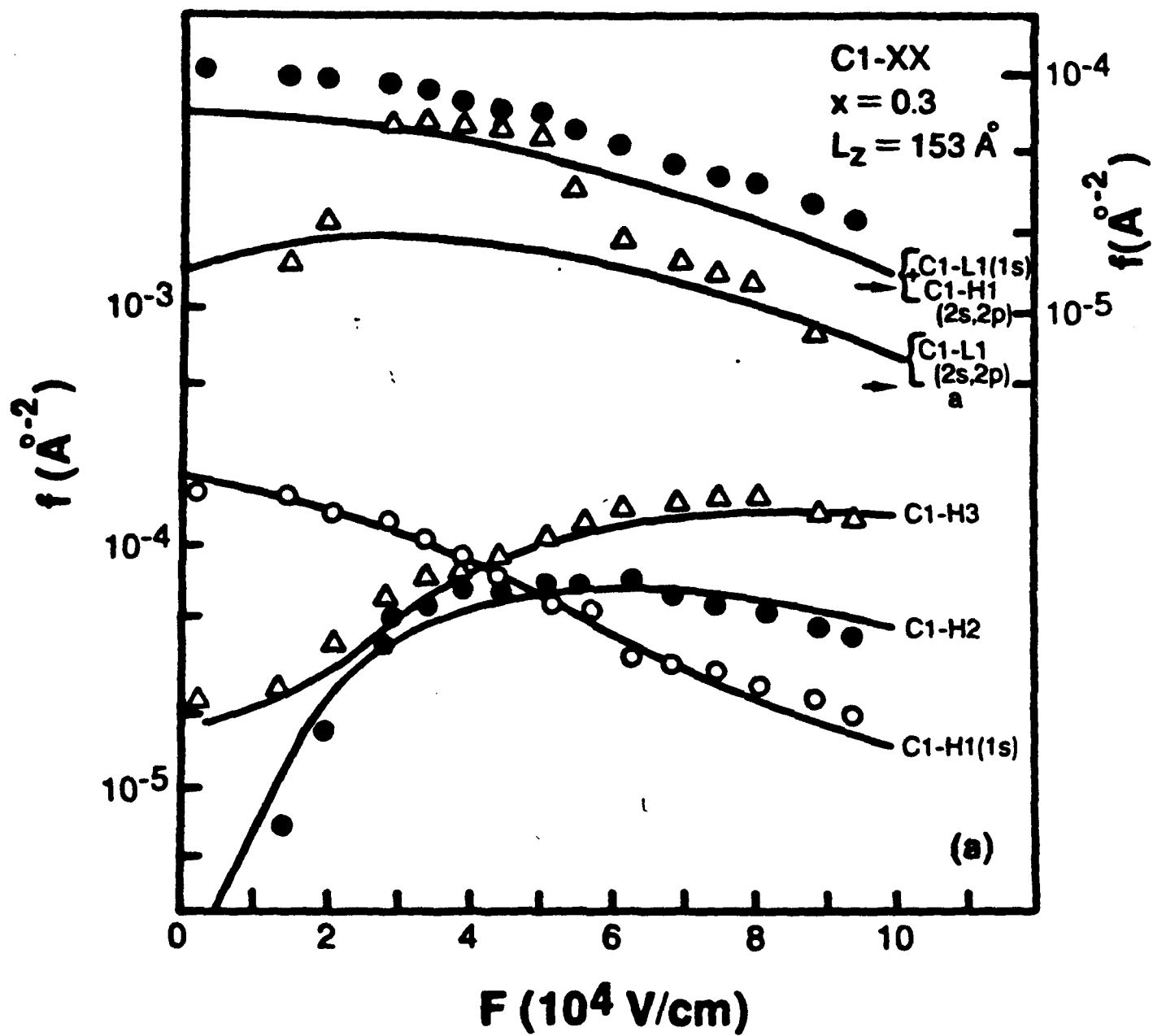


Fig. 9-5. Electric field dependence of the oscillator strength of various excitons in a GaAs/AlGaAs MQW.

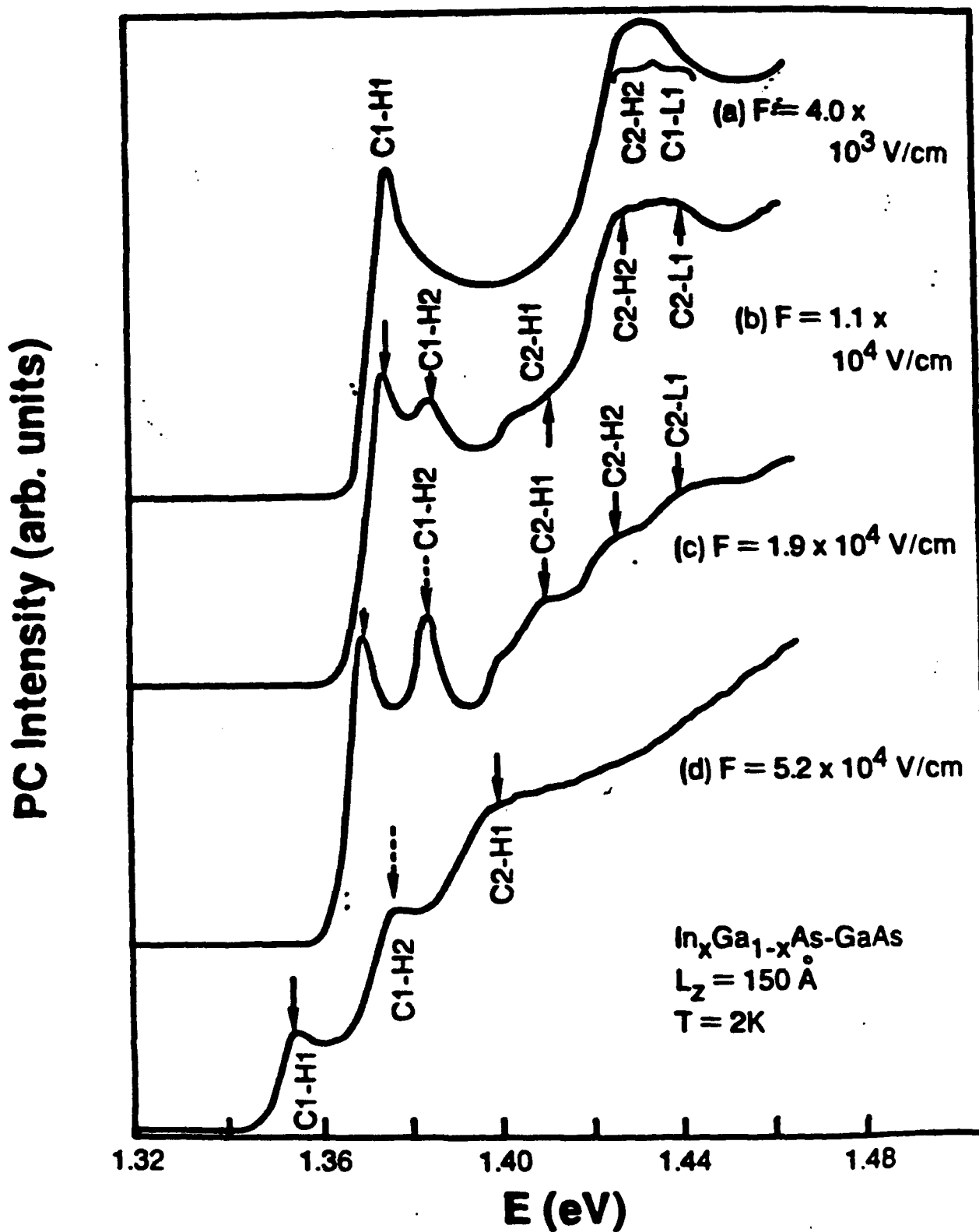


Fig. 9-6. Electric field dependence of exciton transitions in an InGaAs/GaAs MQW.

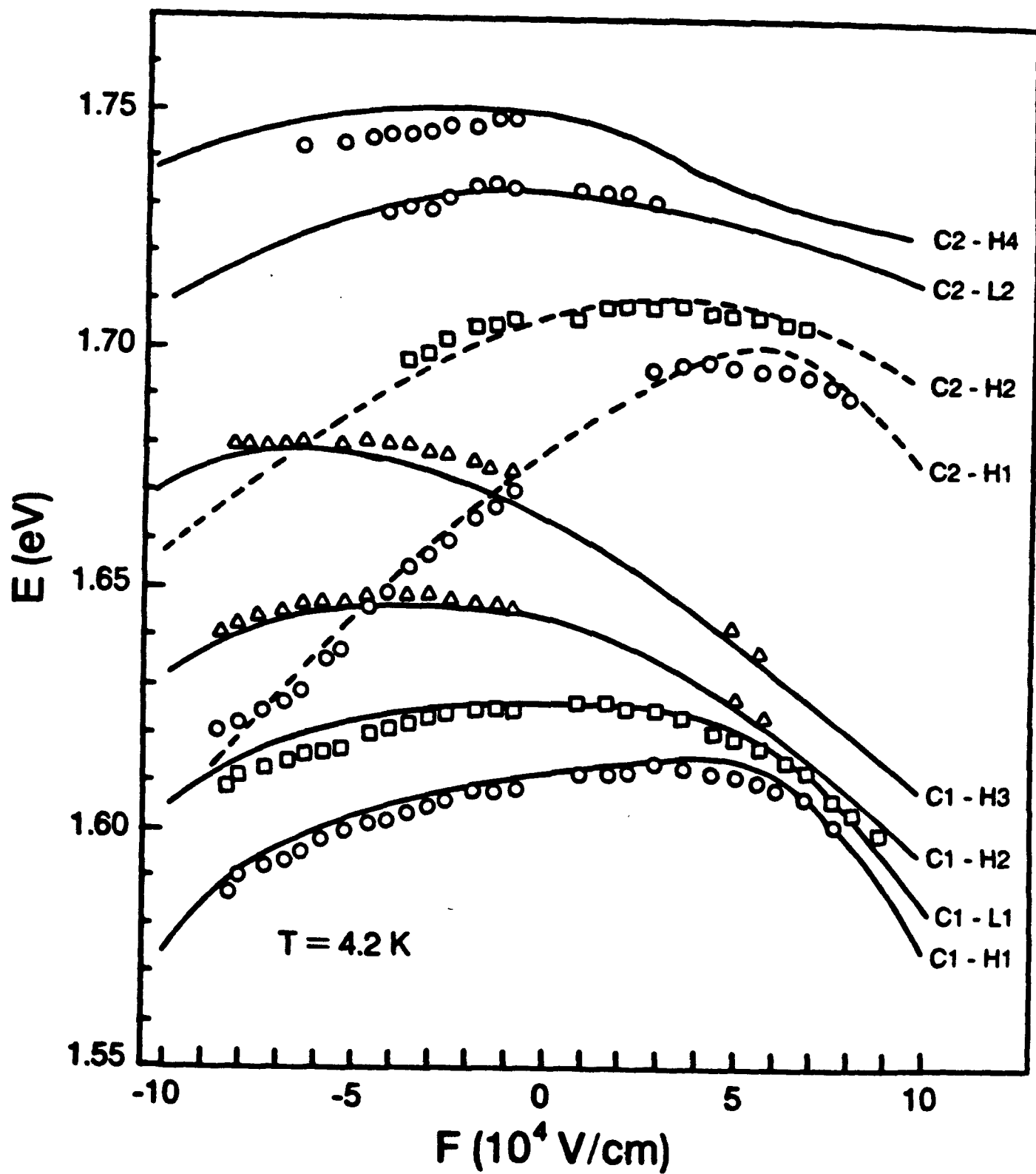


Fig. 9-7. Electric field dependence of exciton transitions in a triangular GaAs/AlGaAs well.

## 10.0 Time Resolved and Magnetic-Field Dependent Photoluminescence in Quantum Wells

High resolution photoluminescence spectroscopy combined with time resolved and magneto optical spectroscopy have proved very successful in identifying extrinsic transitions in quantum well structures. Optical transitions in two different quantum well systems were identified. The system receiving the greatest amount of study is the lattice matched  $\text{Al}_x\text{Ga}_{1-x}\text{As}/\text{GaAs}$  system. This system is essentially strain free, and high quality heterostructures have been produced from this system. The other system that has received considerable attention is the lattice-mismatched  $\text{In}_x\text{Ga}_{1-x}\text{As}/\text{GaAs}$  system. This system can be grown pseudomorphically (without misfit dislocations) with in-plane lattice constant matching, provided the film thickness is below some mismatch-dependent critical value. High quality pseudomorphic quantum wells and superlattices have been grown on GaAs substrates by molecular beam epitaxy. In such structures the InGaAs is under biaxial in-plane compression with an out-of-plane extension in the well layer. The strain removes the degeneracy of the light- and heavy-hole valence bands producing a substantial valence band splitting in addition to the splitting due to well quantization. The bandgap energy also increases with increasing strain. The lifting of the degeneracy between the light- and heavy-hole bands allows the heavy-hole to retain much of its bulk character in the quantum wells. The heavy-hole effective mass will be heavy along the growth direction but light parallel to the growth planes. This property led to speculation of enhanced hole transport<sup>85-88</sup>, suggesting high potential for device applications.

Using magneto-optical spectroscopy the free-to-bound transition was identified in the  $\text{Al}_x\text{Ga}_{1-x}\text{As}/\text{GaAs}$  system. Photoluminescence spectra of a nominal 350Å  $\text{Al}_x\text{Ga}_{1-x}\text{As}/\text{GaAs}$  multiquantum well are displayed in Fig. 10-1. The solid curve shows the spectra in zero magnetic field and the dashed curve in a field of 36 KG which was applied perpendicular to the growth direction. The transition at 1.5172 eV is assigned to the recombination of a free

heavy-hole with a neutral donor located at the center of the well  $D^0_{,h}$ . The assignment of the  $(D^0_{,h})$  transition is based on two criteria. First, the observed transition energy agrees very well with the calculated value obtained from the binding energy of a donor located at the well center and the heavy-hole subband energy in a 350Å well. Second, the observed diamagnetic shift of this transition at 36 KG is 1.2 meV which is considerably larger than that observed for excitonic transitions.

The diamagnetic shift observed for the  $(D^0_{,h})$  transition can be separated into two contributions — one associated with the heavy-hole and one with the neutral donor. Recently, the diamagnetic shift of a neutral donor in a quantum well as a function of well size and magnetic field applied perpendicular to the growth direction has been calculated.<sup>88</sup> For a 350Å-well at 36 KG the calculated diamagnetic shift is 0.7 meV. The difference between the observed diamagnetic shift for  $(D^0_{,h})$  and the calculated shift of the donor level is 0.5 meV and is due the Landau level energy of the free hole; i.e.,  $e\hbar/2M^*C$ , where  $M^*$  is the average hole mass in the Z and Y directions (with Z the growth direction). The measured value of  $M^*$  thus obtained is  $0.41 \pm 0.05 M_0$ . The value of  $M^*$  (defined as  $M^* = M_Y M_Z^{1/2}$ ), using values obtained from cyclotron resonance measurements<sup>89</sup> of  $M_Z = 0.45 M_0$  and  $M_Y = 0.5/M_0$  is found to be  $0.48 M_0$ . The agreement is quite good. Thus, the assignment of the  $D^0_{,h}$  transition in Fig. 10-1 is consistent with the behavior of this transition in an applied magnetic field perpendicular to the growth direction. The low temperature (2K) photoluminescence (PL) signal from a 200Å GaAs-Al<sub>0.3</sub>Ga<sub>0.7</sub>As quantum well structure shows a peak (Q) occurring 1.0 meV lower in energy than the heavy-hole free-exciton (HHFE) transition as shown in Fig. 10-2. Transition Q is neither exciton related nor free-to-bound related and most likely is due to a bound-to-bound transition. Time-resolved PL measurements show that emission from transition Q has a significantly shorter radiative lifetime than that of the HHFE (see Fig. 10-3) while both acceptor- and donor-bound excitons are found to have somewhat longer lifetimes than HHFE.

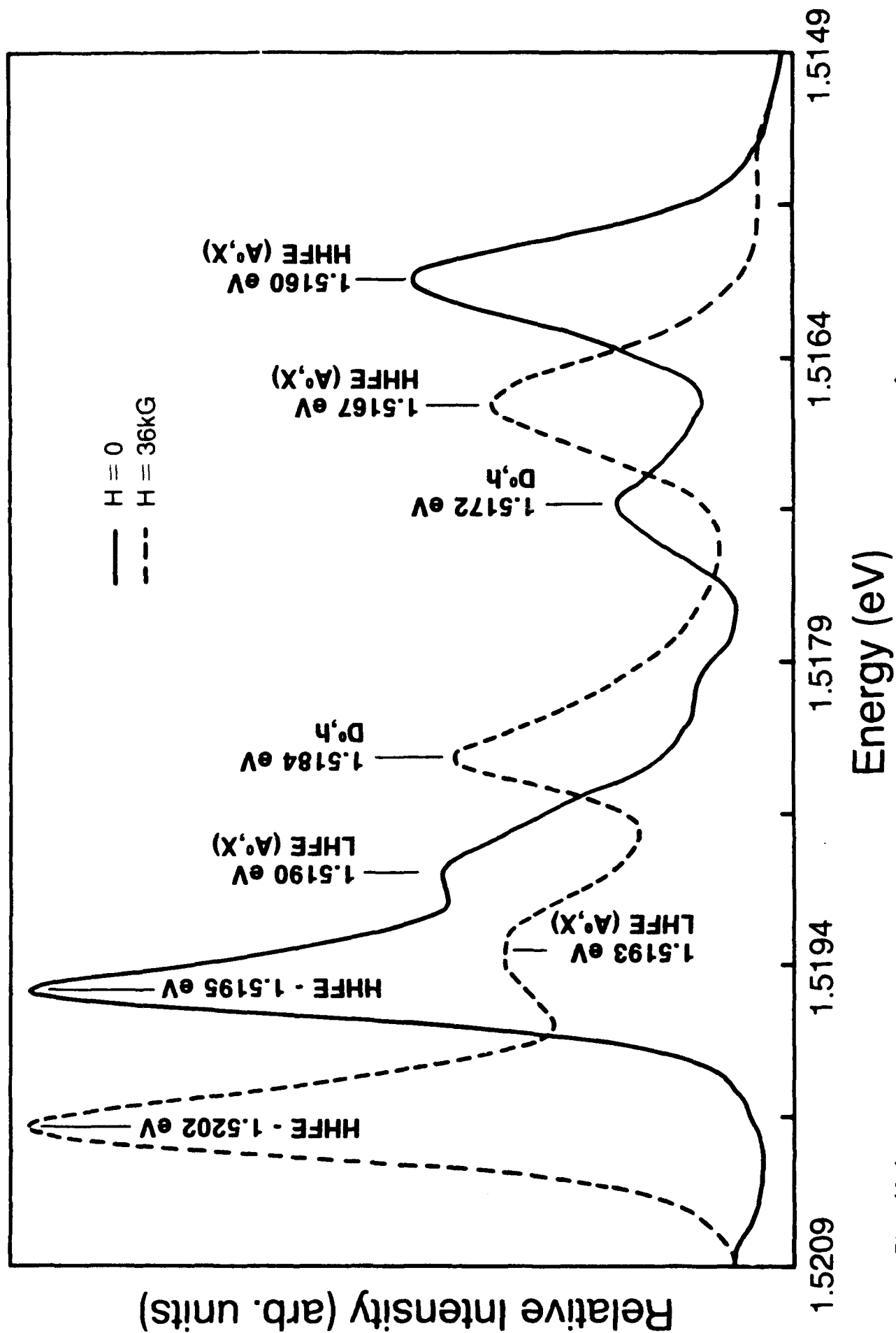


Fig. 10-1. PL spectra obtained at 2K showing the optical transitions from a 350-Å  $\text{Al}_x\text{Ga}_{1-x}\text{As}/\text{GaAs}$  MQW structure in a zero magnetic field (solid line) and a magnetic field of 36 kG (dashed line).



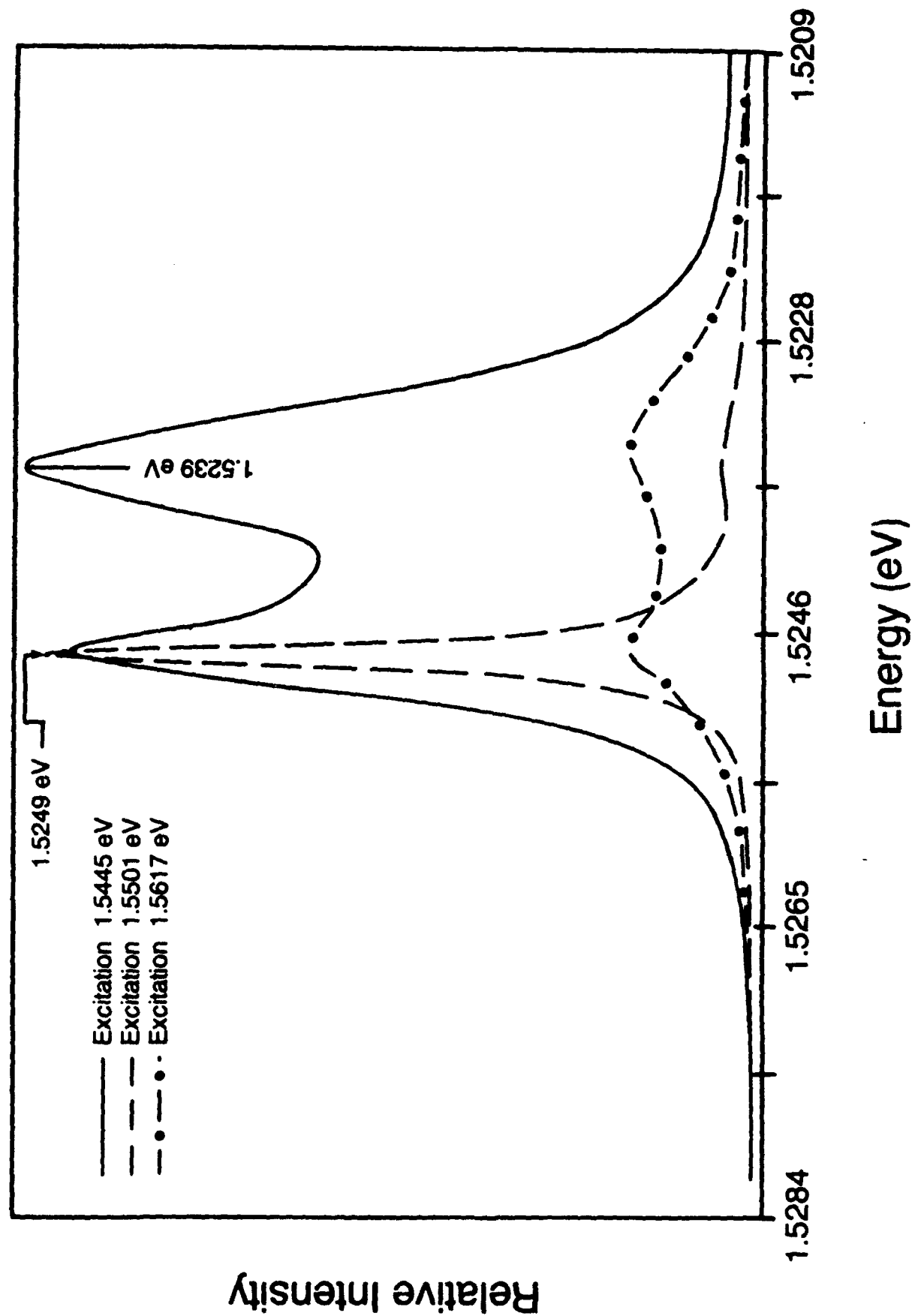


Fig. 10-2. Photoluminescence spectra from a 200-Å GaAs/Al<sub>0.3</sub>Ga<sub>0.7</sub>As QW. Three different spectral curves are obtained from three different excitation energies.

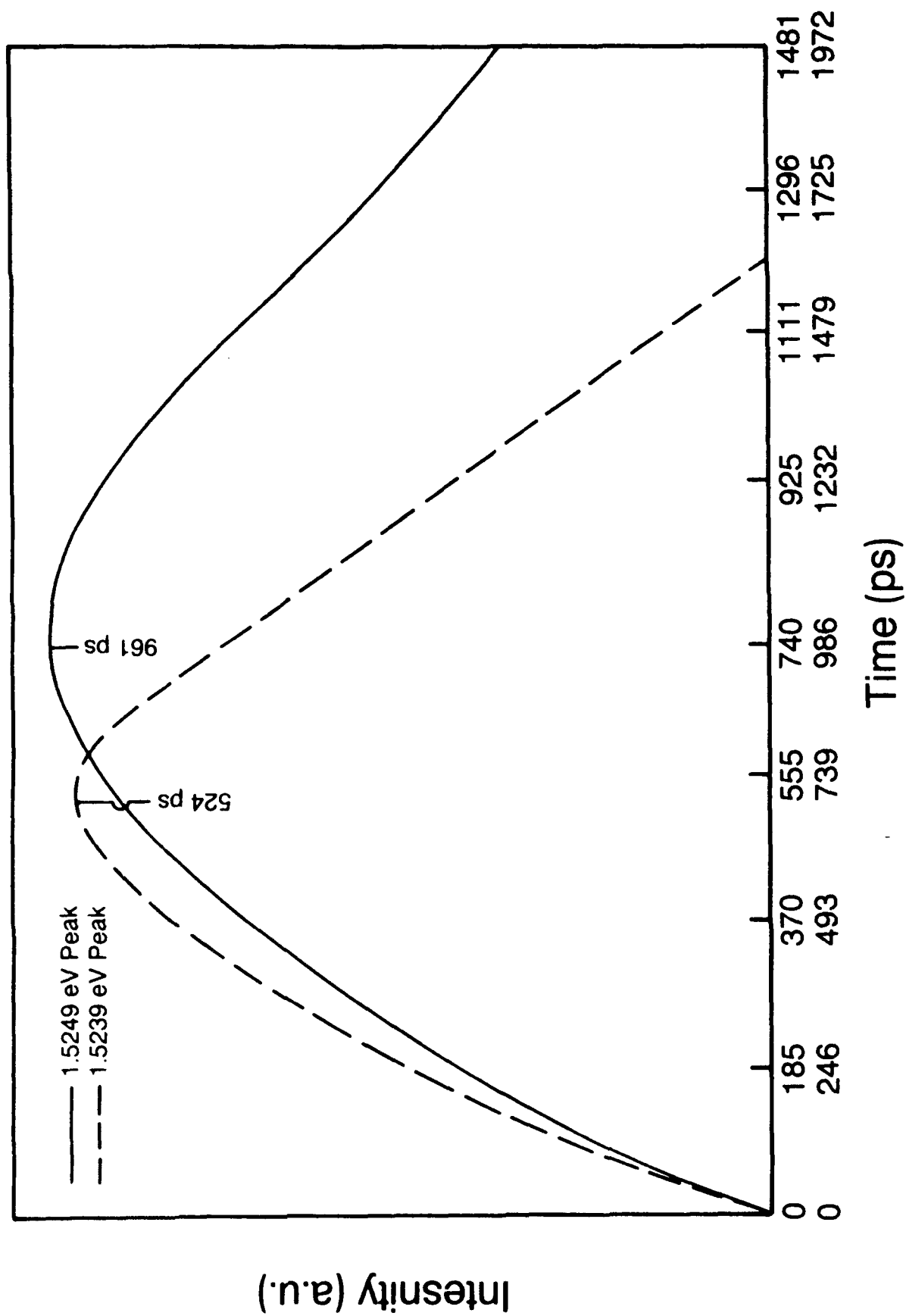


Fig. 10-3. Time response for the HHFE of the sample shown in Fig. 10-2 (solid curve) and for the peak at 1.5239 eV (dashed curve).

Magnetic-field dependent PL measurements show that the diamagnetic shift of transition Q is significantly smaller than that expected for a free-to-bound transition and is consistent with that expected for a bound-to-bound transition. The dramatically reduced lifetime of Q compared to the HHFE can be qualitatively explained as being due to a bound-to-bound transition in which the electron and hole are more closely spaced than they are in the exciton state.

The simplest of bound-to-bound transitions involves the recombination of a shallow bound-electron with a shallow bound-hole. It is known that the energy for such a transition depends on the real space separation of the donor-acceptor pair. Taking the calculated<sup>90</sup> value for the binding energy of a center-of-well donor for a 200Å-well to be 10 meV and a value of 46 meV for the binding energy of the acceptor,<sup>91</sup> the spatial separation of the donor and acceptor can be obtained from the expression:

$$E = E_g - E_D - E_A + e^2/\epsilon R$$

This gives a value of R between 40 and 50Å. The Bohr radius of the exciton for a 200Å-well is approximately 85Å. Thus, the electron and hole are much more closely spaced in the bound-to-bound transition than in the exciton transition. This gives a considerably greater overlap of the electron and hole wave functions which greatly enhances the recombination rate and demonstrates the dominant role of wave function overlap on recombination lifetimes.

A similar transition has been observed in the  $\text{In}_x\text{Ga}_{1-x}\text{As}/\text{GaAs}$  system. The PL spectra from an undoped, two-monolayer  $\text{In}_{0.1}\text{Ga}_{0.9}\text{As}/\text{GaAs}$  QW structure is shown in Fig. 10-4. Two features are observed: the HHFE transition occurs at 1.5133 eV, and another transition is observed to occur 0.7 meV lower in energy at 1.5126 eV. This energy difference of 0.7 meV is considered to be too small to be associated with the binding energy of an exciton to a neutral donor. Also, it occurs at too high an energy to be a free-to-bound transition.

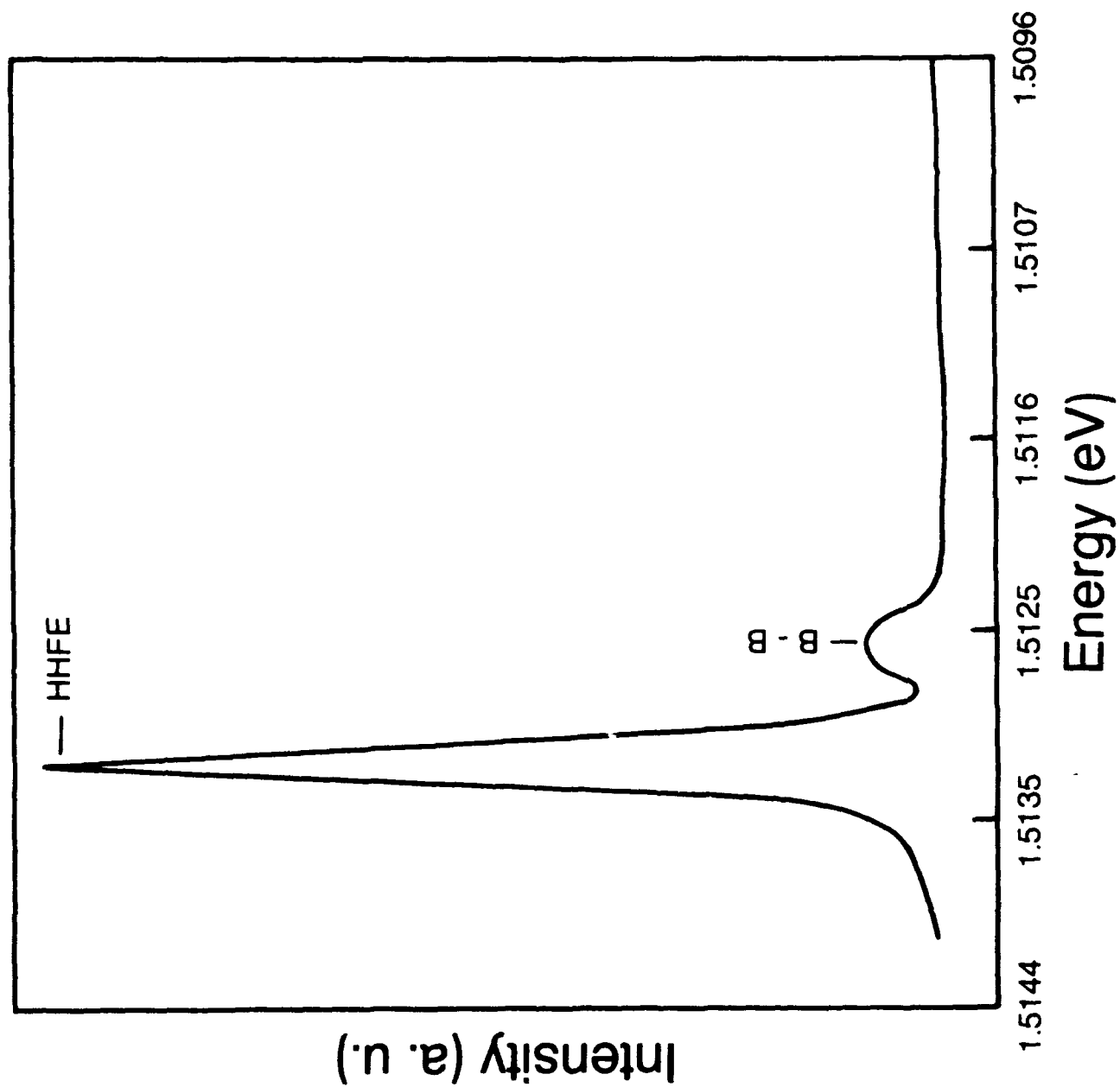


Fig. 10-4. PL spectrum for an undoped, two monolayer-wide  $\text{In}_{0.1}\text{Ga}_{0.9}\text{As}/\text{GaAs}$  QW structure showing the HHFE and BB transitions.

The similar transition observed in  $\text{Al}_x\text{Ga}_{1-x}\text{As}/\text{GaAs}$  QW's was associated with a bound-to-bound (BB) transition. The identification of the BB transition in  $\text{Al}_x\text{Ga}_{1-x}\text{As}/\text{GaAs}$  QW's was based on (1) time-resolved spectra which showed the BB transition to have a much faster time response than either the HHFE of  $\text{D}^0, \text{X}$  transitions, and (2) theoretical arguments which show that the energy position of the transition and its faster time response relative to those of the excitonic transitions are consistent with the BB assignment. A similar behavior is found for the transition occurring at 1.5126 eV shown in Fig. 10-4. Exciting the undoped, two-monolayer-wide  $\text{In}_{0.1}\text{Ga}_{0.9}\text{As}/\text{GaAs}$  QW at the GaAs barrier free-exciton formation energy with a 70-psec excitation pulse gives rise to the time-resolved PL decay curves shown in Fig. 10-5. The solid and dashed curves are the time responses of the HHFE and BB transitions, respectively. Here it is seen that the BB transition has a significantly faster time response than that of the HHFE transition, which is qualitatively similar to the results obtained on  $\text{Al}_x\text{Ga}_{1-x}\text{As}/\text{GaAs}$  QW's.

The same techniques were used to identify both light- and heavy-hole bound exciton transitions in both the  $\text{Al}_x\text{Ga}_{1-x}\text{As}/\text{GaAs}$  and the  $\text{In}_x\text{Ga}_{1-x}\text{As}/\text{GaAs}$  systems. Free-to-bound transitions were also identified in  $\text{In}_x\text{Ga}_{1-x}\text{As}/\text{GaAs}$  QW's.

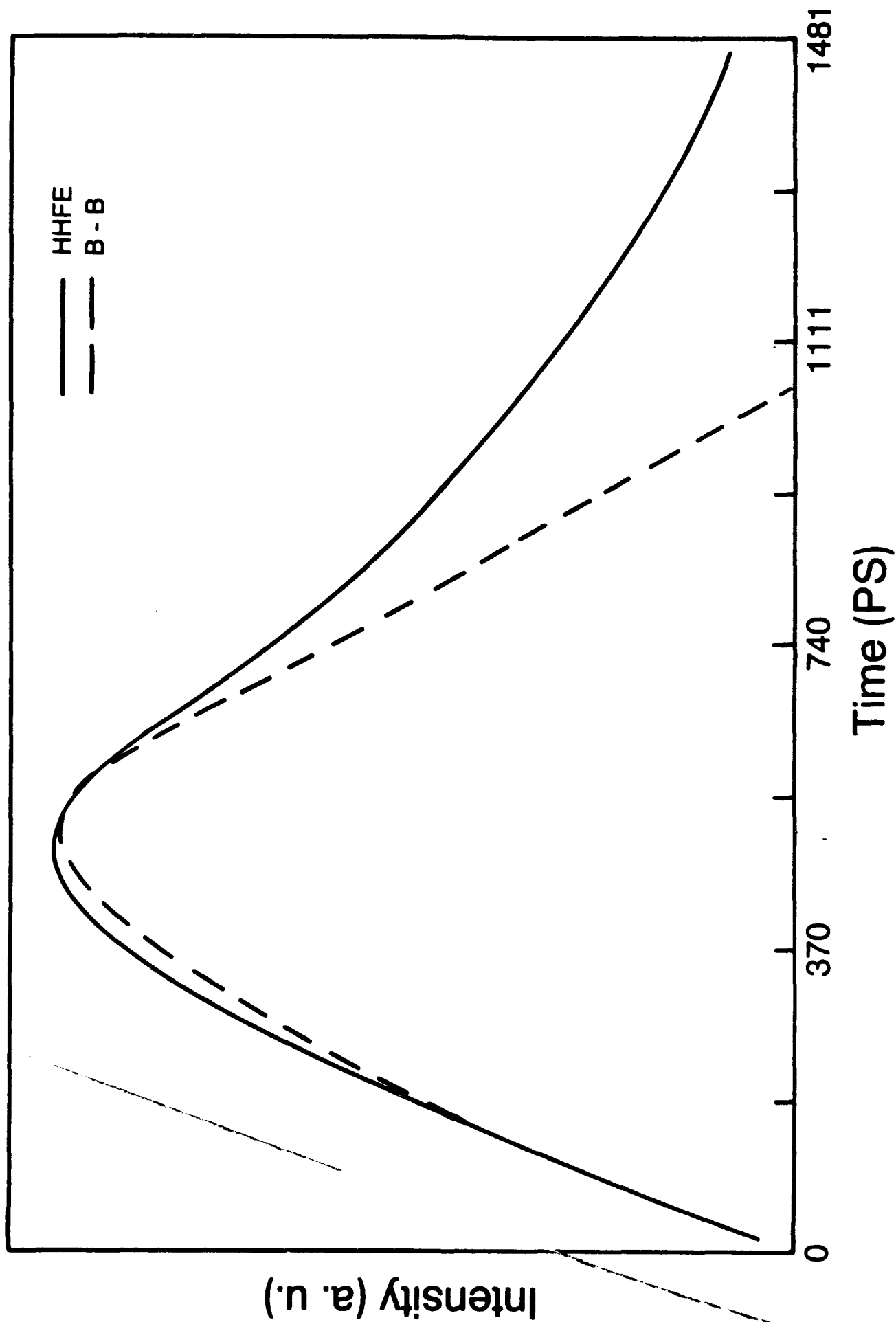


Fig. 10-5. Time resolved PL decay curves for the HHFE (solid) and BB (dashed) transitions for the undoped, two monolayer-wide  $\text{In}_{0.1}\text{Ga}_{0.9}\text{As/GaAs}$  QW structure.

## **11.0. MIMIC Materials/Device Correlation Program**

### **11.1 Management**

This section of the report has been prepared to cover work performed primarily on MIMIC Phase 1, Task 4.E. The management and data analysis part of this effort were added in January 1990. Some description of planning efforts for MIMIC Phase 2 testing and analysis which were conducted toward the end of the contract period in 1991 are also included. All contractors have completed Task 4.E work and data deliveries. End-of-Phase 1 meetings have been held with all contractors. Areas reviewed included materials, uniformity / yield, alignment, and RF/DC correlations. Additional RF/DC correlation work has been accomplished with good correlations on most contractors processes. The MIMIC Phase 2 contracts were signed on 9 August 1991. Since then discussions have been held with all contractors regarding Phase 2 test reticles and testing. The design of an integrated comprehensive test reticle that will combine process control structures, reliability test structures, process limit (defect) test structures, high density FET pairs, and a Standard Evaluation Circuit (SEC) has proceeded well at all contractors. It is planned to continue the ELM/ELR database for government analysis of contractor data. The use of mapping tools will continue at ELM/ELR and is encouraged as a part of contractor data analysis. The number of process lines increases from 6 on Task 4.E to the order of 12 on Phase 2. The number of unique processes will increase to at least 18 at the start with additional processes scheduled for development. Substrate material characterization has been completed with the last Round 3 wafers. Coordination has been maintained with the six participating contractors and other government agencies. All contractors have finished Round 3 on Phase 1. The remaining effort shifted to working with contractors on their Phase 2 test reticle design and test plan. Two GOMAC papers were presented and published in the GOMAC 91 Digest. One of these papers is included below as a summary of technical results on Task 4.E.

### **11.2 Materials**

The goal of the materials subtask in Task 4.E was to determine if present-day semi-insulating (SI) GaAs substrates were, in some cases, adversely affecting devices, and , if so, how they could be improved. First, the standard testing methods, in particular Hall-effect and EL2-absorption

measurements, had to be verified for accuracy and reproducibility among the various laboratories and this was accomplished. Second, new techniques had to be developed in order to obtain dense mapping of dislocation density and subsurface damage, and finally, the materials data had to be correlated with device data. Several conclusions were reached: (1) testing accuracy in the areas of Hall-effect measurements and dislocation counting has greatly improved, and now may be considered satisfactory; (2) material quality, both in bulk and surface aspects, has also improved over the past 5 years, but still is not fully adequate, as evidenced by fourfold symmetry appearing in some device maps, even in MIMIC circuits; and (3) at least two growth methods, the vertical gradient freeze (VGF) and vertical Bridgeman (VB) techniques, show promise of producing greater device uniformity, and should be pursued.

For further information on these subjects, see Publ. No's. 25, 26, 27, 42, 57, 58, 59, 61, 91, 103, 104, 107, and 129, in the List of Publications at the end of this report.

### 11.3 Devices/Contractor Data Analysis

#### 11.3.1 General

End-of-Phase 1 meetings were held with all contractors to review Task 4.E results. Some issues continue to be evaluated on several processes and will be used as a starting point for future Phase 2 work. Five of the six Task 4.E participants are Phase 2 participants. ITT was not selected as a Phase 2 participant but is supported separately under Phase 3 work. Preliminary meetings were held with all Phase 2 teams. There will be a total of at least 12 process lines involved on Phase 2 baseline processes. A summary of results on Task 4.E, and plans on Phase 2 for baseline processes of each team follows.

#### 11.3.2 Texas Instruments / Raytheon / Sanders

Primary issues at TI on Task 4.E were implant uniformity and nitride alignment issues. Experiments were conducted using a rotation half-way through the implant which gave improved uniformity at post-contact. The nitride alignment problem permitted etching into the channel in some areas of a wafer depending on the alignment errors. This leads to degraded FET performance, but more important from a reliability viewpoint, could also lead to poorly passivated devices. These issues will be monitored closely on Phase 2. The TI Phase 2 reticle is large but contains six FET pairs for a fairly good mapping capability. At Raytheon, the main issues on Task 4.E were implant uniformity and gate metal



evaporation run-out. Both will be addressed on Phase 2 as primary areas targeted for improvement. Measurements of Gm at Raytheon Research were faulty; the Gm measurements at the Sudbury pilot line will be verified on Phase 2. The Phase 2 reticle at Raytheon is small and well planned in order to make good use of Task 4.E methodology. Sanders is new to this team and will start Phase 2 without the benefit of Task 4.E experience. They are using some test structures from TI and have a fairly large Phase 2 test reticle.

#### 11.3.3 Hughes / GE / AT&T / M/A COM

Issues remaining at Hughes are gate and/or n+ alignment, recess etch uniformity and nitride passivation effects. Also a result from Phase 1 was a question of FET orientation for best overall performance. Hughes is performing a further evaluation of the effects of orientation with the possibility of switching from V-groove to Dove-tail for increased breakdown voltage. GE concluded Task 4.E with some remaining concerns about their n+ anodic etch methods. GE will not be continuing work with this process under Phase 2. AT&T and M/A COM did not participate in Task 4.E. The Phase 2 reticle for this team will be mostly common, with some areas tailored to foundry specific structures. The reticle is small and has good design for mapping and correlation uses. Minor size variations will result from some foundry modifications and from different Standard Evaluation Circuit sizes.

#### 11.3.4 TRW / Westinghouse

In concluding work on Task 4.E, data on TRW active layer uniformity has been reviewed and comments provided to TRW. It appears that implant or implant anneal may be contributing a consistent gradient. This will be a subject of study under Phase 2. Westinghouse is new to this team and will use the same basic test reticle design as TRW. The reticle will be fairly large but should have adequate mapping and correlation capability. The same basic TRW reticle will be adapted for several base-line processes including HEMT devices.

#### 11.4 Task 4.E Overview

The following is extracted from the GOMAC 1991 paper (Publ. No. 107 in the List of Publications) to provide additional information on the results and methodology on Task 4.E. The following authors contributed to that paper: J. M. King, R. D. Worley, J. R. Sizelove, J. K. Gillespie, T. K. Krueger, R. A. Niedhard, J. L. Brown, S. E. Cummins, and D. C. Look.

##### 11.4.1 Introduction

Task 4.E of the DARPA/Tri-service GaAs microwave and millimeter wave integrated circuits (MIMIC) program employed a DoD-provided high density test reticle for periodic 3-inch-wafer processing by six contractor foundries: Hughes Aircraft, GE, Raytheon, TI, TRW, and ITT. This task provided a high resolution instrument with which to examine substrate quality and wafer process control and promote individual and general wafer processing improvements through DoD, NIST, and contractor data analysis.

##### 11.4.2 Program Methodology

Data originated from a common 4- x 4.5 -mm test-structure reticle repeated some 200 times per wafer and a standardized set of mid- and post-process test procedures. Bare substrates (two per lot), processed wafers (six lots of four wafers each) and all test data were delivered to the Air Force. The reticle contains arrays of orthogonal field effect transistors (FET) pairs (10- and 200- $\mu$ m gate width), Van der Pauw patterns, and TLMs along with standard process control monitor (PCM) structures and a MMIC. Whole wafer testing was conducted on substrates, and during wafer processing (DC tests) at four critical steps. In addition, on-wafer RF testing provided S-parameters at 2 and 4 GHz. Table 11-1 is an abbreviated list of characteristics and test times. The Air Force received and retested wafers to validate data and procedures, extracted equivalent circuit parameters in closed form, and entered all information into a single data base. Approximately 200 characteristics at an average density of 1200 points per wafer were available for analysis.

Table 11-1. Measurements and Test Times

Char/Step	S	O	R	G	F
EL2, EPD, OBS	*				
$\rho$ , $\mu_H$ , Rsh, ns		*			
$I_{sat}$ , $R_{ds}$		*	*	*	*
$I_{ds}$ , $R_s$ , $R_d$ , $G_m$ , $V_{po}$				*	*
$R_g$ , $V_{sat}$ , $V_{dg}$ , $V_{gs}$			*	*	*
Leakage current		*			*
Backgating, Mobility					*
Doping Profile	*				*
$R_c$ , Rsh		*	*		
Sheet Res, Litho	*				*
Cap, Alignment					*
S-Parameters, ECPs 2 & 4 GHz, closed form ECP					

Notes: S=substrate, O=post-Ohmic, R=post-recess,  
G=post-gate metal, F=post-final front side

Table 2. Wafer Process Related Problems

Substrate Variations	*Implant Gradients
Furnace Annealing	Ohmic Anneal Gradients
N+ Anodic Etching	Orientation (C, R, G, F)
*Channel Recess	*Localized Etch Rate
*Gate Deposition	Mask Alignment
*Nitride Deposition	Breakdown Voltage
Transconductance	RTA Variations
Plated metal	*Localized Test Effects

### 11.4.3 Results by Process Step

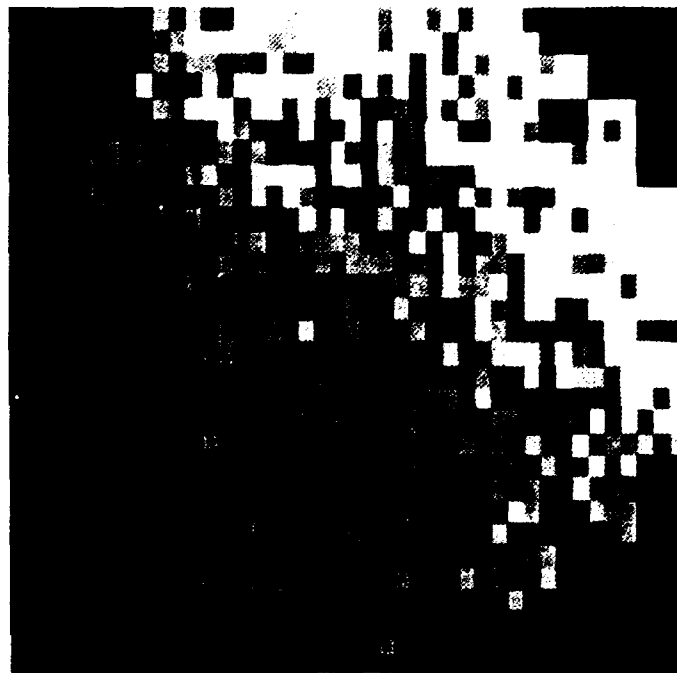
Table 11-2 lists some problem issues encountered during the course of the program. Some are anomalous artifacts of the structures and testing<sup>92</sup> but most are valid representatives of fundamental yield-limiting process problems. Asterisk marked examples will be discussed in this paper.

#### 11.4.3.1 Materials

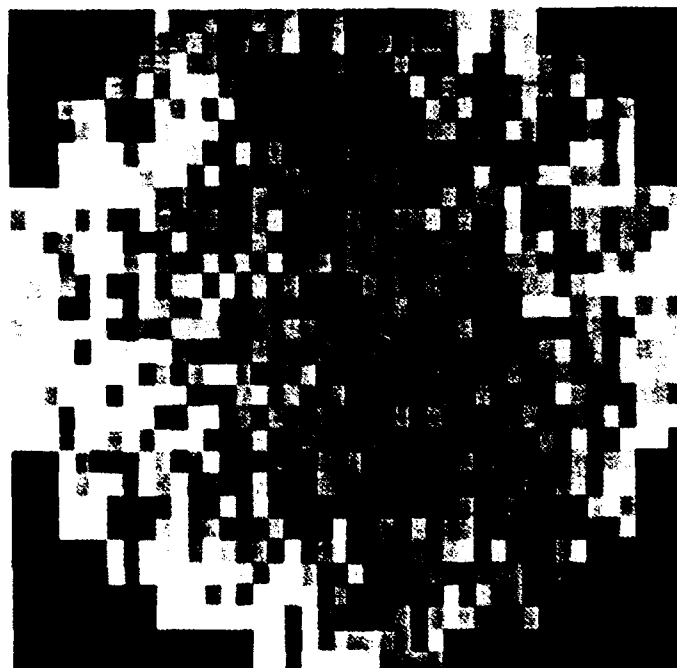
Task 4.E included substrates from eight sources: Airtron, M/A-Com, Spectrum, TI, AT&T, Dowa, Mitsubishi, and Sumitomo. Basic DoD materials characterization on each of two test wafers per process lot consisted of whole wafer mapping ( $>16000$  points) of the deep donor density, EL2; the etch pit density, EPD<sup>2</sup>; and the optical back scattering intensity, OBS. Also, 11 samples across a horizontal diameter were cut for Hall effect measurements. Large differences were observed in these quantities for different manufacturers; for example, Spectrum wafers always showed very low OBS. Many of the wafers displayed very high and nonuniform EPD ( $>100,000 \text{ cm}^{-2}$ , median), but further analysis will be necessary to determine if device uniformity was worse for these materials. For some wafers, when processing was very good, material-induced fourfold patterns in device parameters were clearly evident. As an overall evaluation, however, the materials-related nonuniformities are minimal compared to the process-related nonuniformities for most present-day device fabrication lines<sup>93</sup>.

#### 11.4.3.2 Post-Contact

Measurements and maps at Ohmic or post-contact (C) generally reveal active layer (MBE or ion implanted) and contact metal uniformity. Mapping of  $I_{ds}$ -C shows that most implanted active layers have a gradient resulting from the particular wafer tilt and rotation during implantation (Figure 11-1a). To reduce this effect, one company experimentally rotated wafers  $180^\circ$  after one-half implant dose.  $I_{ds}$ -C symmetry improved (Figure 11-1b, same scale), sometimes with the addition of a mirror plane on the rotated wafer. More elaborate methods are described in the literature<sup>94</sup> but this simple rotation appears to help, and this company is planning its standard use. Other process improvements implemented as a result of post-contact data investigations are annealing furnace configuration redesigns, adjustments to rapid thermal anneal process, and improvements in N+ layer removal methods.



**a**



**b**

Figure 11-1. (a) Map of Ids-C after standard implant, gradient lower-left to upper-right, (b) rotated wafer.

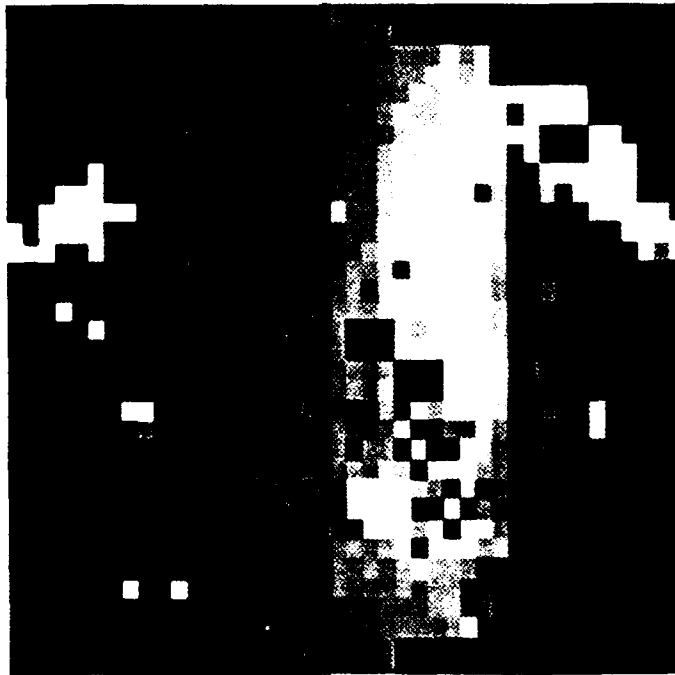
#### 11.4.3.3 Post-Recess

The channel recess-etch process step (R), although intended, in part, to be a fine tuning adjustment to the FET current, has been a major contributor to wafer variations and processing errors. On initial 4.E lots, two companies used manual wafer submersion as a standard etching method. Dramatic evidence of across-wafer variations and discontinuities resulted. Both companies converted to spray etch techniques and subsequent lots show consistent improvements in uniformity. Figure 11-2 shows a comparison of prior (manual) and later (spray) etch results from the same process line. The data sets map over the same grey scale. Map discontinuities can result when partial dipping is used to compensate for apparent gradients revealed from several recess monitor locations. Repeatable improvements due to spray etching have been reported elsewhere.<sup>95</sup>

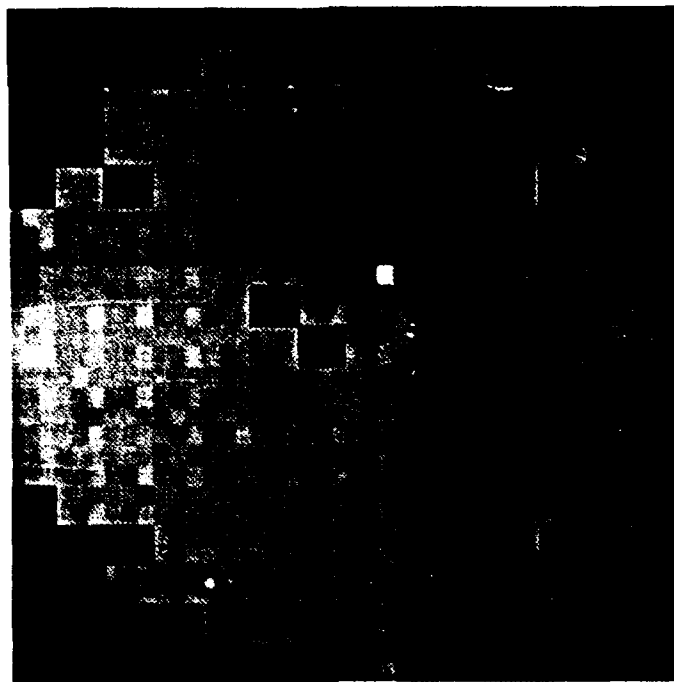
Etch rates can also be affected by local chemistry (e.g., the use of open metal probe pads or nearness of MMICs). Open pads (neighboring TLMs as opposed to Van der Pauw patterns with covered pads) had a strong effect on etch rates for one company. In Figure 11-3a Ids-R data are ranked by percentile and plotted by magnitude. The separation by location is obvious. Another localized effect, in this case due to testing, is illustrated in Figure 3b where FET source inductance data are mapped. FETs adjacent to MMICs create a checkerboard pattern due to capacitive coupling between probes and MMICs during RF testing.

#### Post-Gate

Data taken at post-gate (G) provide the first measurement of complete FET characteristics. These data illustrate the effects of subsequent processing (e.g., nitride deposition) and directly measure FET symmetry through parasitic resistances and breakdown voltages. In typical recessed-gate FET processes, photoresist is opened by optical or E-beam lithography and the recess etch is performed. After etch the gate metal is deposited by evaporation. Since the resist opening is narrow, and undercut for lift-off, deposition shadowing can affect the exact placement of the gate. The Task 4.E reticle, with orthogonal FET pairs, provides an excellent tool for evaluating these and other orientation and spatially dependent processes. Gate metal placement has a strong effect on breakdown voltages from gate to source ( $V_{gs}$ ) and gate to drain ( $V_{gd}$ ). One convenient way to look at this effect is to map the difference  $V_{gs} - V_{gd}$ , i.e., the

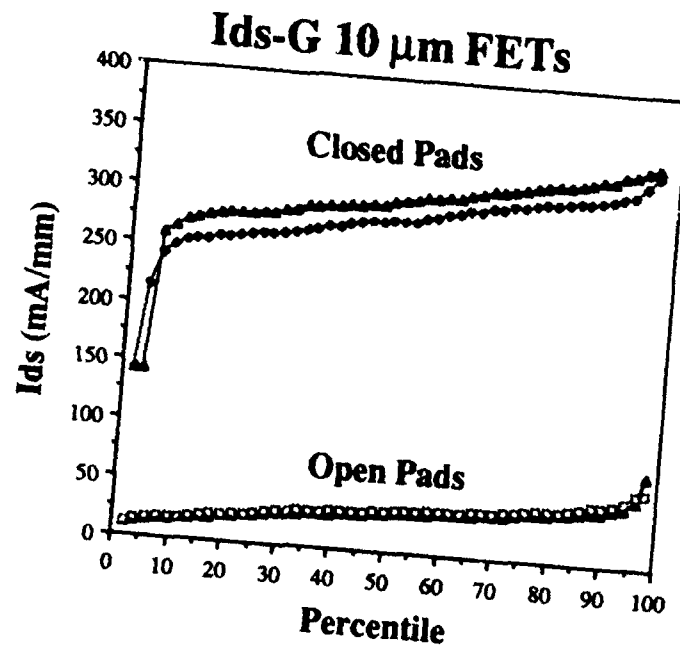


**a**

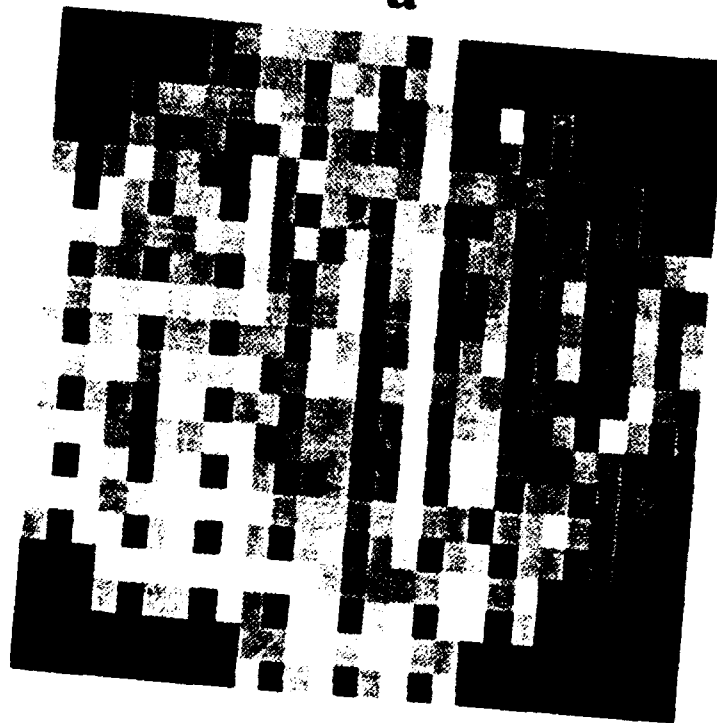


**b**

Figure 11-2. Map of Ids-R for Dip-etched wafer (a), Spray-etched wafer (b) on same grey scale.



**a**



**b**

Figure 11-3. (a) Percentile plot illustrating local etch effects, (b) wafermap illustrating local testing effects.



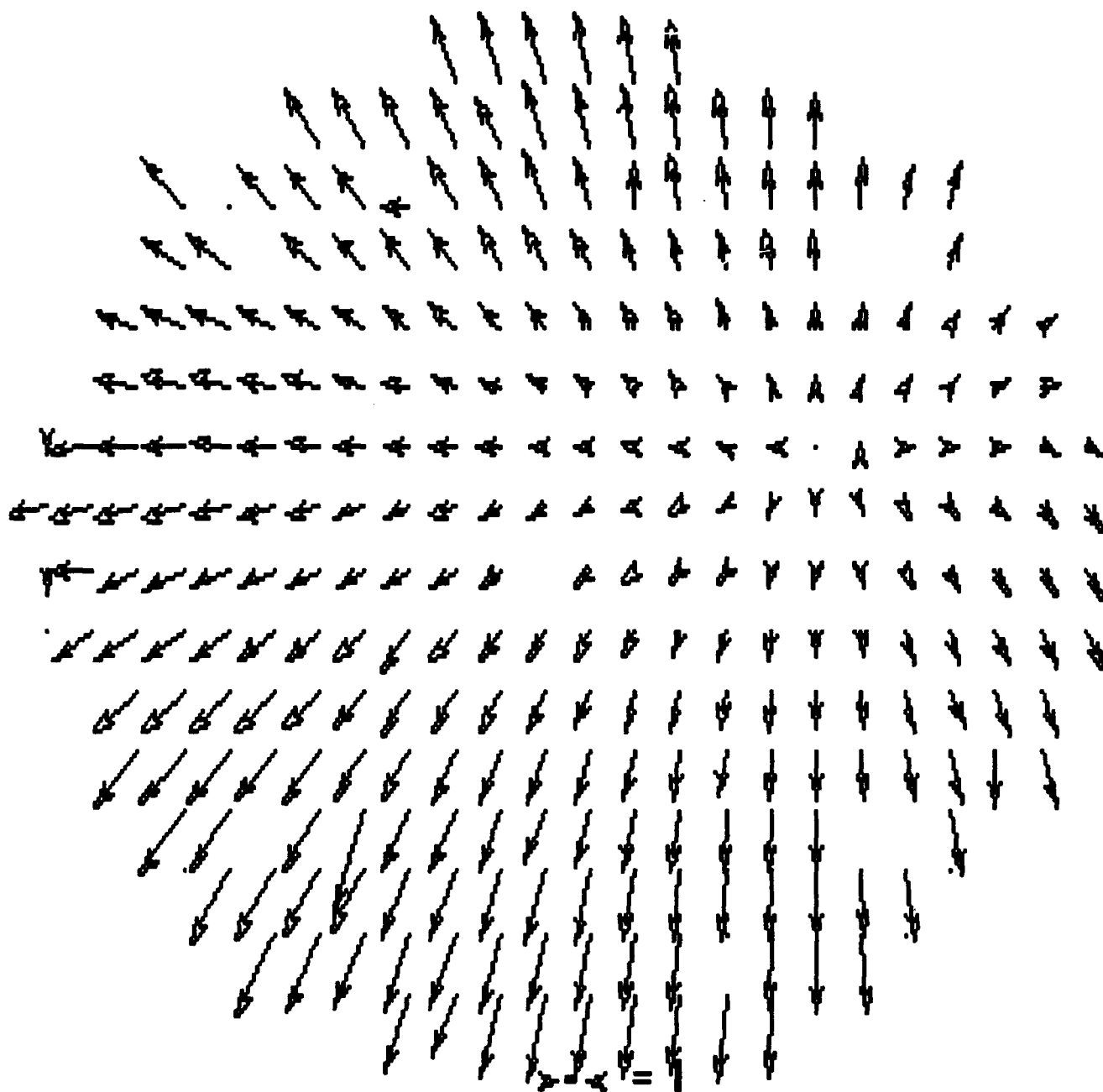


Figure 11-4. Vector map of breakdown voltage variation.

FET symmetry as a function of location on the wafer. The vertically oriented FET is sensitive to horizontal gate alignment and the horizontal FET to vertical alignment. A vector plot using breakdown voltage differences as components is shown in Figure 11-4 for an E-beam processed wafer of symmetrical FETs. The pattern clearly shows the evaporation shadowing effect and the slightly off-center position of the perpendicular to the evaporaton source. The same technique is used to study channel alignment between source and drain by use of the FET parasitic resistances,  $R_s$  and  $R_d$ <sup>96, 97</sup> Our experience shows that the breakdown voltages are most sensitive to the positioning of the gate metal within the channel, while the FET resistances are more sensitive to the channel placement with respect to source and drain.

#### 11.4.3.4 Final DC

More complete testing occurs at final frontside (F), after nitride and thick metal deposition; here most PCM testing and all DoD retesting occur. A good measure of wafer passivaton can be obtained by comparing F vs. G data-sets. Typically, with good quality nitride, the breakdown voltage will drop by less than 10%. FET  $I_{dss}$  will change slightly due to nitride stress effects. Vertical FET (V-groove etch)  $I_{ds}$  generally increases and horizontal FET (dovetail etch)  $I_{ds}$  decreases by a smaller amount. Pinch-off voltage changes correspondingly, while  $G_m$ , though quite sensitive to the nitride process, may vary erratically. Figure 11-5 illustrates changes in  $I_{ds}$  by orientation due to nitride for seven process lines studied. These changes are typical for each line but exceptions occasionally occur. A number of factors affect these changes, including pre-clean etching and nitride stress. Final DC data are important for a number of ongoing correlation studies attempting to predict RF performance from FET DC and PCM data taken inexpensively and early during wafer process.

#### 11.4.3.5 RF - S-parameters, ECPs, MMIC Data

S-parameter data were taken at 2 and 4 GHz for horizontal and vertical 200- $\mu$ m MESFETs (approximately 1200 each orientation per wafer).  $R_g$  was determined using a DC gate length bridge test structure.  $R_s$  and  $R_d$  were determined using DC end-resistance measurements. The intrinsic equivalent circuit model of the FET was then extracted using analytical equations for the seven bias dependent intrinsic model parameters,  $G_m$ ,  $C_{gs}$ ,  $C_{gd}$ ,  $C_{ds}$ ,  $t$ ,  $R_i$ ,  $R_{ds}$ <sup>98</sup>. The RF extrinsic transconductance,  $G_m$ , was determined by converting the measured S-parameters to Y-parameters,  $G_{mextr}$  is the real part

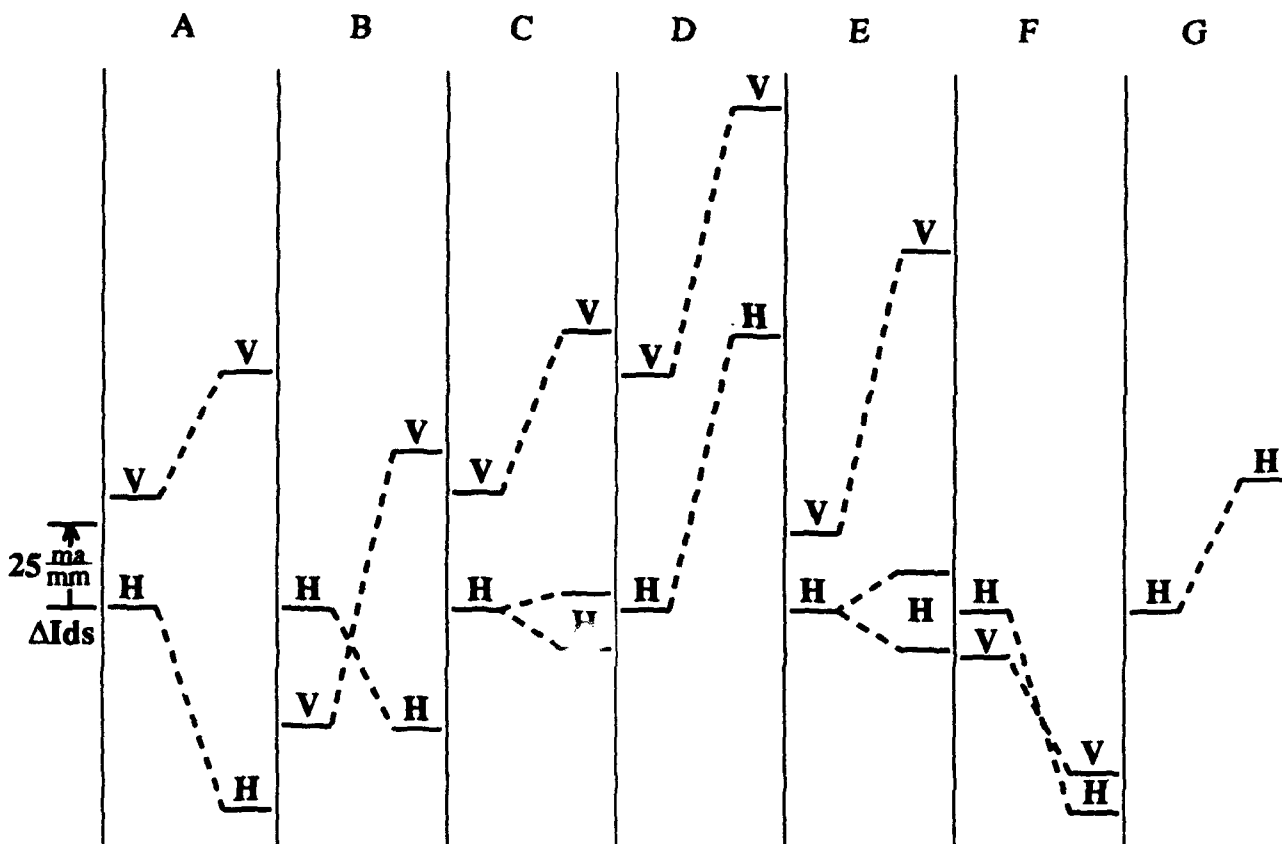


Figure 11-5. Change in  $I_{ds}$  (V vs. H) occurring between post-gate and final DC testing for seven process lines.

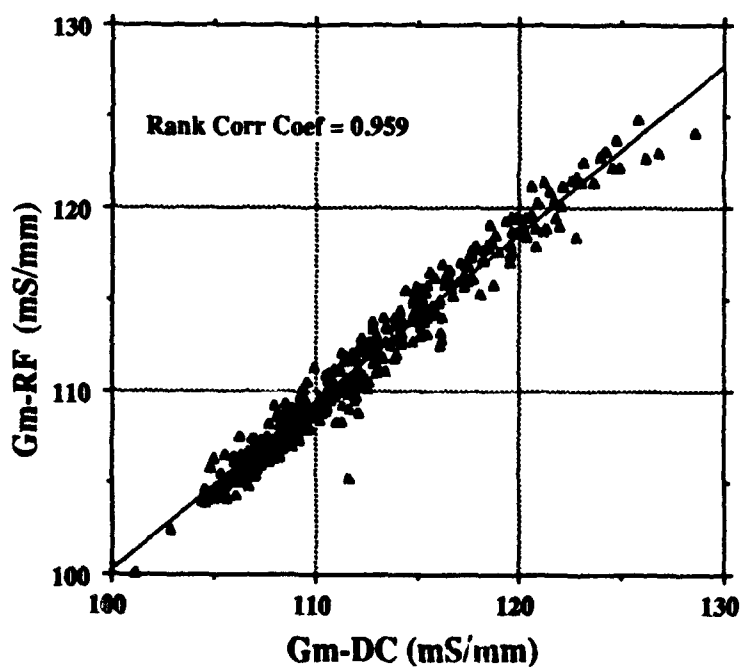


Figure 11-6. Correlation plot of  $G_m$ -RF vs.  $G_m$ -DC.

of  $Y_{21}$ . The RF extrinsic  $G_m$  was found to correlate and give similar absolute values compared to  $G_m$ -DC when measured properly at the same bias condition (Figure 11-6). FET S-parameters, ECPs, MMIC S-parameters, measured gain and noise figure values (where available) are the subject of on-going sensitivity and yield studies to relate variations in device and circuit RF performance to fundamental properties of the GaAs substrates and nonuniformities in wafer processing<sup>99</sup>.

#### 11.4.4 Summary Results

As a result of this program a number of process monitoring test structures have been carefully evaluated<sup>99</sup> and new data analysis techniques have been developed and applied successfully. The use of GaAs process modeling and the application of sensitivity analysis to relate MIMIC performance to substrate and wafer processing issues has advanced significantly.<sup>100</sup> Through the course of this program all participating companies have implemented improvements in response to initial wafer processing deficiencies. In Figure 11-7 a set of box-plots ( $I_{ds}$ -F) for one company's wafers illustrates representative improvements in process control and uniformity made during Task 4.E .

#### 11.4.5 Conclusions/Recommendations

The benefits of high resolution testing for substrate and wafer process evaluation and improvement have been demonstrated. A key element is the orthogonal FET pair at a density sufficient for mapping to resolve variations across a wafer. While all process lines use one preferred FET orientation, the orthogonal pair provides additional useful information on a variety of alignment issues, passivation effects, and other orientation related characteristics. The number of FET pairs could be reduced, and a single size (200  $\mu$ m) would suffice in most cases. Testing, also, could be reduced; post-recess testing could be dropped with only minimal information loss. A minimum density for satisfactory mapping is about 700 FETs per 3-inch wafer. PCM data could be taken at reduced density (approx 200 per wafer) and still provide useful statistical and spatial information. Test conditions should match individual FET designs and processes, and DC testing should reflect biasing for RF operation. The adoption of the DoD test reticle by a number of companies for internal process improvement studies indicates the recognition of these benefits. The trend for the future should be toward reduced density and testing, while permitting continued

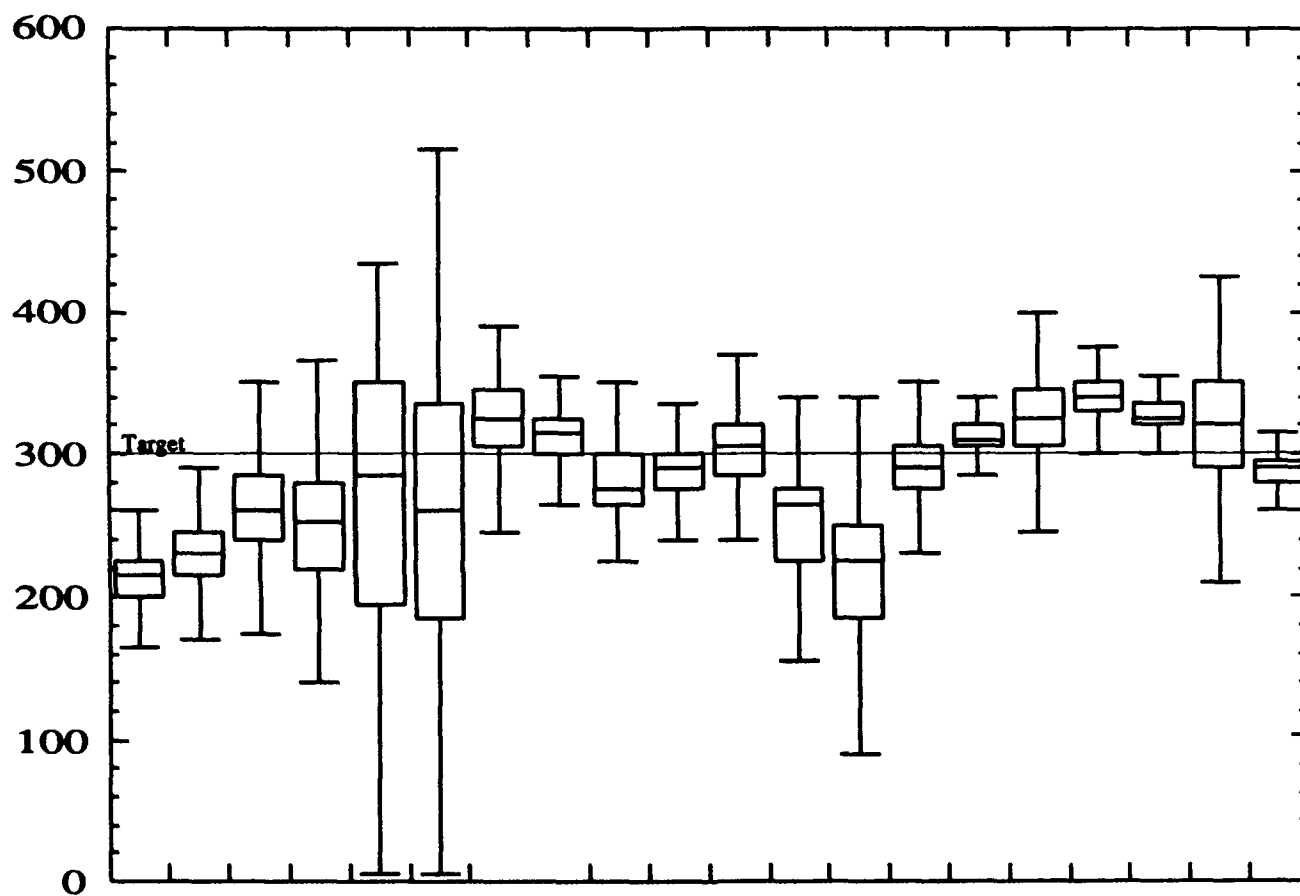


Figure 11-7. Ids-F (mA/mm) boxplots of six lots for one process line.

use of the most valuable structures and methods. A compromise must be made to avoid sacrificing too much wafer area or testing expense while retaining the benefits of general use of these process evaluation methods. A most important point is that many of the problems recognized would have gone undetected (except as a general yield loss) without the high density mapped data of this program.

### References

1. W. Ford, G. Mathur, D. Look, and P.W. Yu, in Semi-Insulating III-V Compounds, Hakone, 1986, ed. by H. Kukimoto and S. Miyazawa (Omsa, Tokyo, 1986) p. 227.
2. J.M. Woodall and J.F. Woods, Solid State Commun. **4**, 33 (1966).
3. D.C. Look, in Semiconductors and Semimetals, ed. by R.K. Willardson and A.C. Beer (Academic, New York, 1983), Vol. 19, p. 93.
4. D.V. Lang, Inst. Phys. Conf. Ser. **31**, 70 (1977), and references cited therein.
5. D. Pons and J.C. Bourgoin, J. Phys. C **18**, 3839 (1985), and references cited therein.
6. S. Loualiche, G. Guillot, A. Nouailhat, and J. Bourgoin, Phys. Rev. B **26**, 7090 (1982).
7. D.V. Lang, J. Appl. Phys. **45**, 3023 (1974).
8. D. Stievenard, X. Boddaert, and J.C. Bourgoin, Phys. Rev. B **34**, 4048 (1986).
9. S. Loualiche, A. Nouailhat, G. Guillot, and M. Lannoo, Phys. Rev. B **30**, 5822 (1984).
10. G.A. Baraff and M. Schluter, Phys. Rev. Lett. **55**, 1327 (1985).
11. G.A. Baraff and M. Schluter, Phys. Rev. B **33**, 7346 (1986).
12. J.W. Farmer and D.C. Look, J. Appl. Phys. **50**, 2970 (1979).
13. N. Braslau, J. Vac. Sci. Technol. **A4**, 3085 (1986).
14. H.H. Berger, Solid-State Electron **15**, 145 (1972).
15. G.K. Reeves and H.B. Harrison, IEEE Electron Device Lett. **EDL-3**, 111 (1982).
16. D.C. Look, IEEE Electron Device Lett. **EDL-8**, 162 (1987).
17. M.D. Feuer, IEEE Trans. Electron Devices **ED-32**, 7 (1985).
18. D.D. Cohen, T.S. Kalkur, G.J. Sutherland, and A.G. Nassibian, J. Appl. Phys. **60**, 3100 (1986).
19. F.W. Smith, A.R. Calawa, C.-L. Chen, M.J. Manfra, and L. J. Mahoney, IEEE Electron Device Lett. **EDL-9**, 77 (1988).
20. M.J. Delaney, C.S. Chou, L.E. Larson, J.F. Jensen, D.S. Deakin, A.S. Brown, W.E. Hooper, M.A. Thompson, L.G. McCray, and S.E. Rosenbaum, IEEE Electron Device Lett. **EDL-10**, 355 (1989).
21. A.S. Brown, U.K. Mishra, C.S. Chou, C.E. Hooper, M.A. Melendes, M. Thompson, L.E. Larson, S.E. Rosenbaum, and M.J. Delaney, IEEE Electron Device Lett. **EDL-10**, 565 (1989).

22. B. J-F. Lin, C.P. Kocot, D.E. Mars, and R. Jaeger, *IEEE Trans. on Electron Devices* **37**, 46 (1990).
23. M.Y. Frankel, J.F. Whitaker, G.A. Mourou, F.W. Smith, and A.R. Calawa, *IEEE Trans. on Electron Devices* **37**, 2493 (1990).
24. P.M. Solomon, S.L. Wright, and F.J. Canora, *IEEE Electron Device Lett.* **12**, 117 (1991).
25. M. Kaminska, Z. Liliental-Weber, E.R. Weber, T. George, J. B. Kortright, F.W. Smith, B-Y. Tsaur, and A.R. Calawa, *Appl. Phys. Lett.* **54**, 1881 (1989).
26. M. Kaminska, E.R. Weber, Z. Liliental-Weber, R. Leon, and Z.U. Rek, *J. Vac. Sci. Technol. B* **7**, 710 (1989).
27. M.O. Manasreh, D.C. Look, K.R. Evans, and C.E. Stutz, *Phys. Rev. B* **41**, 10272 (1990).
28. D.C. Look, D.C. Walters, M.O. Manasreh, J.R. Sizelove, C.E. Stutz, and K.R. Evans, *Phys. Rev. B* **42**, 3578 (1990).
29. M.R. Melloch, N. Otsuka, J.M. Woodall, A.C. Warren, and J.L. Freeouf, *Appl. Phys. Lett.* **57**, 1531 (1990).
30. A.C. Warren, J.M. Woodall, J.L. Freeouf, D. Grischkowsky, M.R. Melloch, and N. Otsuka, *Appl. Phys. Lett.* **57**, 1331 (1990).
31. C.R. Wie, K. Xie, D.C. Look, K.R. Evans, and C.E. Stutz, in Semi-Insulating III-V Materials, Toronto, 1990, ed. by A. Milnes and C.J. Miner (Adam Hilger, Bristol, 1990) p. 71.
32. D.C. Look, C.E. Stutz, and K.R. Evans, *Appl. Phys. Lett.* **57**, 2570 (1990).
33. H. Yamamoto, Z-Q. Fang, and D.C. Look, *Appl. Phys. Lett.* **57**, 1537 (1990).
34. B.R. Nag, Electron Transport in Compound Semiconductors (Springer - Verlag, Berlin, 1980).
35. J.D. Wiley, in Semiconductors and Semimetals, Vol. 10, ed. by R.K. Willardson and A.C. Beer (Academic, New York, 1975), Ch. 2.
36. N.F. Mott and H. Jones, The Theory of the Properties of Metals and Alloys (Dover, New York, 1958).
37. H. Brooks (unpublished).
38. L. Makowski and M. Glicksman, *J. Phys. Chem. Solids* **34**, 487 (1973).
39. S. Fujita, S.M. Bedair, M.A. Littlejohn, and J.R. Hauser, *J. Appl. Phys.* **51**, 5438 (1980).
40. A.W. Nelson and P.N. Robson, *J. Appl. Phys.* **54**, 3965 (1983).



41. K. Masu, E. Tokumitsu, M. Konagai, and K. Takahashi, J. Appl. Phys. 54, 5785 (1983).
42. D.C. Look, D.K. Lorange, J.R. Sizelove, C.E. Stutz, K.R. Evans, and D.W. Whitson, J. Appl. Phys. 71, 260 (1992).
43. S. Adachi, J. Appl. Phys. 58, R1 (1985).
44. P.W. Yu and A. Kangarlou, to be published in the Proceeding of the GaAs and Related Compounds Symposium (1992).
45. A. Kangarlou, H. Guerriella, R. Bernez, and P.W. Yu, Appl. Phys. Lett. 59, 2290 (1991).
46. P.W. Yu, D.W. Fischer, and J.R. Sizelove, to be published in Semicond. Sci. Tech. (1992).
47. P.W. Yu, D.C. Look, and W. Ford, J. Appl. Phys. 62, 2960 (1987).
48. D.C. Look, P.W. Yu, W.M. Theis, W. Ford, G. Mathur, J.R. Sizelove, D.H. Lee, and S.S. Li, Appl. Phys. Lett. 49, 1083 (1986).
49. P.W. Yu and H. Kuwamoto, J. Appl. Phys. 70, 954 (1991).
50. P.W. Yu, Phys. Rev. B 42, 11889 (1990).
51. W.C. Mitchel, L.S. Rea, and P.W. Yu, J. Electronic Mat. 18, 209 (1989).
52. W.C. Mitchel, D.W. Fischer, L.S. Rea, and P.W. Yu, Phys. Rev. B 40, 8431 (1989).
53. W.C. Mitchel and P.W. Yu, J. Appl. Phys. 62, 4781 (1987).
54. M. Baemler, J. Schneider, U. Kaurman, W.C. Mitchel, and P.W. Yu, Phys. Rev. B 39, 6253 (1989).
55. P.W. Yu, S. Ravipati, B.E. Taylor, and W.C. Mitchel, J. Appl. Phys. 67, 1471 (1990).
56. S. Ravipati, P.W. Yu, B.E. Taylor, and W.C. Mitchel, SPIE 1286, 66-73 (1990).
57. D.W. Fischer and P.W. Yu, J. Appl. Phys. 59, 1952 (1986).
58. W.C. Mitchel, G.L. Brown, D.W. Fischer, P.W. Yu, and J.E. Lang, J. Appl. Phys. 62, 2320 (1987).
59. P.W. Yu, D.C. Walters, and W.C. Mitchel, J. Appl. Phys. 60, 3864 (1986).
60. M.C. Ohmer, W.C. Mitchel, G.A. Graves, D.E. Holmes, H. Kuwamoto, and P.W. Yu, J. Appl. Phys. 64, 2775 (1988).
61. D.C. Reynolds, K.K. Bajaj, C.W. Litton, J. Singh, C.K. Peng and H. Morkoc, Appl. Phys. Lett. 48, 727 (1986).
62. D.C. Reynolds, K.K. Bajaj, C.W. Litton, P.W. Yu, D. Huang, J. Klem, and H.

- Morkoc, J. Appl. Phys. 60, 1767 (1986).
63. C.W. Litton, L.W. Kapitan, P.W. Yu, and D.C. Look, SPIE 796, 32 (1987).
  64. P.W. Yu, C.K. Peng and H. Morkoc, J. Appl. Phys. 65, 2427 (1989).
  65. P.W. Yu, C.K. Peng and H. Morkoc, Appl. Phys. 54, 1546 (1989).
  66. K.R. Evans, C.E. Stutz, P.W. Yu and C.R. Wie, J. Vac. Sci. Technol. B 8, 271 (1990).
  67. W.T. Masselink, Y.C. Chang, H. Morkoc, D.C. Reynolds, C.W. Litton, K.K. Bajaj and P.W. Yu, Solid-State Electronics 39, 205 (1986).
  68. K.K. Bajaj, D.C. Reynolds, C.W. Litton, J. Singh, P.W. Yu, W.T. Masselink, R. Fischer, and H. Morkoc, Solid-State Electronics 29, 315 (1986).
  69. D.C. Reynolds, K.K. Bajaj, C.W. Litton, J. Singh, P.W. Yu, P. Pearah and H. Morkoc, Phys. Rev. B 33, 5931 (1986).
  70. D.C. Reynolds, K.K. Bajaj, C.W. Litton, R.L. Greene, P.W. Yu, C.K. Peng and H. Morkoc, Phys. Rev. B 35, 4515 (1987).
  71. D.C. Reynolds, K.K. Bajaj, G. Peters, W.M. Theis, P.W. Yu and H. Morkoc, Phys. Rev. B 37, 7133 (1988).
  72. D.C. Reynolds, K.G. Merkel, C.E. Stutz, K.R. Evans, K.K. Bajaj and P.W. Yu, Phys. Rev. B 43, 1604 (1991).
  73. D.C. Reynolds, K.R. Evans, C.E. Stutz, K.K. Bajaj and P.W. Yu, Phys. Rev. B 44, 8869 (1991).
  74. B. Jogai and P.W. Yu, Phys. Rev. B 41, 12650 (1990).
  75. D.C. Reynolds, K.R. Evans, C.E. Stutz, and P.W. Yu, Phys. Rev. B. 44, 1839 (1991).
  76. P.W. Yu, D.C. Reynolds, K.K. Bajaj, C.W. Litton, J. Singh, C.K. Peng, T. Henderson, and H. Morkoc, Solid State Commun. 58, 37 (1986).
  77. P.W. Yu, D.C. Reynolds, K.K. Bajaj, C.W. Litton, J. Klem, D. Huang and H. Morkoc, Solid State Commun. 62, 41 (1987).
  78. P.W. Yu, G.D. Sanders, D.C. Reynolds, K.K. Bajaj, C.W. Litton, J. Klem, D. Huang and H. Morkoc, Phys. Rev. B 35, 9280 (1987).
  79. P.W. Yu, G.D. Sanders, K.R. Evans, D.C. Reynolds, K.K. Bajaj, C.E. Stutz, and R.L. Jones, Phys. Rev. B 38, 7796 (1988).
  80. P.W. Yu, G.D. Sanders, K.R. Evans, D.C. Reynolds, C.E. Stutz, and R.L. Jones, J. Vac. Sci. Tech. B 6, 6491 (1988).
  81. P.W. Yu, G.D. Sanders, K.R. Evans, K.K. Bajaj, C.E. Stutz, and R.L. Jones, Superlattices and Microstructures 4, 281 (1988).

82. P.W. Yu, G.D. Sanders, K.R. Evans, D.C. Reynolds, K.K. Bajaj, C.E. Stutz, and R.L. Jones, *Phys. Rev. B* 40, 3151 (1989).
83. P.W. Yu, G.D. Sanders, K.R. Evans, D.C. Reynolds, K.K. Bajaj, C.E. Stutz, and R.L. Jones, *Appl. Phys. Lett.* 54, 2232 (1989).
84. P.W. Yu, D.C. Reynolds, G.D. Sanders, K.K. Bajaj, C.E. Stutz, and K.R. Evans, *Phys. Rev. B* 43, 4344 (1991).
85. J.E. Schirber, I.J. Fritz, and L.R. Dawson, *Appl. Phys. Lett.* 46, 187 (1985).
86. G.C. Osbourn, *Superlattices and Microstructures* 1, 223 (1985).
87. I.J. Fritz, T.J. Drummond, G.C. Osbourn, J.E. Schirber, and E.D. Jones, *Appl. Phys. Lett.* 48, 1678 (1986).
88. R.L. Greene and K.K. Bajaj, *Phys. Rev. B* 37, 4604 (1988).
89. M.S. Skolnick, A.K. Jain, R.A. Stradling, J.C. Ousset,, and S.A. Skenasy, *J. Phys. C* 9, 2809 (1976).
90. R.L. Greene and K.K. Bajaj, *Solid State Commun.* 53, 1103 (1985).
91. R.C. Miller, A.C. Gossard, W.T. Tsang, and O. Munteanu, *Solid State Commun.* 43, 519 (1982).
92. C.E. Schuster, L.W. Linholm, J.K. Gillespie, 1991 GOMAC Digest, p. 335.
93. D.C. Look, D.C. Walters, R.T. Kemerley, J.M. King, M.G. Mier, J.S. Sewell, J.S. Sizelove, *J. Electronic Materials* 18, 487 (1989).
94. N. Uchitomi, H. Mikami, and N. Toyoda, *J. Appl. Phys.* 67, 4042 (1990).
95. D.C. Wang, E. T-S. Pan, and W.D. Gray, *Proceedings 1991 U.S. GaAs MANTECH Conference*, p. 64.
96. M. Mah, J. King, R. Worley, J. Gillespie, R. Heidhard, J. Hwang, and W. Melvin, 1990 GaAs IC Symposium Digest, p. 313.
97. S.E. Cummins, J.R. Sizelove, P.D. Mumford, M.Y. Mah, 1991 GOMAC Digest, p. 301.
98. R. Anholt, R. Worley, and R. Neidhard, *J. Microwave and mmW CAD* 1, 263 (1991).
99. R. Anholt, J. King, R. Worley, and J. Gillespie, *J. Microwave and mmW CAD* 1, 271 (1991).
100. R. Anholt, 1991 GOMAC Digest, p.339.

## LIST OF PUBLICATIONS

Contract F33615-86-C-1062  
29 September 1986 - 23 December 1991  
Wright State University

1. W. Ford, G. Mathur, D. Look, and P.W. Yu, "Thermal Cycling of Electrical Properties in GaAs" in Semi-Insulating III-V Materials, Hakone, Japan, 1986 (North-Holland, Amsterdam, 1986) p. 227.
2. D.C. Look, P.W. Yu, W.M. Theis, W. Ford, G. Mathur, D.H. Lee, and S.S. Li, "Semiconducting/Semi-insulating Reversibility in Bulk GaAs," *Appl. Phys. Lett.* **49**, 1083 (1986).
3. W.T. Masselink, Y.C. Chang, H. Morkoc, D.C. Reynolds, C.W. Litton, K.K. Bajaj, and P.W. Yu, "Shallow impurity levels in AlGaAs/GaAs semiconductor quantum wells," *Solid State Elect.* **39**, 205(1986).
4. K.K. Bajaj, D.C. Reynolds, C.W. Litton, J. Singh, P.W. Yu, W.T. Masselink, R. Fischer, and H. Morkoc, "High resolution photoluminescence studies of GaAs/GaAlAs multi-quantum-well structures grown by molecular beam epitaxy," *Solid State Elect.* **29**, 315(1986).
5. D.W. Fischer and P.W. Yu, "Infrared absorption and photoluminescence of defect levels in the 204- to 255-meV range in p-type GaAs," *J. Appl. Phys.* **59**, 1952(1986).
6. P.W. Yu, D.C. Reynolds, K.K. Bajaj, C.W. Litton, J. Singh, C.K. Peng, T. Henderson, and H. Morkoc, "Photovoltaic spectra of undoped GaAs-AlGaAs multiple quantum well structures: Correlation with photoluminescence," *Solid State Commun.* **58**, 37(1986).
7. D.C. Reynolds, K.K. Bajaj, C.W. Litton, P.W. Yu, J. Klem, C.K. Peng, and H. Morkoc, "Excitonic photoluminescence linewidths in AlGaAs grown by molecular beam epitaxy," *Appl. Phys. Lett.* **48**, 727(1986).
8. P.W. Yu, D.C. Reynolds, K.K. Bajaj, C.W. Litton, J. Singh, C.K. Peng, T. Henderson, and H. Morkoc, "Summary abstract: A comparative study of photovoltaic and photoluminescence spectra of undoped GaAs-AlGaAs multiple quantum well structures grown by molecular beam epitaxy," *J. Vac. Sci. Technol. B* **4**, 554(1986).
9. D.C. Reynolds, C.W. Litton, K.K. Bajaj, P.W. Yu, J. Singh, P.J. Pearah, W.T. Masselink, T. Henderson, J. Klem, and H. Morkoc, "Summary abstract: Optical properties of AlGaAs grown by molecular beam epitaxy," *J. Vac. Sci. Technol. B* **4**, 523(1986).
10. D.C. Reynolds, K.K. Bajaj, C.W. Litton, J. Singh, P.W. Yu, P. Pearah, and H. Morkoc, "High-resolution photoluminescence and reflection studies of GaAs-AlGaAs multiple-quantum-well structures grown by molecular beam epitaxy: Determination of microscopic structural quality of interfaces," *Phys. Rev. B* **33**, 5931(1986).

11. D.C. Reynolds, K.K. Bajaj, C.W. Litton, P.W. Yu, D. Huang, J. Klem, and H. Morkoc, "Magnetic and field splitting of the emission lines in the 1.5040–1.5110 eV range," *J. Appl. Phys.* **60**, 1767(1986).
12. D.C. Reynolds, K.K. Bajaj, C.W. Litton, G. Peters, P.W. Yu, R. Fischer, D. Huang, and H. Morkoc, "Lifetimes, ionization energies, and discussion of the emission lines in the 1.5040–1.5110-eV range in GaAs," *J. Appl. Phys.* **60**, 2511(1986).
13. P.W. Yu, D.C. Walters, and W.C. Mitchel, "Photoluminescence determination of effects due to In in In–alloyed semi–insulating GaAs," *J. Appl. Phys.* **60**, 3864(1986).
14. D.C. Look, "Electrical Characterization of Ion Implantation into GaAs: Topography and Depth Profiles," *J. Electrochem. Soc.* **134**, 2527 (1987).
15. D.C. Look, W.M. Theis, P.W. Yu, J.R. Sizelove, W. Ford, and G. Mathur, "Reversible Electrical Properties of LEC GaAs," *J. Electronic Materials* **16**, 63 (1987).
16. D.C. Look, T. Henderson, C.K. Peng, and H. Morkoc, "Mobility and Parasitic Resistance Measurements in AlGaAs/GaAs and AlGaAs/InGaAs MODFET Structures," in *GaAs and Related Compounds 1986*, ed. by W.T. Lindley, Inst. of Phys. Conf. Ser. No. 83 (Inst. of Phys., Bristol, 1987) p. 557.
17. D.C. Look and J.R. Sizelove, "Equivalence of Donor and Acceptor Fits of Temperature–Dependent Carrier Concentration Data," *J. Appl. Phys.* **61**, 1650 (1987).
18. D.C. Look, "Mobility Measurements with a Standard Contact Resistance Pattern," *IEEE Electron Device Lett.* **EDL-8**, 162 (1987).
19. D.C. Look, "Bulk and Contact Electrical Properties by the Magneto Transmission Line Method: Application to GaAs," *Solid–State Electronics* **30**, 615 (1987).
20. D.C. Look, "Equivalence of Donor and Acceptor Fits to Temperature–Dependent Hall Data: General Case," *J. Appl. Phys.* **62**, 3998 (1987).
21. D.C. Look, "High Acceptor Production Rate in Electron–Irradiated GaAs: Impact on Defect Models," *Appl. Phys. Lett.* **51**, 843 (1987).
22. D.C. Look and J.R. Sizelove, "Defect Production in Electron–Irradiated n–type GaAs," *J. Appl. Phys.* **62**, 3660 (1987).
23. D.C. Look, "The Donor Nature of the Main Electron Traps in Electron–Irradiated n–type GaAs," *Solid State Commun.* **64**, 805 (1987).
24. C.W. Litton, L. Kapitan, P.W. Yu, and D.C. Look, "Study and Characterization of Low–Pressure AsH<sub>3</sub> Cracking Cells and Gas–Source MBE Growth of GaAs and (Al, Ga)As," *SPIE Proceedings* **796**, 32, (1987).
25. D.C. Look and E. Pimentel, "Photo–resistivity and Photo–Hall–effect Topography on Semi–insulating GaAs Wafers," *Appl. Phys. Lett.* **51**, 1614 (1987).
26. D.C. Look, D.C. Walters, J. Sizelove, D. D'Agostino, M. Mier, S. Dudley, T. Dundon, and G.L. McCoy, "GaAs Materials/Device Correlation," in *Proc. 1987 U.S. Conf. on GaAs Manufacturing Technology*, ed. by J.V. DiLorenzo, p. 9 (1987).

27. G.L. McCoy, S. Dudley, J. Sizelove, T. Dundon, J. King, S. Labovitz, and D.C. Look, "Observations on the State of the GaAs Processing Technology," in Proc. 1987 U.S. Conf. on GaAs Manufacturing Technology, ed. by J.V. DiLorenzo, p. 37 (1987).
28. L. Peters, L. Phaneuf, L.W. Kapitan, and W.M. Theis, "Non-Contact Doping Level Determination in GaAs Using Photorefectance Spectroscopy," J. Appl. Phys. **62**, 4558 (1987).
29. D.C. Reynolds, K.K. Bajaj, C.W. Litton, G. Peters, P.W. Yu, and J.D. Parsons, "Refractive index  $n$ , and dispersion,  $-dn/d\lambda$  of GaAs at 2K determined from Fabry-Perot cavity oscillation," J. Appl. Phys. **61**, 342(1987).
30. D.C. Reynolds, K.K. Bajaj, C.W. Litton, R.L. Greene, P.W. Yu, C.K. Peng, and H. Morkoc, "Magneto-optical studies of GaAs-AlGaAs multiple-quantum-well structures grown by molecular beam epitaxy," Phys. Rev. B **35**, 4515((1987).
31. K.K. Bajaj, D.C. Reynolds, C.W. Litton, P.W. Yu, C.K. Peng, and H. Morkoc, "Magneto-optical studies of GaAs-AlGaAs multi-quantum-well structures," in GaAs and Related Compounds, 1986, ed. by W.T. Lindley, IOPS Series number 83, 325(1987).
32. P.W. Yu, D.C. Reynolds, K.K. Bajaj, C.W. Litton, J. Klem, D. Huang, and H. Morkoc, "Observation of monolayer fluctuations in the excited states of GaAs-Al<sub>x</sub>Ga<sub>1-x</sub>As multiple-quantum-well structures using photocurrent and reflection spectroscopies," Solid State Commun. **62**, 41(1987).
33. P.W. Yu, G.D. Sanders, D.C. Reynolds, K.K. Bajaj, C.W. Litton, J. Klem, D. Huang, and H. Morkoc, "Determination of transition energies and oscillator strengths in GaAs-AlGaAs multiple quantum wells using photovoltage induced photocurrent spectroscopy," Phys. Rev. B **35**, 9280(1987).
34. P.W. Yu, D.C. Look and W. Ford, "Photoluminescence in electrically reversible (Semiconducting to Semi-insulating) bulk GaAs," J. Appl. Phys. **62**, 2960 (1987).
35. W.C. Mitchel, G.J. Brown, D.W. Fischer, and P.W. Yu, "Characterization of the intrinsic double acceptor in undoped p-type gallium arsenide," J. Appl. Phys. **62**, 2320 (1987).
36. W.C. Mitchel and P.W. Yu, "An antimony related electronic level in isovalently doped bulk GaAs," J. Appl. Phys. **62**, 4781 (1987).
37. P.W. Yu, D.C. Reynolds, K.K. Bajaj, C.W. Litton, J. Klem, D. Huang, and H. Morkoc, "Observation of monolayer fluctuations in the excited states of GaAs-Al<sub>x</sub>Ga<sub>1-x</sub>As multiple-quantum-well structures using photocurrent and reflection spectroscopies," Solid State Commun. **62**, 41 (1987).
38. P.W. Yu, G.D. Sanders, D.C. Reynolds, K.K. Bajaj, C.W. Litton, J. Klem, D. Huang, and H. Morkoc, "Determination of transition energies and oscillator strengths in GaAs-AlGaAs multiple quantum wells using photovoltage induced photocurrent spectroscopy," Phys. Rev. B **35**, 9280 (1987).

39. D.C. Look and J.W. Farmer, "The Type Conversion Phenomenon in Electron-Irradiated GaAs," *J. Phys. and Chem. of Solids* **49**, 97 (1988).
40. D.C. Look, "Contact Resistance Measurements in GaAs MESFET's and MODFET's by the Magneto-TLM Technique," *J. Electrochem. Soc.* **135**, 2054 (1988).
41. D.C. Look, "A Two-layer Magneto-TLM Contact Resistance Model: Application to Modulation-doped FET Structures," *IEEE Trans. on Electron Devices* **35**, 133 (1988).
42. E. Pimentel and D.C. Look, "Resistivity and Hall-effect Topography on Photoexcited Semi-insulating GaAs," *J. Electronic Mat.* **17**, 63 (1988).
43. W.M. Theis, G.D. Sanders, C.E. Leak, K.K. Bajaj, and H. Morkoc, "Electronic Transitions in GaAs/GaAlAs Quantum Wells Observed by Photoreflectance Spectroscopy: Comparison with a First Principles Theory," *Phys. Rev. B* **37**, 3042 (1988).
44. D.C. Reynolds, K.K. Bajaj, C. Leak, G. Peters, W. Theis, P.W. Yu, K. Alavi, C. Colvard, and I. Shidlovsky, "Well Resolved Higher Excited States of the Light- and Heavy-hole Free Excitons in a 225Å AlGaAs Multiple Quantum Well Structure," *Phys. Rev. B* **37**, 3117 (1988).
45. D.C. Reynolds, K.K. Bajaj, G. Peters, C. Leak, W.M. Theis, P. W. Yu, and H. Morkoc, "Correlation Between the Light- and Heavy-hole Free Exciton Fine Structure in AlGaAs-GaAs Multiple Quantum Wells using Photoluminescence Excitation Spectroscopy," *Phys. Rev. B* **37**, 7133 (1988).
46. M.C. Ohmer, W.C. Mitchel, G.A. Graves, D.E. Holmes, H. Kuwamoto, and P.W. Yu, "Thermal properties of semi-insulating GaAs dilutely alloyed with InAs," *J. Appl. Phys.* **64**, 2775 (1988).
47. P.W. Yu, G.D. Sanders, K.R. Evans, D.C. Reynolds, K.K. Bajaj, C.E. Stutz, and R.L. Jones, "Determination of exciton transition energies and oscillator strengths in AlGaAs-GaAs multiple quantum well structures in an electric field using photocurrent spectroscopy," *Superlattices and Microstructures* **4**, 281 (1988).
48. P.W. Yu, G.D. Sanders, K.R. Evans, D.C. Reynolds, K.K. Bajaj, C.E. Stutz, and R.L. Jones, "Summary abstract: Effect of electric field on the exciton transition energies and oscillator strengths of undoped GaAs-AlGaAs quantum well structure determined by photocurrent spectroscopy," *J. Vac. Sci. and Tech B* **6**, 6491 (1988).
49. D.C. Look, "Annealing and Thermal Cycling Effects in Semi-Insulating GaAs," in Semi-Insulating III-V Materials, Malmo, 1988 (IOP, London, 1988) p. 1.
50. D.C. Look, "Magneto-Electric Characterization of Materials and Devices," in Diagnostic Techniques for Semiconductor Materials and Devices, ed. by T.J. Shaffner and D.K. Schroder (Proc. Vol. 88-20, Electrochemical Soc., Pennington, NJ, 1988) p. 221.

51. D.C. Reynolds, K.K. Bajaj, G. Peters, C. Leak, W.M. Theis, P.W. Yu, H. Morkoc, K. Alavi, C. Colvard and I. Shidlovsky, "Deconvolution of the light- and heavy-hole free exciton fine structure in  $\text{Al}_x\text{Ga}_{1-x}\text{As-GaAs}$  multi-quantum wells using photoluminescence excitation spectroscopy," *Superlattice and Microstructures* 4, 723 (1988).
52. P.W. Yu, G.D. Sanders, K.R. Evans, D.C. Reynolds, K.K. Bajaj, C.E. Stutz, and R.L. Jones, "Electric field dependence of exciton transition energies in  $\text{GaAs-AlGaAs}$  quantum wells studied by photocurrent spectroscopy," *Phys. Rev. B* 38, 7796 (1988).
53. D.C. Reynolds, K.K. Bajaj, K. Leak, G. Peters, W. Theis, P.W. Yu, K. Alavi, C. Colvard, and I. Shidlovsky, "Well resolved higher excited states of the light- and heavy-hole excitons in a 225Å  $\text{AlGaAs}$  multiple quantum well structure," *Phys. Rev. B* 37, 3117 (1988).
54. D.C. Reynolds, K.K. Bajaj, G. Peters, W.M. Theis, P.W. Yu, and H. Morkoc, "Correlation between the light- and heavy-hole free exciton fine structures in  $\text{Al}_x\text{Ga}_{1-x}\text{As-GaAs}$  multiple-quantum-well structures using photoluminescence excitation spectroscopy," *Phys. Rev. B* 37, 7133 (1988).
55. D.C. Reynolds and D.C. Look, "Characterization," in Epitaxy of III-V Compound Semiconductors, ed. by R. Malik (North Holland, Amsterdam, 1989) pp. 429-494.
56. D.C. Look, D.C. Walters, J.S. Sewell, S.C. Dudley, M.G. Mier, and J.S. Sizerlove, "A New Technique for Whole-Wafer Etch-Pit Density Mapping in  $\text{GaAs}$ ," *J. Appl. Phys.* 65, 1375 (1989).
57. J.S. Sewell, S.C. Dudley, M.G. Mier, D.C. Look, and D.C. Walters, "Automated and Calibrated Whole-Wafer Etch-Pit Density Measurements in  $\text{GaAs}$ ," *J. Electronic Mat.* 18, 191 (1989).
58. D.C. Look, D.C. Walters, M.G. Mier, J.S. Sewell, J.S. Sizerlove, A. Akselrad, and J.E. Clemans, "Uniformity of Three-inch, Semi-Insulating, Vertical-Gradient-Freeze  $\text{GaAs}$  Wafers," *J. Appl. Phys.* 66, 1000 (1989).
59. D.C. Look, Electrical Characterization of  $\text{GaAs}$  Materials and Devices, (Wiley, New York, 1989) 280 pp.
60. D.C. Look, D.C. Walters, R.T. Kemerley, J.M. King, M.G. Mier, J.S. Sewell, and J.S. Sizerlove, "Wafer-Level Correlations of EL2, Dislocation Density, and FET Saturation Current at Various Processing Stages," *J. Electronic Mat.* 18, 487 (1989).
61. D.C. Look, "Hall-effect Depletion Corrections in Ion-Implanted Samples:  $\text{Si}^{29}$  in  $\text{GaAs}$ ," *J. Appl. Phys.* 66, 2420 (1989).
62. N.C. Halder and D.C. Look, "Deviations from Bulk Transport Measurements in Semi-Insulating  $\text{GaAs}$ ," *J. Appl. Phys.* 66, 4858 (1989).
63. D.C. Reynolds, K.K. Bajaj, W.M. Theis, P.W. Yu, and N. Chand, "Correlation between resonantly excited magnetic-field split donor-bound exciton components with their excited state emission analogues in  $\text{GaAs}$ ," *Appl. Phys. Lett.* 54, 159 (1989).



64. P.W. Yu, C.K. Peng, and H. Morkoc, "Quasi-donor-acceptor pair photoluminescence emission in  $\text{Ga}_x\text{In}_{1-x}\text{As/InP}$ ," J. Appl. Phys. **65**, 2427 (1989).
65. W.C. Mitchel, L.S. Rea, and P.W. Yu, "Observation of difference in the quenching of the photocurrent in GaAs containing EL2 and ELO," J. Elect. Mat. **18**, 209 (1989).
66. M. Baemler, J. Schneider, U. Kaufmann, W.C. Mitchel, and P.W. Yu, "Electron paramagnetic resonance identification of the  $\text{Sb}_{\text{Ga}}$  heteroantisite defects in GaAs:Sb," Phys. Rev. B **39**, 6253 (1989).
67. P.W. Yu, C.K. Peng, and H. Morkoc, "Photoluminescence from carriers confined at a  $\text{Ga}_x\text{In}_{1-x}\text{As/InP}$  single heterojunction interface," Appl. Phys. Lett. **54**, 1546 (1989).
68. D.C. Reynolds, K.K. Bajaj, C.E. Leak, C.E. Stutz, R.L. Jones, K.R. Evans, P.W. Yu, and W.M. Theis, "Determination of binding energy of excitons bound to donors located at the center or edge of the well or center of the barrier in  $\text{Al}_x\text{Ga}_{1-x}\text{As/GaAs}$  multi-quantum wells," Phys. Rev. B. **40**, 6210 (1989).
69. D.C. Reynolds, K.K. Bajaj, C.E. Stutz, R.L. Jones, W.M. Theis, P.W. Yu, and K.R. Evans, "The binding energy of biexcitons in  $\text{Al}_x\text{Ga}_{1-x}\text{As/GaAs}$  multi-quantum wells," Phys. Rev. B. **40**, 3340 (1989).
70. W.M. Theis, G.D. Sanders, K.R. Evans, L.L. Liou, C.E. Leak, K.K. Bajaj, C.E. Stutz, and R.L. Jones, "Extrinsic contributions to photorefectance of GaAs-AlGaAs quantum wells: an investigation of the 'donor-related' feature," Phys. Rev. B **39**, 11038 (1989).
71. W.M. Theis, G.D. Sanders, C.E. Leak, D.C. Reynolds, Y.C. Chang, K. Alavi, C. Colvard, and I. Shidlovsky, "Excited states of the light- and heavy-hole free excitons observed in photorefectance," Phys. Rev. B **39**, 1442 (1989).
72. W.C. Mitchel, D.W. Fischer, L.S. Rea, and P.W. Yu, "Anomalous photoquenching in semi-insulating GaAs attributed to the presence of the deep donor ELO," Phys. Rev. B **40**, 8431 (1989).
73. P.W. Yu, G.D. Sanders, K.R. Evans, D.C. Reynolds, K.K. Bajaj, C.E. Stutz, and R.L. Jones, "Electric field dependence of exciton oscillator strengths in GaAs-AlGaAs quantum wells studied by photocurrent spectroscopy," Phys. Rev. B **40**, 3151 (1989).
74. P.W. Yu, G.D. Sanders, K.R. Evans, D.C. Reynolds, K.K. Bajaj, C.E. Stutz and R.L. Jones, "Photocurrent spectroscopy of  $\text{In}_x\text{Ga}_{1-x}\text{As/GaAs}$  multiple quantum wells," Appl. Phys. Lett. **54**, 2230 (1989).
75. D.C. Look, "Review of Hall Effect and Magnetoresistance Measurements in GaAs Materials and Devices," J. Electrochem. Soc. **137**, 260 (1990).
76. D.C. Look, A.R. Adams, and D.R. Wight, "Hole Mobility, Diffusion, and Lifetime," in Properties of Gallium Arsenide, Second Edition (INSPEC, London, 1990) p. 97.

77. D.C. Look, B.J. Sealy, R.L. Williams, and D. Lee, "Resistivity," Ibid, p. 25.
78. R.A. Stradling and D.C. Look, "Photoconductivity Spectra," Ibid, p. 211.
79. B.S. Ziebro, D.C. Look, J.W. Hemsley, and W. Rice, "In-situ Hall-effect system for real-time electron-irradiation studies," Rev. Sci. Instr. 61, 192 (1990).
80. J.O. Crist and D.C. Look, "Activation efficiencies for a standard qualification implant in GaAs annealed by a rapid thermal process," J. Electronic Mat. 19, 773 (1990).
81. D.C. Look, C.E. Stutz, and K.R. Evans, "Surface and Interface Free-Carrier Depletion in GaAs Molecular Beam Epitaxial Layers: Demonstration of High Interface Charge," Appl. Phys. Lett. 56, 668 (1990).
82. D.C. Look, D.C. Walters, M.O. Manasreh, J.R. Sizelove, C.E. Stutz, and K.R. Evans, "Anomalous Hall-Effect Results in Low Temperature Molecular-Beam Epitaxial GaAs: Hopping in a Dense EL2-like Band," Phys. Rev. B 42, 3578 (1990).
83. M.O. Manasreh, D.C. Look, K.R. Evans, and C.E. Stutz, "Infrared Absorption of Deep Defects in Molecular Beam Epitaxial Layers Grown at 200 °C: Observation of an EL2-like Defect," Phys. Rev. B 41, 10272 (1990).
84. Z-Q. Fang, H. Yamamoto, D.C. Look, K.R. Evans, and C.E. Stutz, "A Comparison of Deep Centers in Low Temperature MBE, As-rich LEC, and Ga-rich LEC GaAs," in Semi-Insulating III-V Materials, Toronto, 1990, ed. by A. Milnes and C.J. Miner (IOP, Bristol, 1990) p. 117.
85. M.O. Manasreh, D.C. Look, K.R. Evans, and C.E. Stutz, "Observation of Deep Defects in As-rich GaAs Grown by the Molecular Beam Epitaxy Technique at 200 °C," in Semi-insulating III-V Materials, Toronto, 1990, ed. by A. Milnes and C.J. Miner (IOP, Bristol, 1990) p. 105.
86. C.R. Wie, K. Xie, D.C. Look, K.R. Evans, and C.E. Stutz, "Low-temperature Grown Semi-Insulating GaAs Layer: Defect Concentration From Lattice Constant and Resistivity," in Semi-insulating III-V Materials, Toronto, 1990, ed. by A. Milnes and C.J. Miner (IOP, Bristol, 1990) p. 71.
87. Z-Q. Fang, H. Yamamoto, and D.C. Look, "Origin and Behavior of Main Electron Traps in Si-implanted GaAs," in Degradation Mechanisms in III-V Compound Semiconductor Devices and Structures, ed. by V. Swaminathan, S.J. Pearton, and M.O. Manasreh (Materials Research Society, Pittsburgh, 1990) p. 93.
88. C.R. Wie, K. Xie, T.T. Bardin, J.G. Pronko, D.C. Look, K.R. Evans, and C.E. Stutz, "Characterization of MBE Layers Grown at 200 °C-300 °C," Mat. Res. Soc. Symp. Proc. Vol. 198, p. 383 (1990).
89. D.C. Look, "Influence of Point Defects on GaAs Devices," in Degradation Mechanisms in III-V Compound Semiconductor Devices and Structures, ed. by V. Swaminathan, S.J. Pearton, and M.O. Manasreh (Materials Research Society, Pittsburgh, 1990) p. 23.

90. M.G. Mier, D.C. Look, D.C. Walters, and J.R. Sizelove, "GaAs Whole-Wafer Dislocation Mapping for Qualifying Substrates," in Proc. 1990 U.S. Conf. on GaAs Manufacturing Technology, ed. by J. Tenedorio, p. 7 (1990).
91. H. Yamamoto, Z-Q. Fang, and D.C. Look, "Non-Alloyed Ohmic Contacts on Low-Temperature MBE GaAs: Influence of Deep Donor Band," Appl. Phys. Lett. **57**, 1537 (1990).
92. D.C. Look, C.E. Stutz, and K.R. Evans, "Unpinning of GaAs Surface Fermi Level by 200 °C Molecular Beam Epitaxial layer," Appl. Phys. Lett. **57**, 2570 (1990).
93. S. Shah, J. Chaudhuri, M. Mier, and D.C. Look, "X-ray Double-crystal Diffractometry Characterization of Semi-insulating GaAs," J. Materials Sci. **25**, 4298 (1990).
94. P.W. Yu, S. Ravipati, B.E. Taylor, and W.C. Mitchel, "Photorefectance measurements of indium content in indium-alloyed semi-insulating GaAs substrates," J. Appl. Phys. **67**, 1471 (1990).
95. D.C. Reynolds, K.G. Merkel, C.E. Stutz, K.R. Evans, and P.W. Yu, "Observation of the donor-bound light-hole free exciton in AlGaAs-GaAs quantum wells," J. Appl. Phys. **67**, 439 (1990).
96. K.R. Evans, C.E. Stutz, P.W. Yu, and C.R. Wie, "Mass-spectroscopic determination of antimony incorporated during III-V molecular beam epitaxy," J. Vac. Sci. Technol. B **8**, 271 (1990).
97. B. Jogai and P.W. Yu, "Energy levels of strained  $\text{In}_x\text{Ga}_{1-x}$  GaAs superlattices," Phys. Rev. B **41**, 12650 (1990).
98. S. Ravipati, P.W. Yu, B.E. Taylor, and W.C. Mitchel, "Photorefectance measurements of indium content in semi-insulating indium-alloyed GaAs bulk substrates," SPIE **1286**, 66-73 (1990).
99. P.W. Yu, "Photoluminescence and photoluminescence excitation of 0.635-eV ELO emission in oxygen-doped semi-insulating GaAs," Phys. Rev. B **42**, 11889 (1990).
100. D.C. Reynolds, T.C. Collins, and K.K. Bajaj, "Electron-mass anomaly as determined from the Zeeman effect of the donor 2P levels in GaAs," Phys. Rev. B **42**, 11208 (1990).
101. D.C. Look, "On Compensation and Conductivity Models for MBE GaAs Grown at Low Temperature," J. Appl. Phys. **70**, 3148 (1991).
102. H. Kanber, D.C. Wang, E.T. Pan, and D.C. Look, "Wafer Level Mapping of GaAs for MMIC Fabrication," 1991 Government Microcircuit Applications Conference Digest of Papers (SLCET-DT, Ft. Monmouth, NJ, 1991) p. 303.
103. H. Kanber, D.C. Wang, E.T. Pan, and D.C. Look, "Wafer Level Mapping of GaAs for MMIC Fabrication," GaAs IC Symp. Tech. Digest 1991, p. 285 (1991).

104. D.C. Reynolds, K.K. Bajaj, and T.C. Collins, "Zeeman electron mass anomaly in InP as determined from orbital and spin splitting of donor 2P levels using high resolution photoluminescence spectroscopy," J. Appl. Phys. 69, 6478 (1991).
105. E.T. Koenig, C.I. Huang, B. Jogai, K.R. Evans, C.E. Stutz, and D.C. Reynolds, "Effect of radial growth rate variation in resonant tunneling diode current-voltage characteristics," Journal of Electronic Materials 20, 223 (1991).
106. J.M. King, R.D. Worley, J.R. Sizelove, J.K. Gillespie, T.K. Krueger, R.A. Niedhard, J.L. Brown, S.E. Cummins and D.C. Look, 1991 Government Microcircuit Applications Conference Digest of Papers (SLCET-DT, Ft. Monmouth, NJ, 1991) p. 331.
107. P.D. Mumford and D.C. Look, "On-Wafer Hall-Effect Measurement System," Rev. Sci. Inst. 62, 1666 (1991).
108. D.C. Look, K.R. Evans, and C.E. Stutz, "Effects of a Buffer Layer on Free-carrier Depletion in n-type GaAs," IEEE Trans. on Electron Devices 38, 1280 (1991).
109. Z-Q. Fang and D.C. Look, "Comparison of Deep Centers in Semi-Insulating Liquid-Encapsulated Czochralski and Vertical-Gradient Freeze GaAs," J. Appl. Phys. 69, 8177 (1991).
110. Z-Q. Fang and D.C. Look, "Infrared Quenching and Thermal Recovery of Thermally Stimulated Current Spectra in GaAs," Appl. Phys. Lett. 59, 48 (1991).
111. D.C. Reynolds, K.R. Evans, K.K. Bajaj, B. Jogai, C.E. Stutz, and P.W. Yu, "Direct coupling of heavy-hole free excitons in InGaAs/GaAs quantum wells with free excitons in the GaAs barrier," Phys. Rev. B 43, 1871 (1991).
112. D.C. Reynolds, K.G. Merkel, C.E. Stutz, K.R. Evans, K.K. Bajaj and P.W. Yu, "Free-to-bound and light- and heavy- hole bound excitons in  $\text{Al}_x\text{Ga}_{1-x}\text{As}$ -GaAs multiple quantum wells," Phys. Rev. B 43, 1604 (1991).
113. P.W. Yu, D.C. Reynolds, G.D. Sanders, K.K. Bajaj, C.E. Stutz, and K.R. Evans, "Electric-field effects of the excitons in asymmetric triangular  $\text{Al}_x\text{Ga}_{1-x}\text{As}$ -GaAs quantum wells," Phys. Rev. B 43, 4344 (1991).
114. D.C. Reynolds, K.R. Evans, C.E. Stutz, and P.W. Yu, "Effect of a magnetic field on the photoluminescence from  $\text{In}_x\text{Ga}_{1-x}\text{As}$ /GaAs and GaAs/ $\text{Al}_x\text{Ga}_{1-x}\text{As}$  quantum wells," Phys. Rev. B 43, 4244 (1991).
115. D.C. Reynolds, K.R. Evans, G. Merkel, C. Stutz, and P.W. Yu, "Photoluminescence due to a bound-to-bound transition in a GaAs- $\text{Al}_{0.3}\text{Ga}_{0.7}\text{As}$  quantum well structure," Phys. Rev. B 43, 9087 (1991).
116. P.W. Yu and H. Kuwamoto, "Photoluminescence of indium-alloyed semi-insulating GaAs subjected to bulk heat treatments," J. Appl. Phys. 70, 954 (1991).

117. D.C. Reynolds, K.R. Evans, C.E. Stutz, and P.W. Yu, "Binding energy of excitons to neutral donors in  $\text{In}_{0.1}\text{Ga}_{0.9}\text{As}/\text{GaAs}$  quantum wells," *Phys. Rev. B* **44**, 1839 (1991).
118. A. Kangarlu, H. Guarriello, R. Berney, and P.W. Yu, "Intrinsic acceptor antisite defects in GaAs under hydrostatic pressure," *Appl. Phys. Lett.* **59**, 2290 (1991).
119. D.C. Reynolds, K.R. Evans, C.E. Stutz, K.K. Bajaj, and P.W. Yu, "Photoluminescence determination of the binding energy of residual donors in  $300\text{-}\text{\AA}$   $\text{Al}_x\text{Ga}_{1-x}\text{As}/\text{GaAs}$  quantum wells," *Phys. Rev. B* **44**, 8869 (1991).
120. Z-Q. Fang and D.C. Look, "Metastable States in Semi-insulating GaAs Revealed by TSC Spectroscopy," in Proc. of the 16th Int. Conf. on Defects in Semiconductors, ed. by G. Davies, G. DeLeo, and M. Stavola, *Materials Sci. Forum* Vol. 83-87, 191 (1992).
121. D.C. Look, D.K. Lorange, J.R. Sizelove, C.E. Stutz, K.R. Evans, and D.W. Whitson, "Alloy Scattering in p-type  $\text{Al}_x\text{Ga}_{1-x}\text{As}$ ," *J. Appl. Phys.* **71**, 260 (1992).
122. H.J. von Bardeleben, M.O. Manasreh, D.C. Look, K.R. Evans, and C.E. Stutz, "Electron Paramagnetic Resonance Study of Low Temperature MBE GaAs," *Phys. Rev. B* (accepted).
123. D.C. Reynolds, K.R. Evans, C.E. Stutz, and P.W. Yu, "Sensitivity of resonant excitation and photoluminescence excitation measurements to exciton localization effects in  $\text{GaAs}/\text{AlGaAs}$  quantum wells," *Appl. Phys. Lett.* **60**, 962 (1992).
124. D.C. Reynolds and K.R. Evans, "Optical and Magneto-optical properties of narrow  $\text{In}_x\text{Ga}_{1-x}\text{As}-\text{GaAs}$  quantum wells," chapter in a book entitled *Semiconductor Interfaces and Microstructures*, to be published by World Scientific Publishing (WSP) Co., Inc.
125. M.O. Manasreh, K.R. Evans, C.E. Stutz, D.C. Look, and J. Hemsky, "Incorporation of Si in Low Temperature MBE GaAs," *Mat. Res. Soc. Symp. Proc.* Vol. (accepted).
126. D.C. Look, J.E. Hoelscher, J. Grant, C.E. Stutz, K.R. Evans, and M. Numan, "Photorefectance and X-ray Photoelectron Spectroscopy in LT-MBE GaAs," *Mat. Res. Soc. Symp. Proc.* Vol. (accepted).
127. Z-Q. Fang and D.C. Look, "Defects in Low-temperature-grown MBE GaAs as Studied by a Variation of TSC Spectroscopy," *Mat. Res. Soc. Symp. Proc.* Vol. (accepted).
128. M.G. Mier, D.C. Look, D.C. Walters, and D.L. Beasley, "Infrared Transmission Topography for Whole-Wafer Gallium Arsenide Materials Characterization," *Solid State Electronics* (in press).
129. D.C. Look, "Point Defect Characterization in III-V Semiconducting Compounds," *Proc. of the 38th Sagamore Materials Conf.* (accepted).

130. D.C. Look, H. Yamamoto, and K. Nakano, "Ohmic Contact Formation on GaAs Layers with Low-Temperature Molecular Beam Epitaxial Caps," IEEE Trans. on Electron Devices (in press).
131. D.C. Look, "Defects relevant for compensation in semi-insulating GaAs," in Semiconductors and Semimetals (ed. by E. Weber) Academic, New York, 1992. (accepted).
132. P.W. Yu, M.Y. Yen, and C.E. Stutz, "Photoluminescence of Mg-ion implantation in low-temperature grown GaAs," Mat. Res. Soc. Symp. Proc. Vol. (accepted).
133. P.W. Yu and A. Kangarlu, "Photoluminescence study of GaAs antisite double acceptor in GaAs under hydrostatic pressure," GaAs and Related Compounds Symp. (accepted).
134. P.W. Yu, J.R. Sizelove, and D.W. Fischer, "Photoluminescence of Ga<sub>As</sub>-related 1.32eV emission in bulk GaAs," Semicond. Sci. Tech. (accepted).

## Patents

D.C. Look and E. Pimentel, "Method and Apparatus for Measuring Photoresistivity and Photo Hall-Effect of Semiconductor Wafers," No. 4,816,755.

D.C. Look and E. Pimentel, "Method and Apparatus for Measuring Average Resistivity and Hall-Effect of Semiconductor Wafers," No. 4,857,839.

D. C. Look, J. S. Sewell, M. G. Mier, J. S. Sizelove, D. C. Walters, and S. C. Dudley, "Whole-Wafer Etch-Pit Density Mapping," No. 5,008,542 (16 Apr 1991).

D.C. Look and P.H. Mumford, "On-Wafer Hall-Effect Measurement System," in process, AF Inv. 20007.